UNIVERSITY OF CALIFORNIA,
IRVINE

Electrochemical Devices Derived from Pyrolyzed Graphitic Polyacrylonitrile

THESIS

submitted in partial satisfaction of the requirements
for the degree of

MASTER OF SCIENCE

in Mechanical and Aerospace Engineering

by

Brandon Ryan Davidovich Pollack

Dissertation Committee:
Professor Marc Madou, Chair
Professor Jaeho Lee
Professor Regina Ragan

2017

DEDICATION

To my friends and family back at home and in the BioMEMS lab.

TABLE OF CONTENTS

LIST OF FIGURES

LIST OF TABLES

ACKNOWLEDGMENTS

I would like to acknowledge the UCI's BioMEMS lab and to thank Dr. Marc Madou for his guidance and advice. Additionally, I would like to acknowledge the C-MEMS team in particular including Sunshine Holmberg, Derosh George, and Lauren (EunByul) Cho for their aid. The visiting scholars Oscar Pilloni and Dr. Arnoldo Salazar also providing me with advice and assistance. An additional thanks needs to go to Dr. Maziar Ghazinejad for his support and passionate encouragement in research and writing.

Many parts of this work were done in collaboration with other members of the BioMEMS lab, and specifically the C-MEMS team. Raman spectroscopy and TEM analaysis were done in collaboration with Sunshine Holmberg. Derosh George and Dr. Ich Tran helped to perform and analyze XPS.

Support for many of the experiments came from various sources including in part the National Science Foundation (NSF) grant #1449397. Equipment access and usage was made possible by UCI National Fuel Cell Research Center (NFCRC) which generously allowed use of their potentialstats for electrochemical experiments. A thank you goes out to UCIs Chemistry Department Laser Spectroscopy for providing access to the Raman microscope, and UCI Integrated Nanosystems Research Facility (iNRF) for access to the clean rooms and related equipment. Additionally, I would like to thank UC Irvine Materials Research Institute (IMRI) and Dr. Ich Tran for access and expertise on SEM, TEM, and XPS which were funded in part by the National Science Foundation Major Research Instrumentation Program under grant no. CHE-1338173.

For use of copyrighted images I would like to thank John Wiley and Sons, Nature Publishing Group, American Association for the Advancement of Science, Royal Society of Chemistry, and Elsevier for permissions. Some of the figures in this thesis are used under CC BY 4.0.

Finally, I must acknowledge Lola and Luna for their unwavering emotional support and unconditional affection.

ABSTRACT OF THE THESIS

Electrochemical Devices Derived from Pyrolyzed Graphitic Polyacrylonitrile

By

Brandon Ryan Davidovich Pollack

Master of Science in Mechanical and Aerospace Engineering

University of California, Irvine, 2017

Professor Marc Madou, Chair

In this work I present a simple route for fabrication of a graphitic carbon and use that to produce hydrogen peroxide sensors. The graphitic carbon was shown to have superior electrocatalytic properties when compared to its more standard fabrication routes. This was done by using the technique of electrospinning to create a nanofibrous mat out of the polymer polyacrylonitrile (PAN). The electrospinning, along with additions of carbon nanotubes (CNT) subjected the nanofibers to a force capable of unwinding the molecular chains of PAN. This unwinding was then maintained by subjecting the nanofiber mats to mechanical stresses, prior to and during a stabilization process which helps the PAN cross-link. Finally, these mechanically treated mats were then pyrolyzed into carbon structures.

Mats were fabricated to have a graphitic nature despite being pyrolyzed at relatively low temperatures (1000 °C). The mats were characterized Raman Spectroscopy, Transmission Electron Microscopy (TEM), and X-ray Photoelectron Spectroscopy (XPS). This showed increased graphitization compared to non-stressed mats and demonstrated interesting elechtrochemical behavior.

In terms of electrochemical properties, the mechanical treated carbons showed an increase in the heterogeneous electron transfer rate. This presented the opportunity to test the carbon mats as an electrochemical sensor. Hydrogen peroxide sensing was performed where it proved

to be on par with other more expensive carbon based materials.

Chapter 1

Introduction

Electrochemistry is all around us. From everyday biological processes such as your brain's neurons firing signals[72, 99], the rust forming on steel left out to moisture[136], the batteries[8] powering technology around us, to sensors/bio-sensors[163] providing information, as well as many more applications. A common material used for electrochemical devices can revolve around inert metals such as gold or platinum[65, 85, 28]. These materials produce excellent properties in their respective functions they are also known for being very expensive and sometimes difficult to machine. Carbons have been used for many years for electrochemical devices although their properties can be lacking compared to the metals since they are often of the amorphous verity. Graphene is known as a carbon material with superior properties and as a possible replacement. Graphene has its own disadvantages though, mainly that it is difficult and costly to fabricate and may need to be functionalized to be used as an electrocatalyst. A popular way to make carbon structures is with performing pyrolysis on polymer precursors. The polymer can be patterned prior to pyrolysis. This will result in a finished structure of carbon structure in the shape of the patterned polymer. Typically, there are two options for this pyrolysis, to use a high temperature (such as 3000 °C) which would allow for the formation of graphitic planes in the carbon allowing for electrical prop-

erties similar to graphene. This temperature would cause the decomposition of most all non-carbon molecules. In electrochemical applications these additional molecules can be necessary. While post-processing can be used to dope in heteroatoms, this can be very destructive to the carbon structure. Alternatively, pyrolysis can be performed at a relatively low temperature (such as 1000 °C) which would leave behind heteroatoms in the structure, but the carbon derived from PAN would be amorphous. Here I present an alternative fabrication route for carbon that would allow for the low temperature pyrolysis and still result in graphitic carbon. This carbon can potentially replace graphene or even rare metals in electrochemical applications.

1.1 Overview of this Work

In order to understand carbon electrochemical devices, it is necessary to first understand carbon. This thesis begins by looking at carbon and its various allotropes. This can provide an understanding of how the structure of carbon can have dramatic effect on virtually every property. Carbon can go from one of the hardest natural materials, known as diamond, to the seemingly opposite as one of the softest natural materials called graphite. These two are naturally occurring carbon allotropes but there are many more (and many still being discovered) such as the recently discovered material of graphene and its rolled up form, the carbon nanotube (CNT). These carbon allotropes are proving to be an extremely popular area of study[120, 67] as graphene and its related forms have incredible properties from excellent mechanical strength[107] to superior conductivity in terms of both thermal[177] and electrical[67]. Graphene also has an incredible range of applications in electrochemistry suitable for most any challenge. Some of graphene's properties comes from the fact that its microstructure is very orderly (or graphitic) as well as inert to many chemicals.

Graphene can potentially be extremely simple to fabricate. By using normal Scotch®

tape, graphene can be peeled off a chunk of graphite [138]. But here lies one of the major disadvantages, cost and scalability. Having a piece of graphene attached to the adhesive side of tape may be interesting, but it is not always practical. This technique would be difficult to scale up to larger volumes. Other techniques are being used such as chemical vapor deposition (CVD)[154] which can produce larger quantities of graphene, although this technique may produce a graphene with impurities, can still be costly, and may involve harsh chemicals.

A discussion is presented of some other allotropes of carbon which can have their own advantages and disadvantages. There is amorphous carbon which has very little order to the structure. Amorphous carbon can be very reactive with dangling bonds and function groups. Then there is glass-like carbon which has improved properties over amorphous carbon with some local order in its microstructure. Glass-like carbon has found many uses because of its hardness combined with good electrical and thermal properties. Typically, it is found in electrochemical applications because of its chemical inertness and high conductivity. Alternatively, it can be found in thermal applications such as a crucible for a high temperature furnace because of its good stability even at high temperatures. Glass-like carbon has another major advantage in its ease of manufacturing. Carbon materials can be very hard to pattern into a desired shape. Glass-like carbon can be fabricated from a polymer precursor. This allows the polymer to be patterned into a desired shape and then undergoes pyrolysis (or decomposed to carbon via heat) to have a carbon structure in the same shape.

Once a background has been established on some of the relevant carbon structures then there is a description of the fabrication process used in this work. Electrospinning was performed to create polymer nanofiber mats. The electrospinning applies strong electrohydrodynamic forces which help to align the polymer molecules. These mats then undergo stabilization while being mechanically stressed to maintain the molecular alignment. The mechanical stressing is used to improve the properties of the final product. After stabilization the

polymer mats are decomposed into carbon through pyrolysis. This now produces an unwoven mat made of carbon nanofibers.

With these carbon nanofiber mats they can be characterized via a wide range of techniques. Raman spectroscopy was used to examine the degree of graphitization based on the crystal structure. This was further supported by an increase in conductivity as tested by a four-probe measurement. Transmission Electron Microscopy (TEM) was used to help confirm the graphitization by the observation of orderly planes in the microstructure as well as by the X-ray diffraction pattern from the Fast Fourier Transformations (FFT). The chemical composition of the samples was observed via X-ray Photoelectron Spectroscopy (XPS) which revealed that there where heteroatoms in the carbon structure. This addition of heteroatoms and the possibility to control their quantity presents the potential to tailor the carbon depending on the application in a single step (that is without some sort of post-processing). Finally, electrochemical testing was performed to show electron kinetics which correlated to what would be expected from a carbon with increased graphitization.

A test study was then able to be completed using the carbon nanofiber mats as electrodes for sensing applications. The electrodes where used as an electrocatalyst for a hydrogen peroxide reduction reaction. This allowed the determination of the quantity of hydrogen peroxide and it proved to do an excellent job creating a sensor with comparable performance with other carbon-based materials including those using more expensive and complex fabrication and materials. This electrocatalysis was not limited to hydrogen peroxide but other important biologically related substances. This opens the potential for the carbon nanofiber to be used in more sensing applications as well as in many electrochemical applications such as a catalyst and electrode for the oxygen reduction reaction (ORR) in fuel cells, electrodes for batteries, and in supercapacitors.

1.2 Motivation

An issue with glass-like carbon is that the properties are not as good as graphite or graphene. Here is where lies the motivation for this thesis, to be able to produce a carbon material that has both graphitic properties as well as retaining some heteroatoms from the original polymer. This would be an as fabricated functionalized graphitic carbon. A technique is being presented that can be used to prepare carbon from a polymer precursor so that it can be patterned as would most glassy-carbons. But a technique is involved that also results in a graphitic structure. To begin an electrical technique known as electrospinning is used which will produce an unwoven mat made of polymer nanofibers. The forces enacted on the polymer from the electrospinning process cause the molecular chains to unwind. The polymer nanofiber mats are then stabilized under mechanical stress so that the molecular chains stay in their aligned orientation for the final step. In this last step the polymer nanofiber mats are decomposed into carbon nanofiber mats inside a 1000 °C furnace.

Chapter 2

Background

2.1 Carbon

Carbon is a truly versatile element that can be tailored to an increasingly large amount of applications. It is one of the fundamental building blocks of all known living organisms because of its flexibility to bond with many other elements. Carbon holds the sixth spot on the periodic table of elements with an atomic weight of 12.011. In its natural state carbon has electron orbitals of $1s^2\ 2s^2\ 2p^2$. An orbital is the probability function of where an electron will be around the atoms nucleus. For example, in the case of the s orbital it forms a sphere around the nucleus while the 2p orbital is made up of two ellipsoids centered around the nucleus. The ellipsoids can be oriented around either the X, Y, or Z axis. The number before the s or p is the energy level. If these orbitals were to share they will form what is a new hybrid orbital in a process known as hybridization.

This new hybrid orbitals will be used to form sigma (σ) bonds (also known as the overlap of atomic orbitals) while the non-hybridized p orbitals will go on to form the pi (π) bonds. A single Carbon carbon bond (C —— C) will be made of a single σ bond, a double carbon bond

(C$=$C) will be made from a σ bond and a π bond, and triple carbon bond (C$\equiv$C) will be made from a σ bond and two π bonds. A σ bond is stronger than a π bond, but a triple bond will be the strongest since there is three of them.

2.2 Allotropes of Carbon

One of the major versatilities of carbon comes from its ability to hybridize and bond with itself. The hybridization of carbon will help determine its physical and electrical properties. When the same chemical element can to take on different forms because of the different chemical bonds taking place, this is known as allotropy. Some of the most famous allotropes of carbon are the diamond and graphite allotropes which have vastly different properties. Diamond is known for being the hardest bulk material, it is optically transparent, has one of the highest thermal conductivity's (of any bulk material), and is an electrical insulator. Conversely, graphite is extremely soft, visually opaque, has very low thermal conductivity, but has a high electrical conductivity. The vast difference in these two allotropes properties are because of the hybridization's associated with them. Carbon has three different hybridization's available to it which are the sp^1, sp^2, and sp^3. In their perfect crystalline form these hybridization's are the structure of carbyne, diamond, and graphene respectively. Here crystallinity is defined by International Union of Pure and Applied Chemistry (IUPAC) as the three-dimensional order of the molecules [129]. These three allotropes have non-mixed hybridization's but there are many mixed hybridization's that form other allotropes and many more are being discovered. The allotropes and their hybridization's are shown in Figure 2.1. Graphene is a two-dimensional lattice of carbons in the vertex of hexagons. It has a thickness of a single carbon atom. It is extremely strong and is an excellent conductor of both electrical and thermal energy. Graphene forms the basis of many other allotropes including graphite (multiple sheets of graphene bonded in parallel together), Carbon Nan-

otubes (CNT, a sheet of graphene rolled into a tube) , and Fullerenes (graphene rolled into a hallow sphere). These materials are what would be called a 2, 1, and 0-dimension material respectively. In this labeling scheme the number refers to the material dimensions that are not solely in the nanoscale. Graphene is considered 2D because it has a thickness that is confined to nanoscale (single atom thick) while the length and width can theoretically be larger than nanoscale. When graphene is stacked into sheets it is called graphite which would be considered a 2D material up until about 10 layers thick[142]. Alternatively, Fullerenes are considered 0D because every dimension is in the nanoscale (it is a nanometer wide sphere).

Carbyne is an allotrope of carbon in a linear chain of repeating triple and single bonds ($(-\!\!-C\equiv C-\!\!-)_n$). It is known to have incredible tensile strength, up to 40x that of diamond[1] and even stronger than that of the previously thought strongest material, graphene. Carbyne does not seem to exist naturally on earth and when fabricated in the laboratories is extremely unstable.

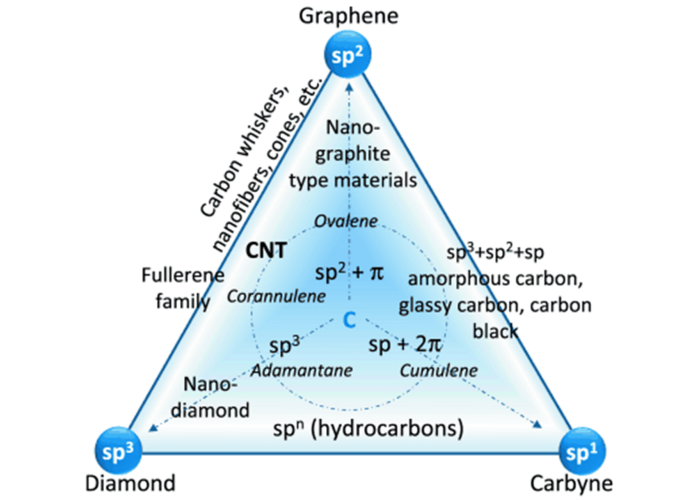

Centi, Gabriele, and Siglinda Perathoner. "Carbon nanotubes for sustainable energy applications." ChemSusChem 4.7 (2011): 913-925.

Figure 2.1: Various carbon allotropes and their hybridization's. The vertices of the triangle are the pure crystalline forms of each hybridization. Permission granted from Centi et al [33]

From Figure 2.1 the non-mixed hybridized carbons are highlighted in the corners as the sp^1, sp^2, and sp^3. As different hybridization's mix then their internuclear bond lengths can differ and thus affect there properties. As an example, a single sheet of graphene is extremely

strong and inert. When it binds with other sheets it will form graphite which on the other hand is known for being very soft and will easily break. This is because of the weak coupling between basal planes (π bonds) would more easily shear which allowed the graphite to be slippery and what is what thought made graphite an excellent lubricant. Studies have gone shone that this is false as there is a need for a vapor (such as water) to be present to facilitate slippery behavior[209].

2.2.1 Graphene

Graphene is an extremely exciting area of carbon and materials science research. It is defined as a flat planar structure of pure crystalline sp^2 bonded carbon in a honeycomb lattice[67]. Initially, atomically thick materials thought possible, but graphene was experimentally proven in 2004[138]. Graphene can be stacked, but when there are more than 8 sheets it starts to be considered graphite[26]. In graphene there are two different structural elements; the basal plane and the edge plane. The basal plan is perpendicular to the 2D carbon sheet and the edge plane is the thickness of that carbon sheet. The edge plane may also be considered defects as this is where there are breaks in the uniformity of the basal plane. The edge plane will have dangling bonds that will often bond with elements in the environment such as hydrogen or oxygen. In the case of oxygen this will form what is known as graphene oxide (GO). The edge is also where there is to be expected a higher electron transfer rate and electrocatalytic ability when compared to the basal plane[211]. It was shown that this 2D material had extremely high crystal quality which is was allows graphene to be incredibly good at being a charge carrier. Therefore, depending on the application it could be advantageous to have a tailored amount of both the basal planes and edge planes. To combine the edge planes reactivity with that of the good structural and electrical properties of the basal plane.

There are many ways to fabricate graphene, one of the simplest and oldest is to start with graphite and through a process known as micromechanical exfoliation, the sheets of graphene can be ripped off of the bulk graphite. This process is as simple as peeling off a layer a graphene. It can even be accomplished with a typical roll Scotch® tape. The tape will adhere to the graphite, and then pull off a single layer[138]. Afterwards the graphene layer can either be left on the tape or the tape can be etched away. This technique is fairly simple to reproduce and it produces very high quality graphene[76], it also produces a very low quantity of graphene. Typically exfoliation techniques are restrained in producing graphene sheets on the scale of about 10 μm. More advanced and scalable techniques are being explored [190, 164, 109, 200] to remedy this.

One of the most common techniques for graphene production is via chemical vapor deposition or CVD[110]. This technique uses a precursor hydrocarbon gas to grow the graphene on a transitional metal such as copper. Copper is often used as it will not be absorbed and bind with the carbon the same way silicon or iron would. The copper (often on a substrate such as silicon) is placed in a reaction chamber with the gas blown in and the temperature is raised to 1000 °C which will decompose the gas. As the temperature is slowly decreased the carbon molecules will form on the copper as a single layer film. The copper can then be etched away such as with iron nitrate ($Fe(NO_3)_3$). By using the CVD technique graphene sheets have are no longer restricted to the micrometer scale and can enter the centimeter range. There is a wide array of other techniques for graphene fabrications as well such as starting with graphite oxide that was fabricated via what is known as the Hummers method and reducing it down to graphene oxide and finally to graphene in the modified Hummers method[200].

Graphene can be considered a parent of many other forms of carbon. In Figure 2.2 we can see how graphene is used as the basis for other important carbon allotropes such as when it curls into a cage in what is known as a fullerene (or buckyball), it can wrap up into a

cylinder to form a carbon nanotube (CNT), or stack into sheets and become graphite. It should be noted though that typical fabrication methods for these structures rarely would involve starting with pristine graphene and shaping it.

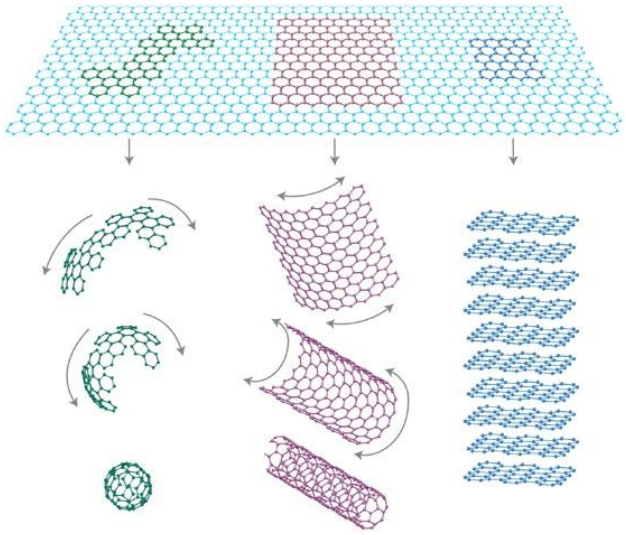

Figure 2.2: Graphene as the precursor for other carbon allotropes. Displayed (from left to right) is the 0D Fullerene, the 1D Carbon Nanotubes, and the 3D Graphite. Permission obtained from Geim et al[67].

2.2.2 Fullerenes

When a graphene sheet is rolled into a hollow sphere it is known as a fullerene. This was named after Buckminster Fuller for his famous Geodesic domes of which these carbon structures resemble. A fullerene will form by a graphene sheet losing its carbons on the edge which will cause pentagons to form and a bowl shape as well. The bowl shape will eventually close into a fullerene[38]. Because of the strain in forming the ball shape, the fullerene will behave different chemically when compared to the planar graphite. The balls the fullerene form are sometimes called carbon cages as they are hallow. They can have a diameter of 0.4 to 1.6 nm[70] depending on how many penta-0 or hexagons it is made up from. The most common form is the C_{60} fullerene which has 60 carbons (vertices) and that is formed

from twenty hexagons and twelve pentagons. The unique structure of fullerene allows it to be used for such the likes as drug delivery[45], photodyanimcs[45, 83], lubricants [18], and catalysts[195].

2.2.3 Carbon Nanotubes

When graphene is seamlessly rolled up into a tube it forms what is known as a Carbon Nanotube (CNT). This was first observed by Sumio Iijima in 1991[86], CNT's have become one of the most widely studied and used areas of nano-carbon materials because of their excellent electrical, mechanical, optical, thermal, and chemical properties. Applications can very as wide as composite materials[178] (to adjust bulk materials properties such as increasing strength and/or electrical conductivity), electrochemical devices[73] (such as sensors and fuel cells), energy storage (such as capacitors and/or batteries)[137, 106, 47], biotechnology[16] (bio-sensing, drug delivery[19], etc), nano/microelectronics[172], molecular circuits[10], and many more.

Although there is a lot of promise in CNT's, there tends to be a bottleneck in their usage due to the cost and production volumes. Typically, CNT's come in two forms; When there is only a single tube then the CNT is called a single walled carbon nanotube (SWCNT). When multiple carbon nanotubes are rolled in a concentric pattern it is referred to as a multi-walled carbon nanotube (MWCNT). It should be noted that unless otherwise specified the term CNT is referring to MWCNT in this work. When rolling the the CNT the orientation of the carbon lattice can have a large impact on the electrical characteristics of the CNT such as allowing it to be either metallic or a semiconductor[156]. This applies to both SWCNT and MWCNT's as the bonding between the multiple walls of a MWCNT's are weak[13]. Like that of of graphene, the electron transport in metallic CNT's will occur without any scattering[63] which allows the CNT to carry large amounts of currents without excessive

heating. Electrons are not the only particle that moves easily through CNT's, phonons also travel relatively unhindered[51]. Additionally, beyond the excellent electrical properties CNT's have excellent mechanical properties as well. A typical CNT will have a modulus of elasticity of about 19 times and a strength of about 56 times that of a steel wire (when normalizing by density)[13]. While there are many ways to synthesis CNT's, the most common methods include carbon-arc discharge (a technique first used by Iijima [86]), laser ablation and Chemical Vapor Deposition (CVD).

In Arc discharge is the process of generating plasma by breaking down a gas from an electricity[9]. Two electrodes are in a gas or liquid immersed chamber where one electrode has a tip of pure graphite (cathode) and the other is filled at the tip with a carbon precursor and a catalyst (anode). An electrical source (in either AC or DC) is applied to the electrodes which are 1-2 mm apart so that there is an arc discharge which produces plasma with temperatures that range from 4000-6000K. The carbon precursor sublimates (turns from solid straight to gas phase) and as a gas will drift towards the cathode where it will cool down and deposit CNT's a long with soot. The CNT's can then be purified out.

Laser ablation is the technique where material is removed from a solid or liquid via irradiation from a laser beam. A laser will hit a target that has a CNT precursor such as graphite. The carbon is ablated (vaporized) by the laser to form a plasma. As the plasma cools down and CNT's and fullerenes are formed. Additionally, larger clusters of carbon molecules will also form to create what is known as amorphous carbon[214].

The third technique mentioned for CNT synthesis is Chemical Vapor Deposition (CVD). This tends to be the most popular of the techniques because of its ease of use, lower production costs, and ability for scaling. The fabrication advantages come from CVD occurring in low temperature and ambient pressures. The downside of CVD comes from the CNT's tend to have inferior properties compared to the other two methods. Using this CVD technique can allow CNT's to be grown in a desired orientation on a substrate[101]. The process of

CVD involves a hydrocarbon that is in a furnace with a catalyst material. The hydrocarbon can be a gas (often known as forming gas) that is flowed into the furnace chamber, a liquid which is heated into a vapor and then pushed into the chamber by an inert gas, or a solid that is simply placed in the furnace with the catalyst. The furnace is heated to a sufficient temperature to decompose the hydrocarbons (typically around 600-1200°C). The catalyst (which is commonly a transition metal such as Fe, Co, or Ni) is pyrolyzed (decomposed via temperature in an inert environment) to release metal nanoparticles. There is no agreed upon mechanism for how the CNT grows, a widely accepted mechanism is that the hydrocarbon vapor will encounter the hot metal nanoparticles which will cause the hydrocarbon to decompose into hydrogen and carbon. The hydrogen can float away while the carbon is dissolved into the metal nanoparticles. When the metal has reached its solubility limit the carbon precipitates out in the form of CNT's[102].

2.2.4 Graphite

One of the oldest known allotropes of carbon is graphite. Graphite is a naturally occurring allotrope that has been used by humans since the beginning of history. It consists of graphitic planes, or sheets of graphene which are weakly bonded. It is the most stable form of carbon and sees uses from the common pencil lead, to batteries, to electrodes, and more. High electrical conductivity and thermal resistance are some of its most used properties.

2.2.5 Graphitization

Carbonization is the process of taking an organic precursor and decomposing it so that the molecules left are a majority of the carbon. While there are many ways to accomplish this process, a common method is via pyrolysis. The pyrolysis technique is defined as the thermochemical decomposition of an organic material in an inert environment (the absence of

oxygen). Some typical environments include argon, nitrogen, or a vacuum[120]. Graphitization is then the process of turning a carbon into a graphitic carbon (carbon with a graphite structure). Carbons fabricated from pyrolysis are typically derived from a polymer precursor. In this context "graphite" is referred to as carbon that has a perfect graphite structure (one that has no defects). A carbon that is graphitic would be considered one that has structure similar to graphite with orderly parallel basal planes. In comparison to graphite, a graphitic carbon display graphitic structure but will also have defects[145].

The nature of what makes a carbon graphitizing or non-graphitizing has been greatly debated. The IUPAC defines non-graphitic carbon as one that can be transformed into a graphitic carbon via high temperature (up to 3000 °C) only. This does not include other types of processing such high pressures and radiation damage. The X-ray crystallographer Dr. Rosalind Franklin (famous for her work in understanding many important molecular structures including that of DNA, RNA, and viruses) in 1951 that certain carbons were to be defined as non-graphitic carbons if they showed graphite like layers in small groups, but not over large areas. In contrast graphitic carbons are those that have the 3D graphite structure. Furthermore, if when a non-graphitic carbon is heated to between 1700 °C to 3000 °C shows that the small groups of graphitic parallel lines begins to align then this carbon can be considered a graphitizing carbon. If there is no alignment of this structure, then the carbon is a non-graphitizing[64]. Franklin stated that non-graphitizing carbons which are highly porous when at low temperatures (500 °C), when higher temperatures are reached the pores would remain. This was compared to graphitizing carbons which would have a compact form and would maintain their compact form during the additional heating. These pores are said to be on the scale of Ångstroms. She goes on to conclude that the non-graphitizing carbons have a rigid cross-linking (bonds between one polymer chain to another) of nuclei of neighboring molecules. This cross-linking are random orientations which prevents the necessary alignment. Not even at the higher temperatures (up to 3000 °C) would be enough to break these cross-links. Graphitizing carbons must then have much weaker cross-links which would

allow for more mobility. It has been speculated that these are sp^3 diamond bonds that have formed which would also explain why non-graphitizing carbons tend to be much harder than that of graphitic ones[145].

With the discovery of Fullerenes and then their related structures there was an advancement of the understanding of sp^2 structures. From this Harris suggested that non-graphitizing carbons may be fullerene-like in their structure[79]. Harris pointed out a flaw in Franklin's theory in that the cross-linking is not well defined and would have to be incredibly strong. This is further emphasized by how sp^3 bonds are unstable at high temperatures. For example, Diamond, which is purely sp^3 bonds, can be transformed into graphite at 1700 °C. Rosalind's incorrect theory may have come from the limitations of the equipment that she was using at the time. Fullerenes are very stable, their formation would inhibit the alignment of of the graphitic layers. Polymers that are graphitizable will have prolonged fusion phases which allow the carbon structure to re-arrange itself to a state of thermodynamic stability of graphite planes. When a polymer undergoes a cross-linking at 300-500 °C it will not undergo this prolonged fusion step which will prevent the re-arrangement of carbons[91, 69]. This can lead to the claim that graphitizability may be an innate property of certain precursors[160, 145, 64, 54, 91].

2.2.6 Amorphous Carbon

When a carbon allotrope contains little to no crystallinity and no long-term order it is known as amorphous carbon[129]. Amorphous Carbon is made of sp^2 and sp^3 bonds so can have short term order and be diamond like or graphite like in specific regions. There is even the possibility of sp^1 bonds[60]. Amorphous carbon will have dangling bonds[167] which allows it to be more reactive and form bonds with other elements. Amorphous carbon typically has properties that may be undesirable such as low electric and thermal conductivity. It is brittle

as well as hard and abrasion resistant. This can limit the applications for amorphous carbon. Most commonly it is simply an intermediate step to the fabrication of another carbon such as a synthetic graphite[145].

2.2.7 Glass-Like Carbon

A type of non-graphitizing or non-graphitizable carbon is called glass-like carbon. This occurs when a polymer undergoes pyrolysis and can maintain the original morphology (or shape) by passing through the plastic phase directly into carbon[89]. It is important to not confuse glass-like carbon with that of amorphous carbon. The major difference between the two is glass-like carbon lacks the dangling bonds of amorphous and glass-like carbon is made up of 2D structural elements[120]. Some other common names for glass-like carbon includes "Glassy" or "Vitreous" carbon, although these are trade names and the IUPAC recommended not to use them[129]. The name "glass-like carbon" comes from both its appearance and properties. When polished the appearance can be very reflective as well as it is very brittle. It must be noted that one of the reasons IUPAC recommends against its other common names is because it cause confusion in that glass-like carbon does not share characteristics with that of silicate glass[129]. Glass-like carbon contains properties of both ceramic and of graphite (there are small areas of graphite-like layers). This allows it to have a hardness of 6-7 Mohs' (for reference Diamond is the hardest at 10 Mohs' and graphite at 1 Moh)[41]. Additionally, when compared to graphite, glass-like carbon has a low gas permeability, on the order of 9-13 magnitudes[41]. Glass-like carbon has good electrical and thermal conductivity (although not quite as good as graphite). While many carbons are chemically inert, glass-like carbon's combination of low permeability and low porosity lends it to be even more inert.

A common challenge for many carbon products is their difficulty in machining. Allotropes

such as diamond are so hard that only other diamonds are used to cut them while graphite is very soft and will crumble if it is cut. This brings up a major advantage of glass-like carbon in that it can be fabricated from a polymer precursor. The advantage in the polymer precursor is that it can be patterned prior to carbonization. Some of the techniques used to pattern the polymer are described in more detail in section 2.6 such as those used in the integrated circuits (IC) industry such as photolithography to create nano- and micrometer scale patterns. When a patterned polymer is then pyrolyzed there will be some shrinkage because of the decomposition of non-carbon molecules out of the structure. This shrinkage tends to be isotropic (uniform shrinkage in every direction) and repeatable. This allows for tight dimensional tolerances to be maintained. Two major applications for glassy carbon include using them in high temperature furnaces as a crucible and in electrochemistry. The use in electrochemistry comes from the mentioned characteristics as well as a wide electrochemical window (the voltage range where the electrode is neither gains or losses an electron) and a low background noise (from the low surface roughness)[119].

2.3 Heteroatoms in Carbon

Many of the topics covered up until this point have focused mainly on pure carbon structures. To further affect the properties of carbon, defects can be added in the form of heteroatoms. This is known as doping which is when a carbon is replaced with a heteroatom (which is simply any non-carbon atom in the molecular structure). The presence of heteroatoms can be accomplished via two basic categories: in situ (where the fabrication process is part of the doping) or post treatment (already fabricated carbon structures are processed to be doped)[203, 56, 194, 187]. The additions of heteroatoms allows for further customization's in the carbon structures and properties such as with increasing the fiber strength for composite materials[98] or changing the electrical properties[96] so that graphene can be used as a

transistor[212, 162]. This can be done by making the material more conductive as an n-type (adding in more electrons)[20, 201] or more resistive. Function groups can also be attached to allow for specific chemical reactions such as oxygen reduction[34]. Some common heteroatoms in carbon can include nitrogen[71, 43, 166, 146], Boron [77, 32], or phosphorous [32].

One of the most common heteroatoms for carbon and one that is of focus of this work is nitrogen. When nitrogen bonds to carbon it can occur in various configurations. In Figure 2.3 there is a molecular diagram of a graphene sheet with various nitrogen heteroatoms and these common bonding configuration onto carbon. The energies in this figure (given as electron volts, eV) are the binding energies of the specific bonds[213]. When a Nitrogen molecule replaces the carbon in a hexagon of carbons it is known as graphitic-N or quaternary-N carbon. If the nitrogen is at the edge of a defect (unbound to another carbon) then it is known as a pyridinic nitrogen (pyridinic-N). The pyridinic-N will consist of the nitrogen having a single bond and double bond to each of its neighboring carbons. When the nitrogen will have a single bond with its neighboring carbons in a pentagon ring it is called a pyrrolic nitrogen (pyrrolic-N). The pyridinic-N and pyrrolic-N can also become oxidized (where an oxygen bonds to it). There is a variety of other ways nitrogen can bond to the carbon structure[143].

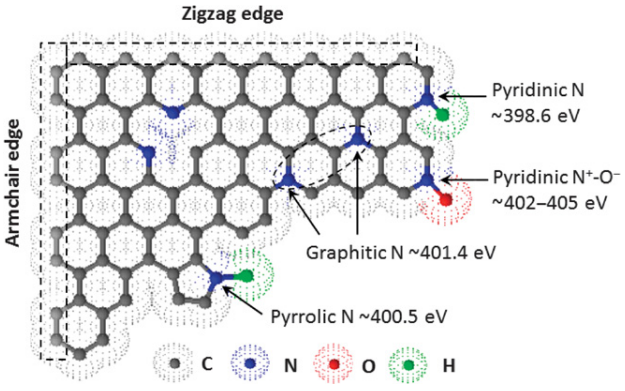

Figure 2.3: A molecular schematic of Carbon with various types of Heteroatoms. From Zhang et all[213]. Reprinted with permission from AAAS.

2.3.1 In Situ Insertion of Heteroatoms in Carbon

The fabrication process for nanocarbons can be slightly altered to include a source of heteroatoms during the formation. One possibility would be the addition of ammonia gas (NH_3) during the fabrication process which would cause the resulting carbon to have nitrogen heteroatoms. An example of this can be seen with the CVD process of graphene. When the hydrocarbon forming gas is added into the chamber (the source of carbon) then some NH_3 gas (the source of nitrogen) can be added in at the same time[193]. Alternatively if the arc discharge method is being used then the NH_3 gas can be added in as the buffer gas for the operation[109]. Laser ablation can also be performed in an NH_3 gas environment for the same results.

Pyrolysis temperature can be a factor in the remaining elements from the polymer precursor. During the pyrolysis process there are various temperatures that are need to be reached in order to decompose the different elements. The temperature required will depend on the specific precursor and the types of bonds. As the precursor is raised closer and closer to the required temperature the remaining non-carbon atoms will reduce. In Cowlard's initial work on glass-like carbon[41] he observed that when a precursor polymer containing up to 2% by weight of bromine, there would be a majority of the initial bromine left in the carbon structure even after pyrolysis (which was carried out up to 1800 °C). Furthermore, it has been shown that when various nitrogen containing polymers where pyrolyzed their remaining nitrogen drops accordingly. At a carbonization temperature of 600 °C there remained the same amount of nitrogen in both the precursor and resulting carbon. As the temperature increased there is a steep drop in Nitrogen to the point where by 1400 °C there is only 0.1 % nitrogen in the final carbon product[87].

2.3.2 Post Treatment Insertion of Heteroatoms in Carbon

Post treatment is an option to use when the carbon structure has already been fabricated. Some of the techniques include thermal, plasma, and hydrazine hydrate (N_2H_4) treatment[187]. It was noted that this style of nitrogen doping is more likely to produce the carbon-nitrogen bonds on the defects such that it produces a majority of pyridinic-N and pyrrolic-N (in comparison to graphitic-N). Most post treatment techniques have a downside where there is a chance of damaging the carbon structure more than the intended doping. The technique of thermal treatment is the process of heating the carbon structure to temperatures of 800 °C and exposing it to a nitrogen source such as NH_3 gas (it was noted by Wang et al [187] that N_2 gas could not be used as it may be too inert to react in this process). The heating can be done by either a furnace [68, 75] or via electrical joule heating of the carbon[201]. The technique of plasma treatment involves the placement of the carbon in a vacuum chamber. Plasma (ionized gas) is then generated from a gas such as N_2 or NH_3. This nitrogen containing plasma is then bombarded against the target which will dislodge some carbon molecules and replace them with nitrogen[164, 187]. Finally, the third technique for post treatment is N_2H_4 treatment. To fabricate graphene from graphene oxide N_2H_4 is used to reduce the graphene oxide into graphene. By adding some NH_3 into the N_2H_4 solution so when the graphene oxide is heated in an autoclave (temperatures ranging from 80-200 °C[114]) the nitrogen will dope the structure.

2.4 Carbon Precursors

Many forms of carbon production come from a variety of precursors that undergo a carbonization process such as pyrolysis. Aromatic hydrocarbons are commonly used, these will yield high levels of carbon. Alternatively, polymers can be used which will tend to have lower carbon yields because they have molecules with heavy weights (such as oxygen or

nitrogen) One of the oldest carbon precursors is cellulose which comes from plant matter such as wood. This has been seen throughout history as the production of charcoal. A list of various common carbon precursors was adapted from Pierson et al[145] and is shown on Table 2.1 with their common uses.

Table 2.1: Common carbon precursors

Precursor	Product	Reference
Methane	Pyrolytic graphite	[159, 50]
Hydrocarbons	Diamond-Like Carbon	[158]
Polyacrylonitrile (PAN)	Carbon Fibers, Electrochemical Electrodes	[98, 15]
poly(ethylene oxide) (PEO)	Nanofibers	[35]
Mesophase Pitch	Carbon Fibers	[126]
Phenolics	Carbon-Carbon	[145]
Furfuryl alcohol	Glass-Like Carbon	[161]
Petroleum fractions	Molded Graphites	[145]
Cellulose (Plants)	Charcoal	[5, 131]

Polyacrylonitrile(PAN, $(C_3H_3N)_n$) is one of the most common precursors used in the industry today for many carbon products from structural elements such as carbon fibers to graphitic carbons such as Toray®. The PAN polymer is inexpensive and can be fabricated into structures simply. One of the more common structures it is used in is in the form of nanofibers.

2.5 Electrospinning to Fabricate Nanofibers

As a fiber shrinks down from the macro, to micro, to nanometer level some interesting properties begin to reveal. This includes the surface area to volume fraction increases greatly, mechanical properties such as tensile strength and stiffness increase, and that there is an increase in the flexibility in surface functionalities[84]. There are many ways to obtain nanofiber such as drawing [140], phase separation [118], and electrospinning[84] among others.

Electrospinning

One technique to produce nanometer scale fibers and a focus of this thesis is electrospinning. This technique employs the use of an electric field to draw a thin fiber from a polymer solution (or polymer melt). The term electrospinning comes from the portmanteau of the words "electrostatic spinning". As early as the 1600 the English physicist William Gilbert (who some regard as the father of Electrical Engineering) was credited with his observation of how electrostatic forces would attract liquids[179]. By 1887 the English Physicist Sir Charles Vernon Boys published his observations on the basic concept of Electrospinning[25]. He observed that as fluid droplets reached the end of an insulating dish (because of the electrostatic pull of an electric field), nanofibers would be drawn out of the droplets.

Modern day electrospinning works on the same principle, a polymer flows through a conductive needle and is pulled via an electrostatic force toward a conductive target (of opposite charge of the needle) as seen in Figure 2.4a. An electrostatic force (also called Coulomb force) is one where stationary charges repel or attract based on like or dissimilar charges respectively. The orientation of the setup is typically done with the needle pointing vertically down towards the collector or horizontally across towards a collector. The polymer is spun against a target (also called a collector) which can have many forms from a flat plate, a rotating drum, or even a pre-patterned structure. Electrospinning is a simple technique to setup and to operate, all that is needed is a polymer reservoir, a "needle" (does not necessarily have to be a needle), and a target. The process can produce nanometer structures without even needing a vacuum to operate. The operating physics behind the operation on the other hand, can be complex as there are many forces and phenomenon in play.

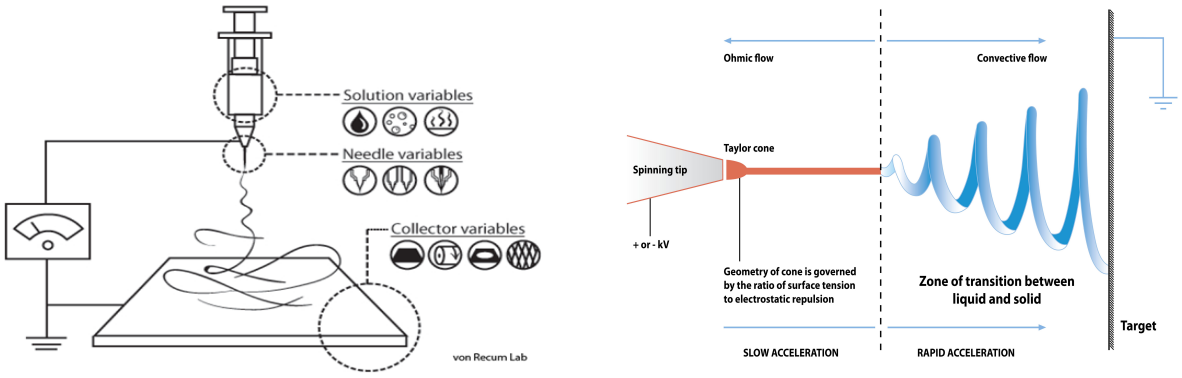

(a) **(b)**

Figure 2.4: A diagram of electrospinning. Images from Ref. [66].

Electrospinning Procedure

A polymer is first prepared by either melting (polymer melt) or dissolving it into a solvent to form a solution. This document will mostly focus electrospinning of a solution. A salt can be added into the polymer as necessary to increase the ionic conductivity (and thus increase the strength of the electrostatic force being pulled on the fiber). Additionally, the solution to be flowed does not have to be a polymer, there have been a wide variety of other substances used in electrospinning beyond polymers such as foods[116, 6], ceramics and semiconductors[108, 153], as well as other materials. It can be noted that the solution preparation is not always as simple as mixing a polymer with a solvent. Often for ceramic solution preparation an alkoxide precursor is used with a polymer as a binder and a sol gel that gets spun. The mat then undergoes a heat treatment to remove everything besides the ceramic[153]. An electrospinning solution can be filled with other additives as well such as carbon nanotubes[52], metals nanoparticles (such as gold and silver)[134], or many other substances to help modify the nanofibers properties as desired. When there are additives in the solution it is important to make sure that the additives are sufficiently dispersed as they may settle during the process.

Once the solution is prepared it can then be flowed (typically via a syringe) through a charged

needle. The needle typically sees a charge of around 5-30 kV[176, 120]). The opposing charge of the needle is attached to the collector. From this an electric field is generated which induces and electrostatic force to pull the fiber out. If the flow rate is too small, then there could be droplet formations (instead of a desired stream). Additionally, there may be Rayleigh instability affects, in that the surface tension will always try to minimize surface area (things move towards a state of less energy). This may be stronger than the viscous forces holding together the fluid stream. As such the stream would be torn apart into droplets. Depending on if the orientation of the needle is horizontal or vertical there could be the force of gravity acting with any electrostatic force (or perpendicular to it in the case of a horizontal orientation). As the electric field is applied to the fluid it will cause the polymer solution to accumulate ions on the surface. The charge of the ions depends on the charge being applied across the needle. Oppositely charged ions will accumulate on opposite sides of the fluid and the electrostatic force will begin to deform the fluid's meniscus layer on the tip of the needle. If the force becomes too large it will break apart the fluid into droplets which is known as electrospraying (this is a separate technique with its own applications)[88]. The breakdown happens more easily if the polymer has a lower molecular weight and viscosity. When the molecular weight is sufficiently high then the polymer chains could be entangled in such that they stretch rather than break. A method to control this breakdown between either electrospraying or -spinning could include adjusting the electric field strength (changing the voltage), changing the solution viscosity (such as with dilution), or changing the solutions ionic conductivity (as in addition of salts). The more salt added to the solution would make it easier for charge migration to occur.

As the fluid is deformed on the tip of the needle it forms what is known as a Taylor Cone[173, 207]. This happens because there is an accumulation of surface charges on the fluid droplet which start to repel and will cause the elongation and formation of the Taylor cone. A

critical voltage can be found by Equation 2.1[120, 174]:

$$V_c^2 = \left(\frac{2L}{h}\right)^2 (\ln\left(\frac{2h}{R}\right) - 1.5(0.117\pi RT) \tag{2.1}$$

Here the critical voltage, V_c, is the voltage needed so that the electrostatic forces overcome the surface tension of the polymer and create the cone. The critical voltage is a function of the distance between the charged needle and the opposite charged collector, L, the length of the needle, h, the radius of the needle, R, and the temperature, T.

Through the formation of a Taylor cone there is a significant reduction in cross section of the polymer stream down to a nanometer diameter. The cone's shape is determined by the solution's surface tension and the electrostatic force pulling on it. In Figure 2.5 there are an examples of a Taylor Cone formation. In Figure 2.5a there is a schematic representation of how the charge accumulation occurs on the surface of the fluid and forms the cone. The viscous force of the liquid is resisting the deformation while the electrostatic force causes the cone to form. In Figure 2.5b there is an image of a Taylor cone formation from Han et al[78]. The solution's properties (such as viscosity) and electric field (intensity and fluids ionic conductivity via salts) can be adjusted accordingly to create different shapes and thus different fiber diameters.

As the droplet is being formed by the electric field, the charges are accumulating at the tip of the Taylor cone causing the cross-section to rapidly decrease. Because of the decreasing cross-sectional area, the viscous force begin to shrink until the electrostatic force overcomes this causing the polymer to jet off towards the collector. Because of the large polymer chains of high molecular weight polymers, their entanglement will help prevent the polymer jet from breaking apart into a spray and will result in a continuous fiber [120].

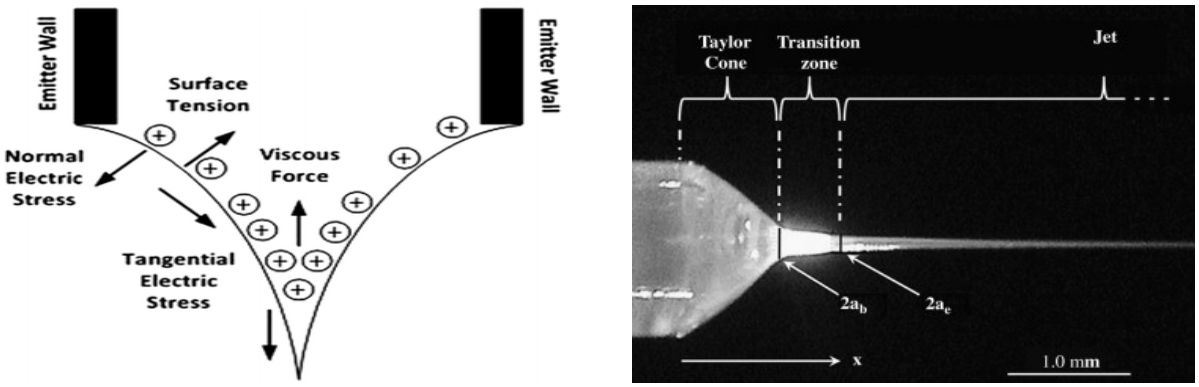

(a) **(b)**

Figure 2.5: A diagram of electrospinning Taylor Cone. (A) Reproduced from Ref. [198] with permission from the Royal Society of Chemistry. (B)Reproduced from Ref. [78] with permission from Elsevier.

As the jet forms, it will continue to elongate because of the charges that it carries[155]. These charges allow the jet to remain initially stable and flow in a straight line. As the jet flows in this straight line there will be a balancing of charges where the excess ions will move towards the edges of the jet, so the jet is at equilibrium. Given enough distance the polymer will solidify into a a nanofiber either by the evaporation of the solvent or the solidification of the polymer melt. As this happens the ionic charges are then frozen in place aligned along the surface of the polymer jet. The solidification plays an important factor in the final product. If solidification does not happen before the fiber reaches the target, then there may be merging fibers. It can be important to carefully optimize all the parameters so that uniform and continuous fibers are achieved.

The region of stability and the straight-line flow can be called the near-field region. If the collector is placed within this region then it is called near-field electrospinning (NFES). From this stability it becomes possible to have a fine control over the deposition of a single continuous fiber. If the collector is placed further away from the needle, then the polymer jet will enter an unstable region. This is the far-field region and is used to create nonwoven mats of a continuous nanofiber. As such this style of electrospinning is referred to as far-field electrospinning (FFES).

In the unstable region there is a variety of forces that will act on the polymer jet to cause it to undergo a whipping motion. The electric field caused all the ions to be aligned on the outer surface of the polymer jet. These ions, now frozen in place because of polymer solidification, will have an electrostatic repulsive force since they are all the same polarity. As such a whipping affect will occur causing a rapid acceleration and a mechanical pulling on the fiber (thus further shrinking the fiber diameter). All of this happens while the fiber is being pulled by the electrostatic force towards the collector. In addition to the electric field and surface charge related forces there are other forces on the fiber as summed up by Madou et al[120]. These are gravitational, viscoelastic, surface tension, and frictional forces. The force of gravity can have a different affect depending on the orientation of the needle (horizontal and thus perpendicular to gravity or vertically down and thus in the direction of gravity). This gravitational force is affected by the fluids density. The viscoelastic force is that of the fluid trying to resist being pulled apart which is a product of the solutions components. Additional to viscoelastic force there is also surface tension forces at play holding the polymer jet together. This force is affected by both the same solution properties as the viscoelastic force, as well as the possibility for additives to be used such as surfactants which could affect the surface energy of the solution. The final force mentioned is that of frictional forces that are a result of the fluid flowing through the environment.

As mentioned above there are many materials that can be used for electrospinning into nanofiber mats. For the context of this work the ones that are generally of interest are those which are carbonizable. Once the polymer nanofiber mat has been fabricated it can then be pyrolyzed to create a carbon nanofiber mat (CNF). This CNF mat can be used on it's own as something such as water filtration [150, 74] or an electrode [148]. Or the CNF can be spun over a preexisting structure to form something such as a membrane [53] or even a single fiber as a gas sensor[215].

Far-Field Electrospinning (FFES)

In its simplest form far-field electrospinning is a charged needle jetting a polymer towards an oppositely charged collector. As described above the polymer will chaotically whip around to create a random pattern on the collector. This will create a mat of a continuous nanofiber. A distinction to make is that this is not a textile or fabric as there is no interweaving of nanofibers (and thus why it is called nonwoven). The mat will tend to be of consistent thickness for as the nanofibers accumulate on the target they will cover the collector and thus the localized electric field will be weaker compared to an uncovered area. As the process continues the fiber will tend to accumulate on the areas of lowest thickness.

The collector has up until now not been described in too much details. A common style is simply a flat sheet of conductive material in a simple shape such as a copper square or silicon wafer. Depending on the final goal, the nanofibers may want to be removed from the collector or remain. If there is sufficient distance for the polymer to fully solidify then there may not be any stiction between the nanofiber mat and the collector and it can simply be peeled off. Alternatively, the collector may be wrapped in a thin layer of foil or wax paper (such as parafilm®) in order assist in ease of removal.

Additional forms of collectors can be used to create a wide range of end results. When the collector is a solid flat plate the nanofiber mat will be a solid flat mat with random orientation. Alternatively, a solid rotating drum[128] could provide a more uniform mat, although it may increase the chance of a fiber breakage. This would result in randomly oriented fiber unless the speed of the rotating drum is increased then the fibers can align[30]. To gain further alignment in the fibers the collector could be made from two plates[95, 108]. In this setup the nanofibers will deposit on the plates and across the gap between the plates. If the plates are parallel, then the fibers will mostly be perpendicular to the two plates. The basic principle is the fiber will deposit onto the conductive collector and reach across

to other collectors (or typically anything conductive in the vicinity). Figure 2.6a shows a schematic of the electrospinning setup depositing across two plates. The fibers will align perpendicularly across the plates as seen in Figure 2.6b. Here the target collector was made of four parallel plates, this can be seen by the thick grey bars and the aligned fibers span between them. The end result can be compared in Figure 2.7a which is a carbon nanofiber mat deposited on a solid plate while Figure 2.7b shows aligned fibers. Additional collector setups have been described by Li et al [108].

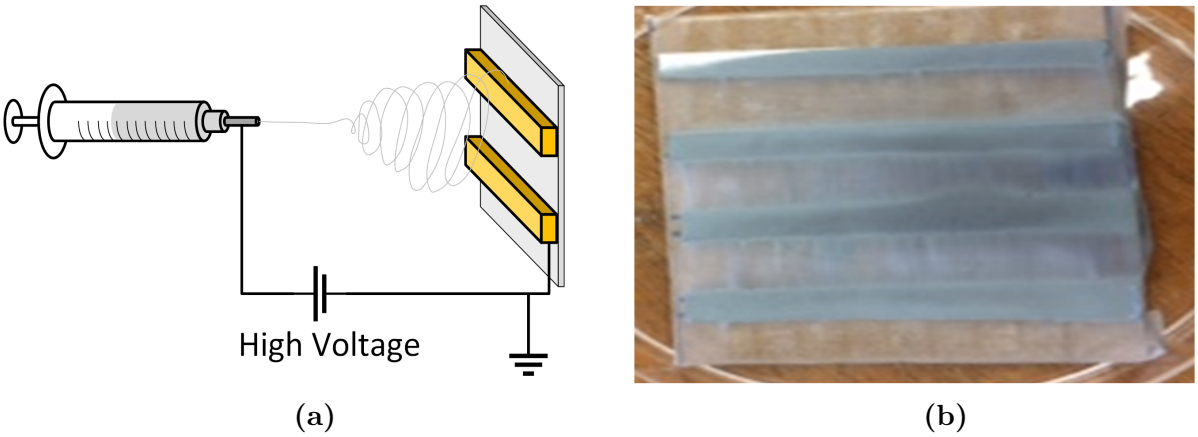

Figure 2.6: A diagram of electrospinning over parallel plates (A) a schematic representation of 2 plates and (B) a finished mat from 4 parallel plates.

Manipulations of the electric field can also be incorporated. A conducting wire can be laid across the collector such as a rotating drum[128] or placed behind the collector in a specific pattern[176]. Needles or targets with sharp points can be used which will concentrate the electric field to single points[175]. Charged electrodes (with the same charge of the needle) can be placed around the path of the spinning to change the electric field[175, 48].

Near-field Electrospinning (NFES)

When the collector is placed inside the stable or near-field region of the polymer jet then it becomes the process of near-field electrospinning (NFES). This style of electrospinning can occur at lower voltages to further reduce any instabilities. The process allows for precise

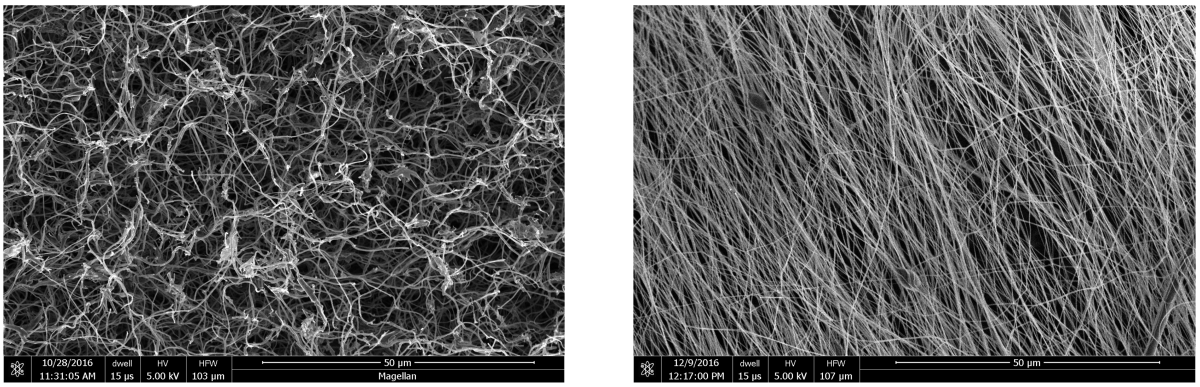

(a) **(b)**

Figure 2.7: SEM images of carbon (A) randomly oriented fibers and (B) fibers aligned via parallel plates

control of the individual fiber. It was first introduced by Sun et al[170] in 2006 as a method which took advantage of the linear and stable regions so that controls of the fiber could be precise and predictable. This precision allows for a direct patterning of the fiber where the needle can move in a plane parallel to that of the collector. In this way NFES can act such as a printer and on a standard movable stage. The resolution can be limited to that of how fine the stage can move (which potential is in the order of nanometers). Beyond the typical setup, there is the Atomic Force Microscopy (AFM) electrospinning that can be used for a process known as nanoelectrospinning[199].

In FFES the the nanofiber is self-initiated, where the electrostatic forces are enough to overcome the surface tension of the fluid. In contrast this may not always be the case for NFES when at the lower voltages. There needs to be an initiation method, for once the fiber has started to spin it will continue to. One popular strategy is via a mechanically initiation where something is used to touch the fluid droplet form the needle and connect it to the collector. This could be done by physically moving the needle towards the collector until it initiates and then backing it up to the desired location. This can be dangerous as arcing might occur if you get too close at such a high voltage. Alternatively, a rod can be used to agitate the droplet and bring the first fiber to the target. There is currently work at the

UCI BioMEMS lab in electrostatic initiation via a glass rod where it brings a localized field to start the spinning process which would be contact free.

Electromechanical Spinning (EMS)

One of the downsides of NFES is that while the jet remains stable because it is in the linear region, the fiber will not undergo the mechanical stretching from the whipping motion of the far-field regime. As such the fibers tend to be larger in diameter when compared to ones fabricated from FFES. One solution is to incorporate a mechanical aspect the NFES setup to stretch and thin out the fibers into the nanometer scale. This process is known as electromechanical spinning (EMS)[31]. This technique can operate at lower voltages which helps to reduce electrostatic instabilities and make the deposition more controlled.

2.6 Carbon Manufacturing

Carbon can be very difficult to pattern since it tends to be brittle (such as with glass-like carbon) or very soft (such as with graphite). Traditional manufacturing techniques such as cutting or milling do not work well. This section reviews some of the basic concepts of ways to pattern.

Carbon Microelectromechanical Systems (C-MEMS)

Carbon Microelectromechanical Systems (C-MEMS) are a subsection of the Microelectromechanical Systems (MEMS) category. MEMS are microdevices that merge mechanical features such as movement with electrical. Some of the most common products of this category include microphones and inertial navigation units (gyroscopes and accelerates). In the case

of a microphone there will be a diaphragm that vibrates with the inputted sound. This vibration is then transduced into an electrical signal which can be amplified as sound on a speaker. In terms of an inertial navigation unit there can be micro features that vibrate and as inertial changes are felt (such as accelerations or rotations) which causes vibration changes. This vibration is transduced into electrical signals that can be read to determined what the change in inertia was. Their fabrication procedures were originally derived from the Integrated Circuit (IC) Industry.

2.6.1 Photolithography

One of the most common micro/nanofabrication techniques is the use of light to pattern a photosensitive polymer in what is known as photolithography. A simplified process overview can be seen in Figure 2.8. Here a polymer is deposited to a uniform thickness. A mask is placed on the polymer so that it will selectively block ultraviolet (UV) light from affecting the polymer under it. The polymer is developed to reveal a patterned structure.

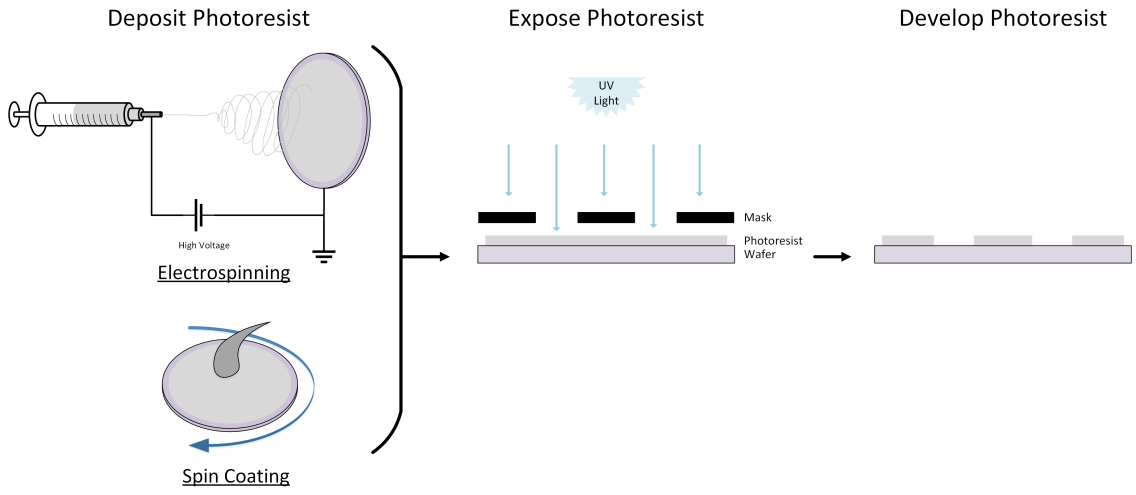

Figure 2.8: Photolithography diagram, the photoresist is first deposited using a techniques such as electrospinning or spin coating. A mask is then used to selectively expose the photoresist into a desired pattern (note that the example in this Figure is for a negative photoresist). Finally the photoresist is developed to leave behind only the desired structures

For the first step of photolithography a polymer material is deposited onto a substrate (such as a silicon wafer). A common technique is called spin coating, although electrospinning can also be used[165]. In spin coating a polymer is dispensed onto the substrate, they are then spun around at specific RPM. This will distribute it uniformly across the surface. The speed of rotation along with the known viscosity of the polymer solution will determine the thickness coated. This polymer is known as a photoresist.

The next step is to pattern the photoresist. This is done with a photo mask. Depending on the size of the features needed the mask can be expensive, made from a chrome plated fused quartz substrate, to the very economical polymer transparency that was laser printed. The goal of the mask is to selectively block UV light. The mask is placed above the photoresist and then exposed to UV light. The photoresist type would determine the mask layout. When exposed to UV light a positive photoresist will experience polymer scission while a negative photoresist will experience polymer cross-linking. After the photoresist is exposed it is developed to remove any undesirable areas. In the case of a positive resist the areas that experiences scission will dissolve more easily while the areas that experienced cross-linking in a negative resist will remain.

At this point the patterned photoresist can act as either a mask or the structure itself. In traditional IC fabrication the photoresist can be used as a mask for selective doping. Here the silicon wafer would be placed in a furnace and exposed to typically either boron (P-type) or phosphorous (N-type) to selectively give the silicon substrate more holes or electrons respectively. The photoresist can then be removed. In MEMS devices the photoresist can act as a mask for etching where the structure under the mask selectively removed. In C-MEMS this photoresist layer can become the basis of the structure itself. The photoresist is the precursor polymer that after being patterned can then be pyrolyzed into a carbon structure. During this process there is a loss of mass and shrinking of the structure occur.

2.6.2 Nanoimprint Lithography

An alternative technique for micro- and nanopatterning is Nanoimprint lithography (NIL)[37]. In this technique a material (typically a polymer) is imprinted with a nanoscale mold (also called a stamp or template). This will produce nanoscale patterns with dimensions down to the 25 nanometer range[37].

A polymer is deposited onto a substrate typically with spin coating (or possibly electrospinning). The mold is then pressed down on the polymer to deform the it. During the molding process the polymer can be cross-linked or stabilized via UV light through a transparent mold[144] or via heating of the mold and polymer[94]. The heating of the polymer could allow the polymer to deform more easily. With the patterned polymer additional fabrication steps can be completed. The imprinting will typically not completely remove the polymer material but rather create a difference in height between features. One common technique to isolate the patterns is to etch via reactive ion etching (RIE)[94]. This will etch all the surfaces equally, thus it can be stopped once the etching reaches the substrate on the low portions. Figure 2.9 demonstrates schematically a typical process of NIL. Once the structures have been patterned they can then be pyrolyzed to produce a finished nanometer scale patterned carbon structure.

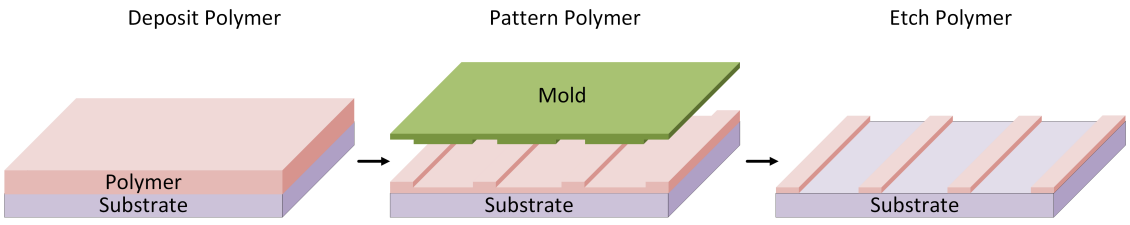

Figure 2.9: Nanoimprint lithography procedures. A polymer is deposited onto a substrate. A mold then can imprint a desired pattern. Finally etching can be used to remove thin sections of the patterned polymer allowing for isolated features.

There are many advantages to NIL such as such as nanometer resolution, excellent aspect ratios (can pattern vertical walls), low costs, and high throughput. Even larger throughput

can be achieved with techniques such as Roller NIL[171]. Here there is a mold in the shape of a cylinder (or roller) that can be pressed against the polymer to imprint the pattern continuously. This would allow for a continuous manufacturing process. Additionally, NIL allows for nanoscale features on a wider range of materials rather than simply photosensitive ones as seen in photolithography. As such many carbon precursors, such as PAN[217], can be patterned in this manner and then pyrolyzed. Some additional considerations for NIL include the polymer deformation when it is imprinted. The polymer will be compressed and pushed to the side. There may raised edges as well to accommodate incomprehensibility. The fabrication of the mold must also be considered. Here it is necessary to make a mold that has nanoscale features and can ideally withstand multiple uses. This can be done with photolithography where a photoresist is patterned to form a mask against an etching process (such as RIE). The mold can be made from many materials such as silicon or aluminum.

2.7 Techniques For Carbon Characterization

Once the carbon has been fabricated it must then be characterized to understand its properties. There are a wide variety of techniques that can be used Each technique can provide different information and have value in their uses. A few techniques are described here that were used in this work. The main considerations in choosing these techniques was the property of interest for examination as well as the availability of the equipment.

2.7.1 Electron Microscopy

The ability to look at the very small structures is very useful when studying microstructures. Optical microscopy has been a reliable technique in the sciences since the early 1600's. This technique uses visible light to illuminate a sample and an optical lens to focus the light.

Through the years there have been many improvements, but the practical limit can see a resolution down to 200 nm and magnifications of around 2,000 times. To be able to examine smaller structures it is possible to replace the illumination source from visible light to electrons. This is the foundation of electron microscopy which can produce images as great as 10 million times and has a resolution in the Ångstrom scale.

Electron microscopes will have a high voltage across a filament such as tungsten. This is the source of electrons (known as primary electrons). The high voltage will cause the electrons to break away from the filament and where they then can be focused with electromagnetic lenses (in lieu of optical lens) towards a target. This operation must be performed inside of a vacuum environment as even oxygen molecules could cause collisions with the electrons. What happens when the electron reaches its target depends on the style of microscopy that is being performed. In Scanning Electron Microscopy (SEM) the electron is scattered off the surface of the sample as it is rastered across. Alternatively, the electron can pass through the sample (which must be very thin) in what is known as Transmission Electron Microscopy (TEM).

Scanning Electron Microscopy

Scanning Electron Microscopy produces images by using accelerated electrons to scan across a sample's surface. When the electrons hit the surface, they will produce many signals as the electrons interact with the atoms of the sample. Typically, the main image is produced by the release of secondary electrons from the sample. These electrons will have different energy levels depending on the height where they hit the sample. This can translate into different intensities in the image. An image from a SEM is grey-scale for this reason, but artificial coloring for contrast purposes or for artistic reasons can be added over the image. Imaging from SEM can have a resolution down to 0.5 nm. Typically, SEM is considered a non-destructive technique as the primary electrons will only interact with the surface of the

sample (typically only nanometers deep). One of the primary features SEM is used for is of the sample's topology. A consideration for SEM is the sample being examined must be electrically conductive. If an insulating sample is used, then the primary electrons will begin to accumulate on the sample which would affect the next incoming electrons. To solve this nonconducting samples are often coated with nanometer thick layer of metal.

Transmission Electron Microscopy (TEM)

Transmission Electron Microscopy (TEM) produces the data by using the accelerated electrons to pass through a sample. This is the original form of electron microscopy that has been used since 1931. The electron beam will pass through the sample onto a collector on the far side. As the electron interacts with the sample it will change the energy of that electron. This allows the TEM to show images of phases and crystal structures. Because of the need for an electron to pass through the sample it requires the sample to be extremely thin, typically no larger than 100 nm. As such sample preparation can be more difficult than that of SEM. For TEM the sample must be sliced thin or ground up into a nanoscale powder. Additionally, TEM samples must also be conductive for the same reasons as SEM samples. A nanometer metal coating can be applied in the same manner.

2.7.2 Raman Spectroscopy

To examine the crystallinity of a structure the technique of Raman spectroscopy can be used. Raman spectroscopy is named after the Indian physicist Sir C.V. Raman who won the Nobel prize in physics for his contributions towards the understanding of molecular scattering of light. As light enters a transparent material there are some photons which will have their wavelength change in a phenomenon known as Raman Scattering [152, 151]. When photons are scattered by a molecule or atom a phenomenon known as Rayleigh Scattering occurs

where there is a conservation of kinetic energy of these photons (elastic scattering). This means the photon will maintain the same frequency and wavelengths. Raman Scattering is the observation that a small percent of the photons will scatter inelastically, in that their frequency and wavelength will be different. This inelastic change comes from a transference of energy from photons and molecular vibrations[183].

When using a known incident photon source, the scattering information of the inelastic photons can be used to decipher the molecular structure of what the photons scattered off of. This is the basis for the technique of Raman spectroscopy. It has become an extremely versatile technique that can be used with almost no sample preparation[183]. Simply place the sample under a target, shine a laser to excite the sample, and measure the resultant photons for their wavelength. The results of Raman spectroscopy are then measured by what is known as a Raman shift (expressed in cm^{-1}) and Intensity (expressed as an arbitrary unit, a.u.). The units here are arbitrary because it is compared against itself. The Raman shift is defined as the difference between the scattered light and incident light [183].

Raman spectroscopy is well suited for the study of graphene and graphene related materials[59]. When graphene is excited there are lattice vibrations (a phonon which is the quantum of vibrational energy) from the stacked layers of graphene. These vibrations are sensitive to any sort of defects in the graphene structure[21]. The various vibrational information is broken down into different bands. At around 1500-1630 cm^{-1} there is the G-band[60] which is the vibrations of the first order Raman mode. This is activated by the sp^2 bonds of the pure graphene[14]. While this band will be present in any carbon with sp^2 bonds, the shape of it will depend on the quality of the samples[92].

At around 1300-1400 cm^{-1} there is the D band (for "Defect" or "Disorder"[21, 121]). This band will excite when there is a defect in the structure. Causes of these defects can come from a variety of areas such as sp^3 bonds. These defects are adding disorder to the system and moving the carbon away from a graphitic structure towards that of an amorphous one.

The height of the D and G peaks are (I_D and I_G respectively) often compared and used to determine the level of order or graphitization of a carbon. As such the ratio I_D/I_G approaches 0 as it becomes more graphitic[59, 21]. To see these peaks the Raman data can then be fitted via techniques such as Lorentzian distribution[123]. When the laser excited the material, it is only exciting the surface atoms which makes Raman a surface technique. This will not give any information about the bulk of a material.

2.7.3 X-ray Photoelectron Spectroscopy

While Raman spectroscopy is a very powerful technique, it is not perfect. As mentioned, the D band will get excited because of a defect, this can still leave the question of what the defect is. A technique known as X-ray Photoelectric Spectroscopy (XPS) is widely used a compliment with Raman as a means to determine the elemental composition of a sample. The foundations of XPS are based on the excitation of photoelectrons from a material by the excitation of photons (as explained by Einstein[55]). The process occurs when a portion of a material is irradiated by a X-ray beam. This process causes electrons to be emitted which can then be measured in their quantity and energy. Much like Raman, XPS is also limited to the surface of a sample (0-10 nm). Because of this small layer of irradiation this technique is considered non-destructive. Unlike Raman though, XPS requires a more complicated setup. Typically XPS is performed in a high or ultra-high vacuum (10^{-8} to 10^{-9} millibar respectively) environment, although there have been some recent advances towards ambient pressure XPS [57]. The information obtained from XPS can not only give the user what elements are present but potentially what type of chemical bonds are present as well. When the XPS experiment is run the data is typically plotted with intensity as an arbitrary unit (this is the number of electrons) versus the binding energy of those electrons in eV (electron volts, 1.6×10^{-19} J). The binding energy is the amount of energy holding molecules together. This is a characteristic of the various elements and correspond to the electron

configuration. For the purposed of this work we tend to be most interested in the levels of carbon, nitrogen, and oxygen in our carbon samples. In carbon the XPS can provide information about heteroatoms. They can be identified with their bonding nature such as if a nitrogen is pyridinic, pyrrolic, or graphitic[117, 193].

2.7.4 Conductivity Measurements

Surface conductivity is the measurement of the ease of electron's ability to move through the material. For more graphitic materials it would be expected that the conductivity would be high compared to a more amorphous sample. In electronics the resistance (which is the inverse of the conductivity) of something can be measured with a multimeter. A voltage is sent though the material and the drop in voltage that occurs can then be calculated as caused as the resistance. Unfortunately, this does not work well at very low resistivity and as such a different technique is needed. One such technique to measure the surface resistance of a material is known as four-terminal sensing. Here two pairs of probes (all spaced out to a known distance) are touched to a surface. In one pair a fixed current, I, is applied. The other set of probes measures the voltage, V. Ohm's law ($V = IR$) can then be used to solve for the resistance, R.

Chapter 3

Carbon Nanofiber Fabrication via Electrospinning

Carbon nanofibers were produced through electrospinning and pyrolysis to create nanofiber mats. The procedure used to fabricate the carbon nanofiber (CNF) mats are described in Figure 3.1. Here there is the breakdown of the four processes involved to fabricate the mats. The first step is the solution preparation (Figure 3.1A), where the three components are combined and thoroughly mixed. The solution is then electrospun onto a drum (Figure 3.1B) to make a polymer nanofiber mat. This mat undergoes mechanical treatment and stabilization (Figure 3.1C) to prepare it for pyrolysis. Finally, the nanofiber mat is decomposed into carbon via pyrolysis in a tube furnace that is purged of air with flowing nitrogen gas (Figure 3.1D).

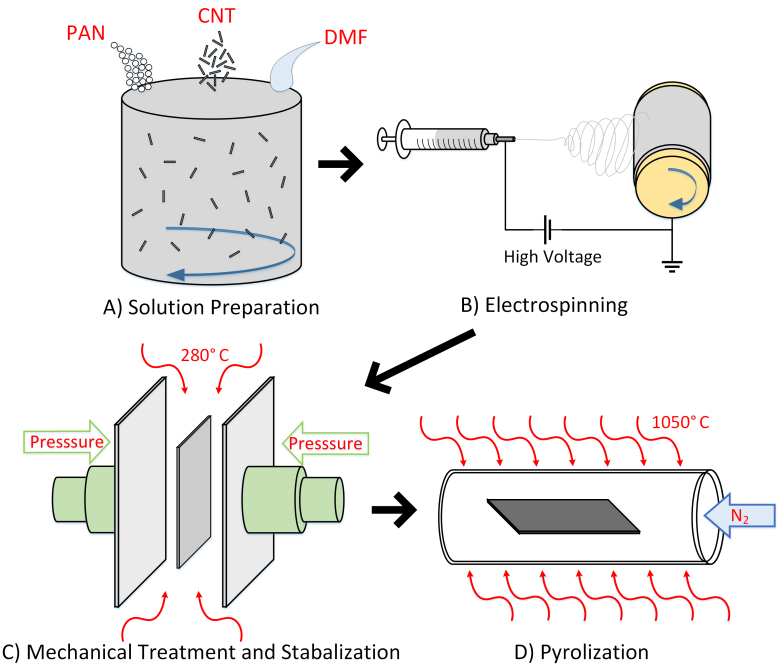

Figure 3.1: Fabrication schematic for CNF mats. The process is broken into four steps: (A) solution preparation, (B) electrospinning, (C) mechanical treatment and stabilization, and (D) pyrolysis.

3.1 Carbon Nanofiber (CNF) Mat Preparations

3.2 Solution Preparation

For electrospinning a solution was prepared with Polyacrylonitrile (PAN) dissolved in the organic solvent dimethylformamide (DMF) with mixed in Multi-walled carbon nanotubes (MWCNT). The final ratio of this of the nanofibers will be 8% PAN and 1% MWCNT's. To create this solution the MWCNT's and DMF are first mixed and placed under ultrasonication for 1 hour which will evenly disperse the MWCNT's. Afterwards, this solution can mix at room temperature for 24 hours on a stir plate. The PAN is then mixed with the MWCNT and DMF solution to create a mixture that is 8% PAN by weight and 1% MWCNT-DMF solution by volume. This new solution is then placed on a hotplate while stirring to be heated to 40 °C for a minimum of 24 hours. The solution can remain on the hotplate for

several days although it is always best to use a freshly prepared solution. At all mixing steps the container should be sealed tightly and wrapped with Parafilm® to help prevent contamination's (such as during ultrasonication) and evaporation.

3.3 Far-Field Electrospinning

Once the solution is prepared it can then be spun into the nanofiber mats via electrospinning. It is important begin electrospinning the solution as soon as possible after it has been taken off the hot plate/stir plate to prevent the MWCNT's from settling. In the electrospinning setup a rotating drum was used as the target to be spun on. The drum has a diameter of 63.6 mm and a width of 37.5 mm. The drum is wrapped in a conductive metal such as copper or aluminum foil. The foil should be as smooth as possible to ease with pulling the finished nanofiber mat off and to help keep the nanofiber mat itself as even and smooth as possible. The drum is grounded to the electrical source (this can usually be done with a wire brush) and is spun at approximately 120 RPM as measured by a laser tachometer prior to spinning. The solution is loaded into a syringe with a flat metal needle of 21 gauge (0.02025 inch inner diameter). The syringe is loaded with the solution and placed on a syringe pump to dispense the solution at a rate of 0.25 mL/hr.

The power source is set to 16 kV and this potential is applied with the positive on the needle and the negative on the target. Electrospinning occurs for 1-2 hours (and consumes about 1 mL of solution) which will typically result in a mat with a thickness of about 100 μm and have individual fiber thickness of about 100-300 nm. The thickness can be controlled by increasing or decreasing the time of spinning. The nanofiber mat will be very electrically charged and is best handled with anti-static tools such as alumina tipped tweezers. The color of the as spun mats will tend to range from white if it is pure PAN to a grey if there are MWCNT's mixed in. When the mats are removed off the drum they will be in a cylindrical

shape. They can be cut once across the width so that they can be laid flat without any part overlapping. In Figure 3.2 there is an image of a CNF mat using a laser confocal microscope. The confocal image was taken on a Keyence VK-X250 Laser Confocal Microscope.

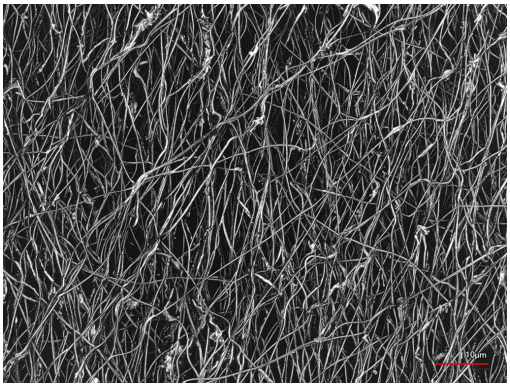

Figure 3.2: Laser confocal image of the CNF mat. The scale bar is 10 μm.

3.4 Mechanical Treatment and Stabilization

Prior to stabilization of the nanofiber mats they are compressed in a laminator to impart mechanical stress as well as surface uniformity. A single sheet of A4 Paper is folded in half and a plastic laminate is used to coat the paper to protect the nanofiber mats from sticking to it. The mat is placed in the paper and the paper is folded to enclose the mat on both sides. The paper is loaded into the laminator to compress and flatten it. That mat is rolled 4-5 times.

The now flattened nanofiber mat is loaded into a compressive device to be stabilized in the oven. The compressive rig typically entails two flat plates made of a material that can withstand the 280 °C such as stainless steel. An example is seen in 3.3 where the sample is loaded in the clamp and torqued to 4 in-lbs. Silicon wafers were not be used as the nanofiber mat will stick to it during compression. The plates are always cleaned with isopropyl alcohol (IPA) and blown dry (preferably by clean N_2 gas). The mats are loaded into the rig where compressed to the desired compression level with a torque wrench and torquing the clamp

to 4 in-lbs which is about 20kPa of pressure. While under pressure the rig loaded with the nanofiber mat is loaded into the oven which is at room temperature. The oven temperature is raised to 280 °C and let to dwell at there for 5 hours. The oven is then shutoff and allowed to cool naturally. This process is open to atmosphere during the heating as the PAN nanofiber mat needs oxygen to stabilize. The mats should be brown in color. If they were stabilized in the absence of oxygen they may have a yellow color until they oxidize to brown.

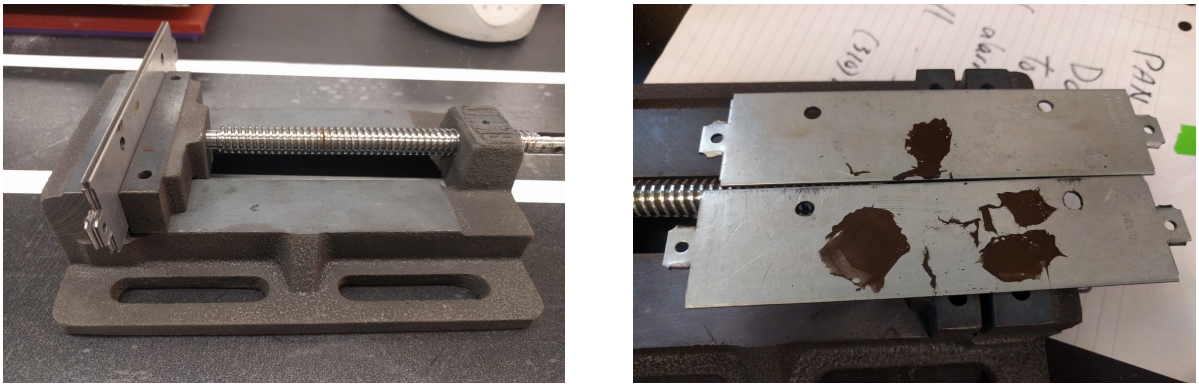

(a) **(b)**

Figure 3.3: A mechanical stabilization device: (b) Device is compressing the mats and is ready to be stabilized, (b) The steel plates are opened to show the stabilized nanofiber mat.

3.5 Pyrolysis

The nanofiber mats are now ready to undergo pyrolysis and become a carbon nanofiber (CNF) mats. The stabilized polymer mats are loaded into a tube furnace. The samples in the furnace will sit at room temperature while nitrogen gas (N_2) is flowing through it. This is done in order to purge the furnace of any oxygen content. The gas is flowing at a rate of 9000 sccm (standard cubic centimeter per minute). This rate is maintained for the entire duration of the pyrolysis. The nanofiber mats are stored inside alumina crucibles for the pyrolysis process. Care should be taken to avoid the mats from being blown away by the flowing N_2 and the exhaust port it flows into as the mats are very light and easy to lose when loading. It is recommended to leave the samples purging in the furnace for a minimum

of 8 hours. After an 8 hour purge the oxygen content in the furnace has been measured at 20 ppm.

For pyrolysis it is important to follow a strict temperature profile as that will help determine the final carbon structure. The temperature is ramped from room temperature to 300 °C at a rate of 4.5 °C/min. The furnace will remain at 300 °C for 1 hour. The temperature will then raise to 1050°C at a rate of 2.5 °C/min. This temperature will remain at 1050 °C for 1 hour until which the heat is turned off and the furnace is allowed to cool to ambient temperature naturally. An example of a tube furnace in the midst of a pyrolysis run can be seen in 3.4A. The temperature profile is plotted in Figure 3.4B. Once the pyrolysis is complete and the furnace cools down then the PAN nanofiber mats are now carbon and are ready to use.

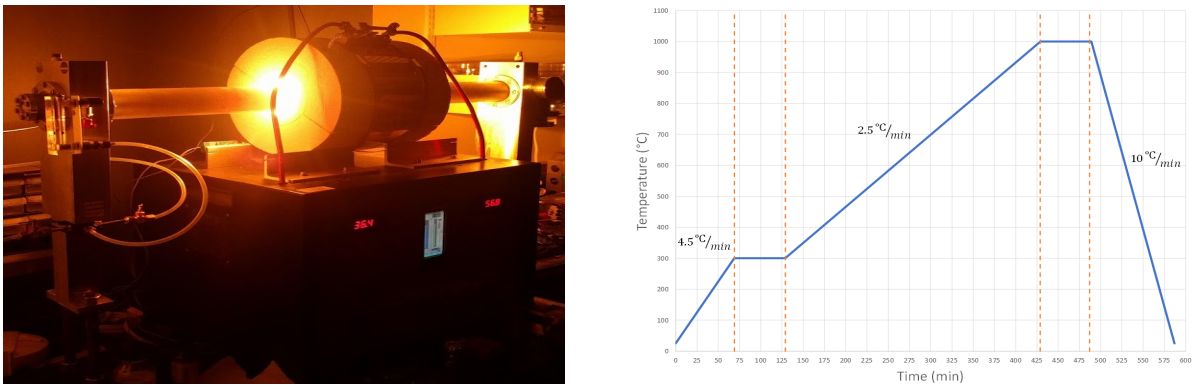

(a) **(b)**

Figure 3.4: (a) tube furnace during pyrolysis and a (b)typical temperature profile of a pyrolysis run .

Alternative Carbon Nanofiber mats

The fabrication process for the carbon nanofiber mats describes the final desired product. In order to validate the fabrication process a variety of samples were made to use as controls. There are many variables that could be adjusted in terms of every step. The chemistry could be modified for the solution in a number of ways. The electrospinning setup could

have been varied in factors such as voltage, collector style, spinning environment as well as other parameter changes. During the mechanical treatment and stabilization there could be modifications to ramp rates and amount and style of stress induced on the sample. Finally, during pyrolysis there could have been modifications to areas such as the inert gas being used and ramp rates.

For this manuscript the focus was on the fabrication process and how that led to graphitization and heteroatoms. As such the variables that were modified were the addition of CNT's as well as the effect of mechanical stress. For this reason, the control samples that were tested included using a pure PAN sample (no CNT's were added) that did not undergo any mechanical stress during stabilization. This sample is referred to as PAN CNF. A sample that had CNT's added to the PAN solution but underwent no mechanical stress during stabilization is called PAN-CNT CNF. A sample that pure PAN (no CNT addition) but did go under mechanical stress during stabilization is known as PAN-M CNF. And finally the sample that had both the addition of CNT's and underwent mechanical stress during stabilization is known as PAN-CNT-M CNF.

Chapter 4

Method for Carbon Nanofiber Fabrication

4.1 Preparation for Electrochemical Testing

The Carbon nanofiber mats (CNF) come out of the furnace ready to use and can be characterized as desired. The CNF mat in this context is also referred to as an electrode. Technically, electrochemical tests can be conducted on the bare CNF material as is. Though there are some considerations which would make electrochemical testing easier. The CNF mats are extremely fragile and will break very easily from many forces such as a stray breeze (as one might expect in a fume hood) or even breaking when it is unable to penetrate the surface tension of a liquid electrolyte. In initial electrochemical tests a CNF mat was simply attached via metal alligator clips and then dipped into the solution for testing. Some further issues that would present are the piercing of the CNF mat to the point of breaking it. Furthermore, there are issues where when running a CV there was an unexpected peak. When examined this peak matched that of the copper reduction, as in the metal clip and/or the

wore were coming in contact with the solution. Additionally, corrosion can be seen on the clip which deteriorates the signal. This corrosion can sometimes be seen in both the solution and the CNF (Such as with reddish-brown colored substance).

4.1.1 Coating the Contact Point of CNF Mat

A solution to contamination and CNF mat weakness would be to coat the contact area. Then the metal clips can pierce through the coating which should in theory protect the clips from any solution that may creep up from capillary forces as well as help reinforce the CNF mat from breaking. One issue with dip coating the CNF mat into a coating such as wax is controlling the area being coated. The CNF mats seem to show an extreme hydrophilicity. This was demonstrated with a contact angle testing. In this setup a droplet was placed on the mat and viewed on a high-speed camera. In theory there should be a droplet with a visible contact angle that is measured via the camera. In the case of the CNF mat the droplet was absorbed almost instantaneously (at least faster than the camera could see). While it may not be true hydrophilicity in the technical term, the highly porous mat absorbed the water. When coating the CNF mat with a liquid that will solidify this same absorption issue is seen. It is critical to prevent the coating liquid from creeping too far into what would be expected to be the working area of the electrode. With a wax coating it can be seen via a white wax color but some other coating's such as a Polytetrafluoroethylene (PTFE, common trade name is Teflon®) solution have the issue that it dries clear. Some examples of the issues of plain and coated setup are shown in Figure 4.1.

From Figure 4.1 there are three examples of common problems. In Figure 4.1A the CNF was unable to break the surface tension of the liquid and as such it bent, potentially breaking the electrode as well as not exposing the maximum surface area into the liquid. In Figure 4.1B the arrow is pointing to some salt that precipitated from the evaporated solution. The

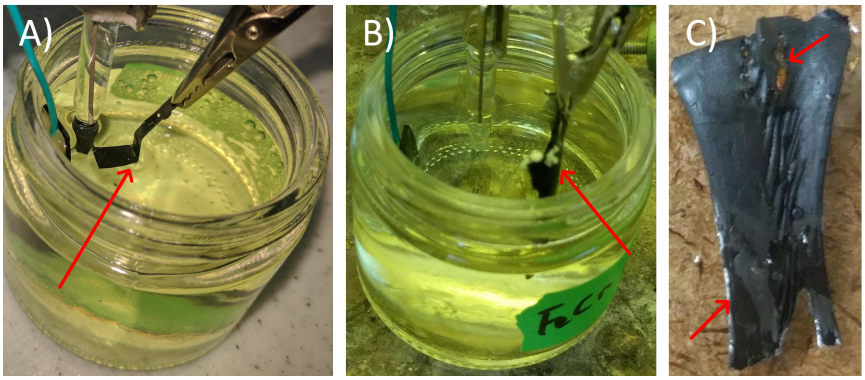

Figure 4.1: Electrochemical test setups' where the CNF electrode was coated with either wax or PTFE and a clip was used to hold the electrode in the solution. (A) The CNF electrode failed to break through the liquid's surface tension and thus bent, (B) The coating failed to stop liquid from being drawn up via capillary force and evaporating leaving precipitate of salt, (C) The wax coating proved difficult to control as the bottom arrow points to the dark portion of the CNF electrode which is the only area that remains uncoated. The top arrow shows how the wax failed to prevent the liquid from creeping upwards and corroding the metal clip.

point of interest is that the solution climbed up the CNF electrode (due to capillary forces) and started to evaporate. Finally in Figure 4.1C there is an electrode that was removed from the solution post testing. Two points of interest are seen on this electrode, starting from the bottom arrow there is a clear color difference from the wax coating. The arrow is pointing to a darker area which is the uncoated portion of the CNF electrode. The lighter portion is where the wax coated. The procedure of coating the CNF involves dipping the section that will be clipped into hot wax. The problem is the wax creeps through the electrode potentially covering significantly more area than expected or desired. Furthermore, the wax failed to stop any liquid from creeping up to the metal clip and corroding it. The top arrow shows some redish-brown liquid which is evidence of this corrosion.

4.1.2 Preparation of Carbon Electrode with PDMS

One solution to the issue of fragile CNF was to use a silicon-based organic polymer to protect and reinforce the CNF known as Polydimethylsiloxane (PDMS, Sylgard 184 Silicone

Elastomer, Dow Corning Corporation). PDMS is a type of silicone that is often used in microfluidic devices as it is optically clear, inert, and hydrophobic (meaning water will not stick onto it). PDMS is simple to use as it is mixed from typically two parts, a base and a curing agent. The two parts are weighed out to the manufacturers specified ratio and then are mixed thoroughly. A mold was made by laser cutting sheets of acrylic. Alternatively, molds can be made from by CNC machining or 3D printing. Of note, many Stereolithography (SLA) resins can contain inhibitors that will prevent certain types PDMS from curing. The thoroughly mixed PDMS can then be poured into the mold and set to cured. To remove bubbles the PDMS (already in the mold or before) can be placed in a vacuum or pressure chamber to be degassed. This may not be necessary since perfect optical clarity is not required. Care can be taken to prevent small bubbles from breaking through and causing leaks when mixing the PDMS. The PDMS is set to cure over heat such as a hot plate or in an oven. If the mold material cannot stand the heat then it can be cured at ambient temperature at a much slower rate. Any unused PDMS can be kept in the fridge which will slow the curing time. Once all the PDMS has been cured then they can be carefully removed from their molds. A layer of PDMS is also poured over a piece of glass (such as a microscope slide) to allow for future tests with chemicals such as hydrochloric acid (HCl) which will etch through glass but not PDMS. Using the remaining PDMS from the fridge the parts of the mold is then assembled and bonded with uncured PDMS. The CNF working electrode is bonded on its edges against the floor of the cell and the remainder of the PDMS cell is bonded on top of it.

An edge of the CNF should be sticking out of the PDMS so that a wire can be connected. Thin 32-gauge magnet wire was used to establish an electrical connection between the CNF and the potentiostat. First the enamel coating of the magnet wire is stripped off both ends of the wire with a flame, then cleaned with a razor blade, and finally polished with a high grit sand paper. One side of the stripped wire is bonded using Conductive Carbon Paste (Structure Probe, Inc.). The paint is allowed to dry fully (which can be accelerated with

heat) and then PDMS is placed on top of it as a form of strain relief. In Figure 4.2 there is a sample of the full PDMS cell. It is self-contained and holds the CNF in place while isolating the electrical contact from contaminating the solution. Figure 4.2A shows that original intent of the mold to have the CNF working electrode bonded vertically in the center. While this potentially has the advantage of shortening the path between the working electrode and the other electrodes, it proved to be practically difficult as the fragile CNF working electrode would break with the adding and removing of fluids. By placing the CNF working electrode along the bottom of the cell as seen in Figure 4.2B and C then the electrode was much more secure and more likely to survive multiple tests. This change eventually led to the final version of preparation.

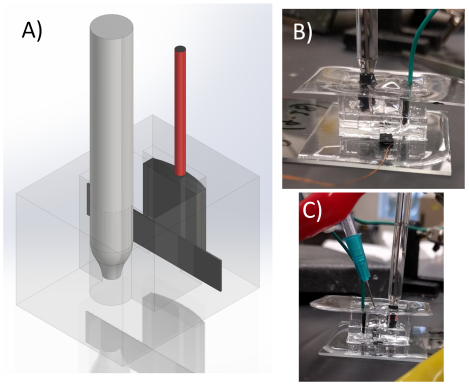

Figure 4.2: A PDMS mold that encloses the carbon nanofiber mat. (A) A CAD rendering of the cell, the original design had the CNF working electrode placed vertically in the center. (B) A side view of the cell in use, (C) a side view of the cell in use. In this instance there is a needle piercing the top of the cell. This needle can be used for access to the cell.

This preparation had a major advantage of allowing potential variables such as liquid volume and electrode spacing to be held constant between multiple tests setups. The CNF electrode could then be cut to a predetermined size each time and molded around. Additionally, the mold had built in slots for the Reference and Counter electrodes which allowed them to be held in place by the PDMS which made it easier to setup. Unfortunately, there was an issue with the volume of liquid that the cell was capable of testing. The test cell worked when using fixed concentration of an analyte. It became impractical to use this configuration when small concentrations of an analyte. There were also complications with tests such as in

chronoamperometry when standard additions are injected in the electrolyte. The cell volume was 1 mL, so any additions would change the total volume to greatly. This volume change could be compensated in the experimental analysis, it still left the issue of over flowing.

PDMS Backbone for Electrodes

The final iteration of PDMS molding was a simple method to add support to the electrode as well as isolate the electrical contact. The PDMS was poured into flat sheets. When cured it would be cut into either a larger piece for a back-plane or a smaller one for support right at the point of electrical contact. Figure 4.3 shows how this setup looked in both a schematic representation (Figure 4.3A) and in a photo of a sample ready to be tested (Figure 4.3B).

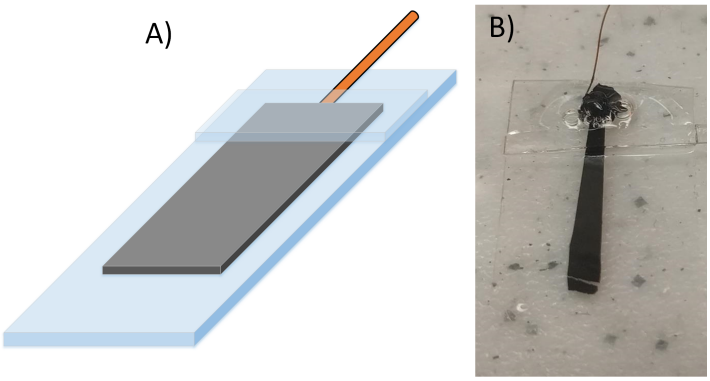

Figure 4.3: The final setup for the PDMS backing and support used for electrochemical testing. (A) A schematic representation of the PDMS back-plane and the actual electrode (B)

The CNF electrode is cut in dimensions of about 2mm x 5mm and then placed on sheet of PDMS that is larger than the sample. This will form the back-plane or backbone of the PDMS support. A strip of magnet wire is prepared in the same manner as before and bonded to a short edge of the CNF electrode with the conductive carbon paste. After the paste has dried a small piece of PDMS strip is bonded with some uncured PDMS directly under where the wire was bonded. Some additional uncured PDMS can once again be added to the point where the wire was bonded to add strain relief and make the assembly more

durable. The assembly is cured on a hot plate and is ready to use. If the CNF electrode is too long then another strip of cured PDMS can be bonded to the bottom section of the CNF to help flatten it. After the assembly has cured the geometric area of the electrode can be calculated by measuring the footprint of the exposed CNF electrode. The electrode can be supported by clipping to the PDMS for support with another clip attached to the wire for electrical contact.

Electrochemical Test Cell

Once the CNF electrode has been reinforced with PDMS it is ready to be tested. To do this a test cell was devised from a 50 mL conical tube made of Polypropylene (PP). The lid of the tub had multiple holes drilled into the top so that they are ports for the various parts of the test setup. This can be seen in Figure 4.4. In this configuration there is room for approximately 30mL of fluid (the total volume should be precisely measured but will determine on how high/low the electrodes are placed from the lid). Alligator clips will hold the PDMS portion of the CNF working electrode so that it never touches the liquid. The reference electrode can be placed directly into the cell and the counter electrode can be supported by either its wire (presuming it has a thick enough wire to support this) or by another alligator clip. The entire setup is then suspended over a stir plate so that there can be some mixing of the solution when needed.

4.2 Electrochemical Testing Methods

Electrochemical testing was performed with a three-electrode setup. This includes a reference, counter, and working electrodes. The working electrode is the CNF mat that was just prepared with PDMS. The reference electrode (RE) is a Silver/Silver-Chloride (Ag/AgCl)

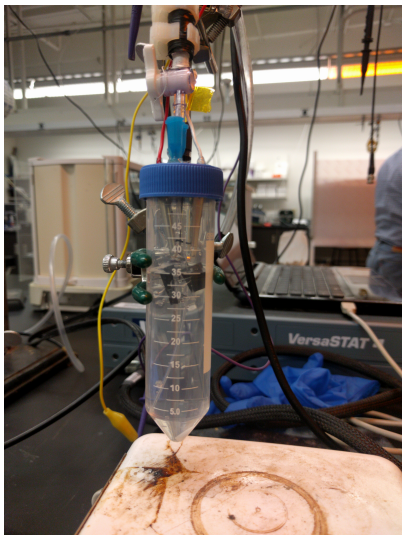

Figure 4.4: Full electrochemical setup in a 50 mL conical tube and all the attachments piercing through the lid.

electrode that is in saturated 3.0 M NaCl. This electrodes are purchased and used as is. A counter electrode (CE) is a glassy carbon electrode that had a geometric surface area 5x5 mm^2.

The Glassy Carbon electrode is initially purchased, it has no wire connections. To add one a wire is stripped and bonded to one side of the glassy carbon tile with the conductive carbon paste. Once the paste has dried a two-part epoxy is used to secure and insulate the bonded area. This will protect it from any future liquid it will be submersed during testing. The epoxy is made to cover the entire bonded area including up a little past the insulation of the wire. Any type of wire from a thin gauged magnet wire to 22-gauge wire can be used. By using thicker wire then the wire can itself be used as support. The Glassy Carbon electrode is polished by using an alumina slurry. The slurry is placed on a polishing pad and using a repetitive and constant motion the electrode is moved around in figure-eight patterns. To help prevent uneven polishing the electrode is rotated periodically, and the direction of movement is reversed. This is done for approximately 1-2 minutes. The electrode is then rinsed with methanol or IPA and then wiped dry with a lint free paper towel. Prior to each electrochemical test this polishing procedure should be followed to ensure the best

performance from the counter electrode.

4.2.1 Electrochemical Solution Preparation

The electrolyte supporting solution for electrochemical testing was carried out typically in either 2.0 M potassium chloride (KCl) or in 1X Phosphate-Buffered Saline (1X PBS). The PBS is a buffer solution (helps maintain a constant pH) with 136 mM sodium chloride (NaCl), 2.7 mM potassium chloride (KCl),10 mM disodium phosphate (Na_2HPO_4), and 1.8 mM monopotassium phosphate (KH_2PO_4). They were all dissolved into di-ionized water (DI water). This will result in concentrations of 0.14 M NaCl, 0.0027 M KCl, and 0.010 M PO_4^{3-}. The pH of 1X PBS was desired to be at 7.4. In order to achieve this a solution was made with about 10% less DI water then is required, and the pH is tested. To bring the pH to 7.4 either HCl or sodium hydroxide (NaOH) was added to decrease or increase the pH respectively. After the pH is balanced, DI water can be added to the final volume. For convenience, a solution of PBS is made that is 10 times the concentration (known as 10X PBS). In this case the PBS is diluted down to 1X PBS and then pH balanced in a similar manner prior to being used. Typically, the pH of a 10X solution will be approximately 6.8 but will change to 7.4 after dilution.

The analytes used came in either a solid or liquid form. When using a solid the weight was measured out based on the molarity and volume desired by Eq. 4.1.

$$FW * C * V = m \tag{4.1}$$

Where FW is the Formula or Molecular weight in grams/Mol (which should be given by the manufacturer), C is the concentration in Mol/Liter, V is the volume in liters, and m is the

mass in grams. When the analyte is a liquid then the concentration is needed so that Eq. 4.2 can be solved.

$$C_1V_1 = C_2V_2 \tag{4.2}$$

Here C is the concentration in Mol/L and V is the volume in liters. The subscript 1 and 2 represent the initial and final concentrations.

4.2.2 Electrochemical Techniques

A major set of tools used to characterize the CNF electrodes are electrochemical techniques. Here the setup of the techniques as used for testing are described. Three popular techniques were used in this report. The techniques were Electrochemical Impedance Spectroscopy (EIS), Cyclic Voltammetry (CV), and Chronoamperometry (CA). Each technique offers its own insight in the electrochemical reactions occurring on the electrodes surface.

All electrochemical experiments were performed using the VersaSTAT 4 Potentiostat by Princeton Applied Research. The potentiostat was running the included software of VersaStudio 2.48.5. All experiments were performed in either 1X PBS solution or 2M KCl solution with the appropriate analyte added in as necessary. The CV was typically performed at scan rates of 10, 20, 30, 40, 50, 100, 200, 300, 400, 500, 1000, 2000, 3000, 4000, and 5000 mV/s in that order. Each scan rate was run for three times prior to moving on automatically to the next scan rate. The voltage window was selected based on the analyte testing. The EIS experiments were done automatically at the end of all the CV experiments. The frequency's ranged from 10,000 Hz down to 0.1 Hz. Chronoamperometry was performed at a potential which was determined by the CV of the same analyte. This potential was determined when

the current was maximum in the CV. All the values were normalized by the active surface area.

For chronoamperometry the signal to noise can be found via Eq. 4.3[125] and using the standard signal to noise ratio of 3 (S/N = 3). In this equation σ is the standard deviation of the signal from the stable blank solution (typically taken right before the additions of the analyte). This is in essence the noise of the signal. A standard curve is created from the CA of the concentration versus the current. The curve will have a slope, S, which is needed to calculate the LOD as well.

$$LOD = \frac{3\sigma}{S} \tag{4.3}$$

4.2.3 Surface Area Calculations

A crucial component to understand electrochemistry is the surface area of an electrode as all electrochemical reactions happen on the surface. The Randles-Sevcik equation can be used as seen below in Eq. 4.4[26] as am analytical technique. The area can be determined if using a well understood analyte (such as ferri/ferrocyanide) in which the diffusion coefficient is known. Cyclic voltammetry can be run to obtain a peak reversible current (I_p^{Rev}) and thus the Eq. 4.4 can be solved for the Surface Area (A).

$$I_p^{Rev} = \pm 0.446 nFAC\left(\frac{nFDv}{RT}\right)^{\frac{1}{2}} \tag{4.4}$$

The remaining variables in Eq. 4.4 are the number of electrons (n), the Faraday Constant

(F), the analyte concentration (C), the scan rate (v), the universal gas constant (R), and the temperature (T). A systems reversibility can be determined if the plot of I_p^{Rev} versus $v^{\frac{1}{2}}$ is linear. The Randles-Sevcik equation presents an issue in that it is applicable to flat electrodes. The complex 3D geometry of the nanofiber mats presents a challenge and as such another technique should be used.

An alternative technique, and the primary one used in this work, is the use of EIS. When using EIS the results can be approximated as an electrical circuit. This circuit can then be solved using iterative techniques for the various elements which are analogs for various phenomena that are occurring. A basic type of equivalent circuit is the Randles cell[12] as shown in Figure 4.5. Here there are 3 basic elements being used to model the system. The resistance of the solution is modeled as R_S. This value can be modified by changing the solution's electrolyte concentrations so that there are more or less charge carriers available in the solution. The properties of the electrode are modeled as the double layer capacitance (C_{dl}). This capacitance is caused from the double layer that is formed at the interface between the the electrolyte solution and solid electrode. It is formed from the buildup of ions that are adsorbed on the surface of the electrode. There will be a buildup of charge at this layer and as such a nanometer wide insulated space. This could be ideal or detrimental depending on the application. The final element in the Randles cell is the charge-transfer resistance (R_{ct}). This value is based on the electron's difficulty from transferring from one phase (such as liquid) to another (such as solid). The Randles cell in Figure 4.5 offers a simple method to model the system as well as a good starting point for modeling.

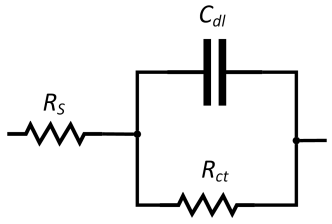

Figure 4.5: The Randles cell equivalent circuit

The circuit needs to be updated slightly to better represents the phenomena that is occurring in the CNF mats. To do this the standard capacitance model of a C_{dl} is replaced with a constant phase element (CPE). and an additional element was added in series with the R_{ct} known as Warburg element (W) as well. The resulting circuit can be seen in Figure 4.6. The CPE element is used since the capacitance does not behave in the same ideal behavior as an electronic capacitor. The CPE locks the phase such that the capacitance is not frequency dependent. A Warburg element (W) is used to model the diffusion effects on the system. Additional elements could be added to the circuit as the phenomena that is occurring is better understood. This would lead to better fitting between the actual data and the circuit model.

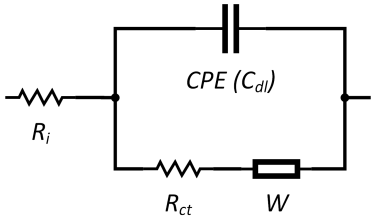

Figure 4.6: Equivalent circuit used for Carbon Nanofiber mats

With this model it can then be fitted iteratively to the data obtained from the EIS. This fitting will allow values to be solved for the different elements. This is typically done with software, in our experiments the free software "EIS Spectrum Analyser" [22] was used. When EIS was performed in a blank electrolyte solution then the electrochemically active surface area was solved from the values obtained from the equivalent circuit. Using the specific double layer capacitance (C_{dl}) then Eq. 4.5[169, 12] can be solved. It should be noted that the C_{dl} should be in units of $\frac{F}{cm^2}$ and as such needs to be normalized by the surface area of the electrode. To solve this issue an approximation is made where the geometric surface area is used to normalize the C_{dl} and thus solve Eq. 4.5. The double layer charging current, I_c, and the scan rate, v, can be obtained from cyclic voltammetric experiments of the same

electrode in a blank solution.

$$A_{act} = \frac{I_c}{C_{dl} v} \tag{4.5}$$

Chapter 5

Characterization of Carbon Microstructure

The goal of this manuscript is to describe a route for fabricating graphitized carbon nanofibers to be used for electrochemical devices. The fabrication steps as described in Section 3 were designed and optimized to produce graphitic nanofibers at a low pyrolysis temperature. Each step of the process plays an important role to this goal. This section uses various characterizations to understand the level of graphitization and elemental composition of the CNF mats. The more graphitic structure will allow for better electrical properties while the additions of heteroatoms (such as nitrogen) will allow for better electrocatalyst. Both of these properties would allow for a more effective electrochemical sensor.

The CNF mats underwent a variety of tests, both non-destructive and destructive (typically in that order so that the samples can be reused as many times as possible). The non-destructive tests included Raman spectroscopy which was used to gain insight into the graphitization, XPS which allowed further insight into graphitization as well as the material composition, and four-probe conductivity tests. The destructive tests that then followed

included TEM, which involved the grinding up of the sample to view the microstructure, and electrochemical tests which required the CNF mat to be bonded to a PDMS backbone as was described in Section 4.1.

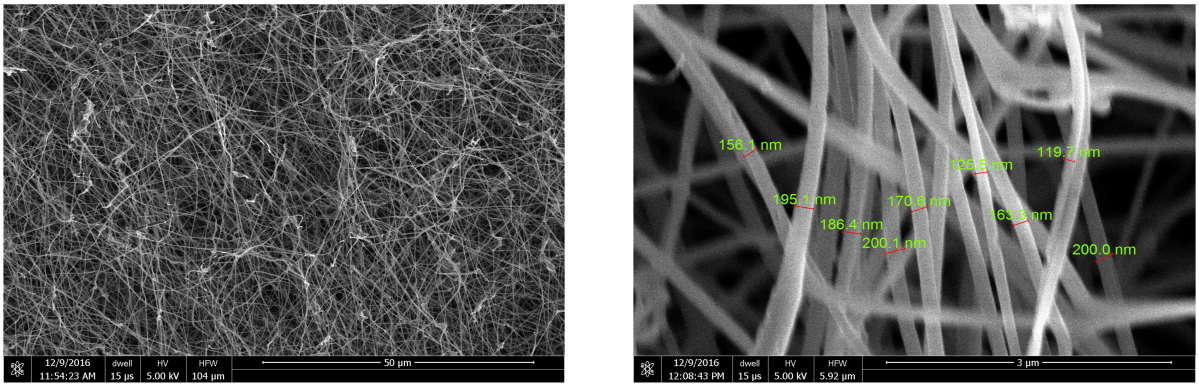

(a) **(b)**

Figure 5.1: Images of the carbon nanofiber mats taken on an SEM; (a) is a zoomed out image of the mat, (b) is a zoomed in portion of the same CNF mat with individual fiber diameters.

The CNF mats were examined under SEM which normally would be considered a non-destructive test. In preparation of using the SEM a sample will be mounted to a pedestal (typically via conductive double-sided tape). It then becomes difficult to remove the CNF mat as they are very fragile and will tear. Some SEM images are seen in Figure 5.1. In Figure 5.1a the overview of the CNF mat can be seen and in Figure 5.1b a zoomed in view allows a sampling of the diameters of the individual fibers. All SEM images were conducted using a FEI Quanta 3D FEG Dual Beam SEM.

Often in this work the CNF mats are compared to commercially obtained Toray graphitic fibers. The Toray fibers are seen to be much larger than that of the electrospun fibers as shown in Figure 5.2. From this figure there is an overview of the Toray sample in Figure 5.2a and a zoomed in view with dimensions of individual fibers in Figure 5.2b.

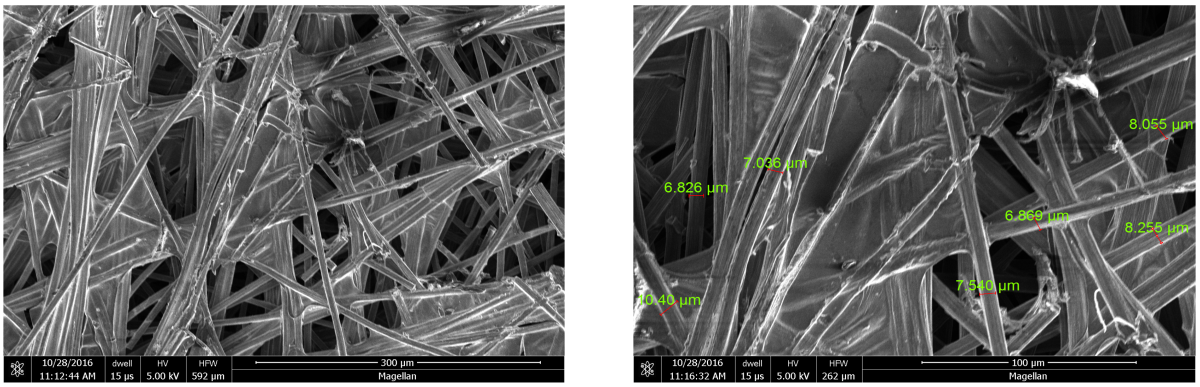

(a) **(b)**

Figure 5.2: Images of Toray graphitic fibers taken on an SEM. In (a) there is an overview of the mat, in (b)there is a zoomed in portion of the same Toray mat with fiber diameters.

5.1 Graphitization of Mechanically Treated Carbon

Evidence of Graphitzation

When the carbon nanofiber mats become more graphitic there are an assortment of improvements in properties that can be expected when compared to that of the more amorphous variety. One such simple test is the conductivity of the mat. Using a four-probe conductivity measurement a rough value can be obtained. There would be an expectation for an increase in conductivity as the carbon became more graphitic. The four-probe measurement was carried out on a Signatone SP4 probe station controlled by a Keithley 2400 SourceMeter. Multiple currents were tested typically ranging from 7 mA to 10 mA and the results averaged out. It should be noted that this would provide more of an estimate since the mats are very porous and randomly oriented. The conductivity values are shown in Table 5.1 where a pure PAN sample, A PAN sample with CNT's added (PAN-CNT), and a PAN sample with CNT that also underwent mechanical treatment (PAN-CNT-M). There is an expected (but modest) increase in conductivity from simply adding CNT's. While the addition of the mechanical treatment made an order of magnitude increase in conductivity.

Table 5.1: Conductivity (values obtained from Ghazinejad et al[69])

Material	Conductivity, $\sigma(S/m)$
PAN	150 - 250
PAN-CNT	450 - 600
PAN-CNT-M	4900 - 5000

Raman Spectroscopy

This data alone is not enough to demonstrate increased graphitization of the CNF mats. Raman spectroscopy was performed on all three of the samples seen in Table 5.1. From the Raman spectra a comparison of the two peaks can provide insight. Using a Renishaw InVia Raman Microscope and an excitation laser of 532nm wavelength the samples were characterized. The collected data was then plotted with the D ($1355cm^{-1}$) and G ($1583cm^{-1}$) peaks fitted using Lorentzian distributions[42, 124]. Three Raman spectra are plotted in Figure 5.3 for the samples of Pure PAN, PAN-CNT, and PAN-CNT-M.

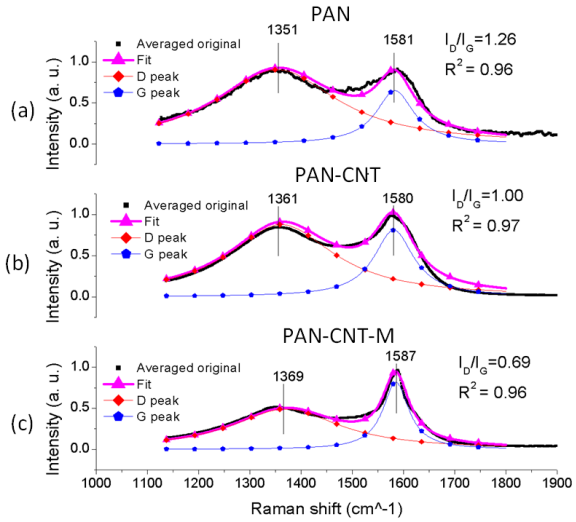

Figure 5.3: Raman spectra for the (a) Pure PAN CNF, (b) PAN-CNT (c) and PAN-CNT-M. Figures adapted from Ghazinejad et al[69]

Figure 5.3 shows the G (I_G) and D peaks (I_D), which from Section 2.7.2 are known to be representative of the in-planes vibrations and sp^2 structural defects respectively[180]. The ratio of the two peaks (I_D/I_G) helps provide an understating into the level of graphitization,

where a smaller value would indicate more graphitization and larger implies more defects. When comparing the three different spectras in Figure 5.3 their ratios can be compared. There is once again the same trend as seen before in the conductivity's where the addition of CNT's helps the overall graphitization to a small degree. It is not until the mechanical stress during stabilization that there is a much larger and noticeable increase in order (graphitization) compared to the disorder. In Figure 5.3 this is seen as the PAN sample (Figure 5.3a) has an (I_D/I_G) ratio of 1.26 while the PAN with CNT's added (PAN-CNT, Figure 5.3b) shows a ratio of 1.00 leading to about a 20% decrease in disorder. When comparing the mechanically treated sample (PAN-CNT-M) which has a ratio of 0.69 (Figure 5.3c), the decrease can be seen as much as over 45% when comparing to the pure PAN sample. This further supports that this increase in graphitization is due to the combination of both the CNT's and the mechanical stabilization and not simply the addition of already graphitic CNT's.

Transmission Electron Microscopy

Beyond the Raman results, an additional validation of the graphitic nature can be observed via a FEI Titan S/TEM High Resolution Transmission Electron Microscopy (HRTEM). For simplicity HRTEM is referred to as the more generic TEM. By using a TEM micrographs can be obtained with enough resolution to be able to see the actual layers of graphene sheets in the Ångstrom scale. Four different samples where viewed under TEM and their results are shown in Figure 5.4. The carbon samples are the pure PAN, PAN-CNT, PAN-CNT-M, and finally plain CNT's for reference in Figures 5.4a, b, c, and d respectively. This figure is broken up into three sections with the main image on the left. On the upper right is a Fast Fourier Transform (FFT) which shows the diffraction pattern, this is indicative of the crystallinity order. On the lower right is a zoomed in and processed image of the lattice fringes.

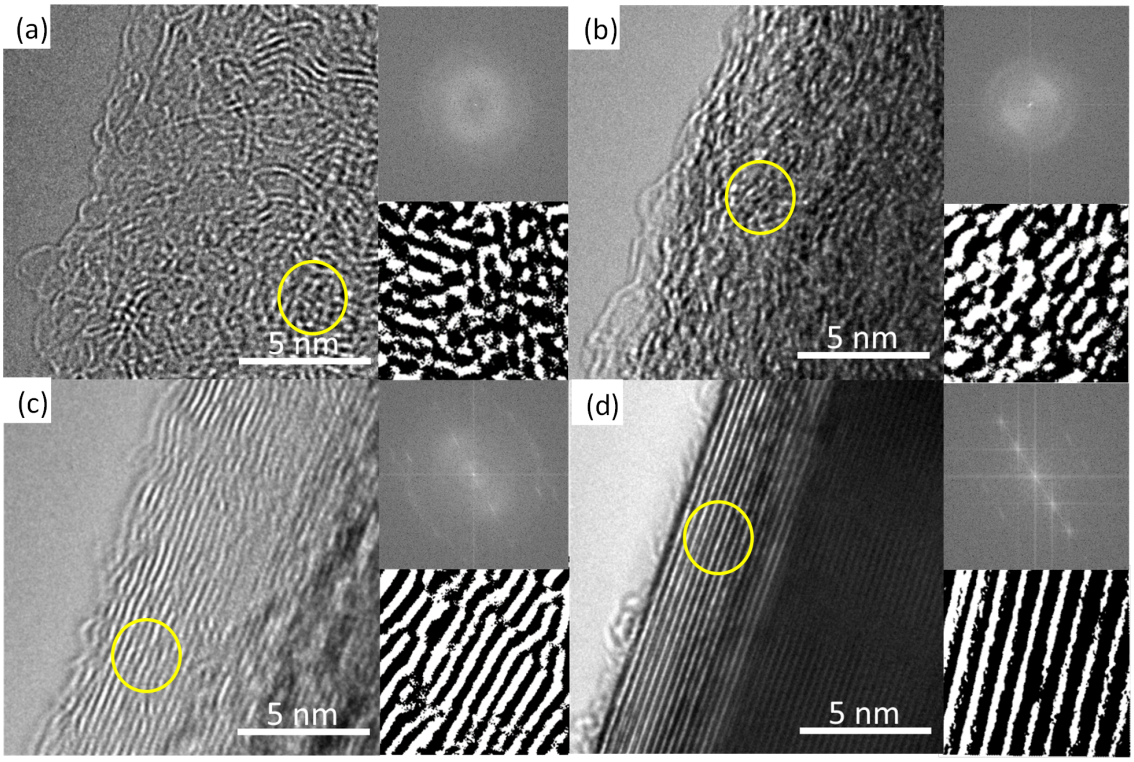

Figure 5.4: TEM Micrographs of (a) Pure PAN CNF, (b) PAN-CNT, (c) PAN-CNT-M, and (d) CNT's. Each image has an inset on the upper right of the Fast Fourier Transform and lower right of a zoomed in processed image for clarity. Figure is from Ghazinejad et al[69]

From Figure 5.4 the increase in graphitization is clear. The example of what a graphitic structure should look like is seen in Figure 5.4d where there are very long and orderly planes. These planes are known as the fringes. From the FFT there are very distinct point sources in the image representing the orderly nature of the crystal structure. When measured the inter layer spacing is 3.4 Å which corresponds with literature for the spacing expected in CNT's[97]. In comparison, this can be compared to the pure PAN sample of Figure 5.4a. This provides an excellent example of an amorphous carbon. Here it is seen there is lack of long term order in the way that the planes are fragmented and seemingly random in orientation. By looking at the FFT of the PAN sample it is a symmetric ring which is indicative of a chaotic amorphous structure. The addition of CNT's to the to the PAN solution is seen in Figure 5.4b. The results arguably show a slight increase in order, but overall the planes are short and chaotic. Again, the FFT for this image is of symmetric

rings. This helps to demonstrate that the graphitic gains by the addition of CNT's are limited. Any gains that may have arisen from the CNT's during the electrospinning process may have been lost during stabilization. With the addition of the mechanical treatment of the PAN-CNT sample there is a noticeable improvement in the order as seen in Figure 5.4c. The planes are orderly and more similar to that of the plain CNT sample seen in Figure 5.4d. Although it should be noted there are more defects (where the planes are broken). This could be advantageous though as it adds more edge planes when compared to the pure CNT's. These edge planes will make the PANC-CNT-M samples more electrochemically active when compared to the long defect free basal planes of plain CNT's[211].

5.2 Heteroatom Content

The existence of heteroatoms (non-carbon atoms in the carbon structure) can allow for a multitude of modifications including enhanced electrocatalytic properties which is important for sensing applications. The Raman plot can be further deconvoluted to discover other peaks in the data. When fitting the Lorentzian, a peak at $1220cm^{-1}$ can be seen. This is demonstrated in Figure 5.5. The peak can often be interpreted as the presence of heteroatoms[189, 4, 42, 124]. It is not entirely clear the reason for this peak as depending on the form of the heteroatom could result in different spectra. There may be more defects if the nitrogen is pyridinic as this could potentially create nanoholes[111]. Alternatively, if the nitrogen is graphitic then there may not be any defects as a result. Further investigation of heteroatoms was accomplished with X-ray Photoelectric Spectroscopy (XPS) on a Kratos AXIS-SUPRA surface analysis instrument that was using an X-ray source of a monochromatic Al Kα.

An XPS spectra is presented in Figure 5.6 of the PAN-CNT-M sample. From here various peaks can be observed indicating presence of heteroatoms. There can be seen three major

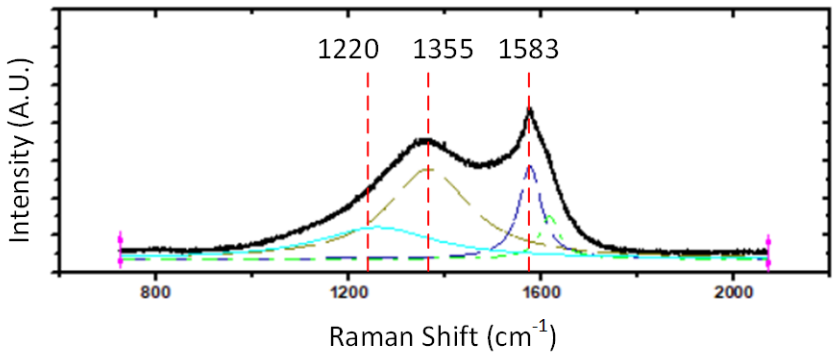

Figure 5.5: Raman spectra for PAN-CNT-M with Lorentzian fitting for the I (1220 cm^{-1}), D (1355 cm^{-1}), and G (1583 cm^{-1}) peaks. Figure adapted from Pollack et al [148].

peaks, one for Oxygen (O 1s), a Nitrogen peak (N 1s), and a Carbon peak (C 1s). The data obtained from these spectra shows that the composition of the sample has 94.5 ±0.1 at. % (atomic ratio) carbon, 4.4 ±0.5 at. % nitrogen and a small 1 ±0.3 at. % of oxygen. In contrast the pure PAN sample shows a concentration of 86.5 ±0.1 at. % (atomic ratio) carbon, 2.80 ±0.5 at. % nitrogen and a much larger oxygen at 10.30 ±0.3 at. % of oxygen.

There is an additional peak labeled "C KVV" on the XPS spectra of Figure 5.6, this is around 1200 eV. This peak is from auger emissions [133]. When the X-ray from the XPS causes a photoelectron to be emitted there will be a vacancy in a lower electron orbit which will be filled by one from a higher orbit in what is known as relaxation. The excess energy from this process will be emitted as an auger electron. Because these emissions where induced by X-rays they will show up on the XPS spectra [80]. The nomenclature "KVV" refers to the electron orbit that the initial vacancy was in (in this case K shell) followed by where the double vacancy will be (here it is in the valence shell). This auger peak can provide data on chemical speciation as well provide some insights on the ratios of sp_2 and sp_3 carbons [2]. Further investigation of this peak would need a technique known as Auger Electron Spectroscopy (AES) which is very similar to XPS except it uses electrons instead of X-rays for excitation.

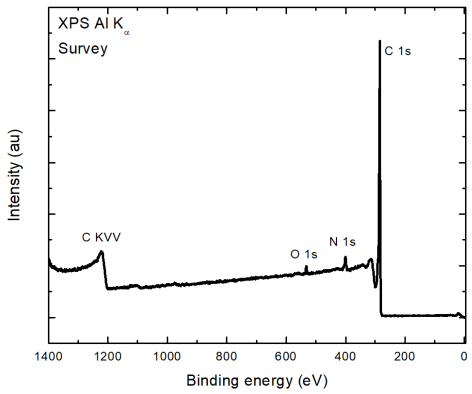

Figure 5.6: Full XPS spectra of PAN-CNT-M sample. Figure from Pollack et al [148].

5.2.1 Nitrogen Heteroatoms

Nitrogen can be seen in the sample by the presence of a peak at around 400 eV. Further examination of this peak is accomplished via deconvolution and the results are plotted in Figure 5.7. Here the two samples that were examined under XPS are pure PAN and a PAN-CNT-M in Figures 5.7a and 5.7b respectively. Fitting this deconvoluted N 1s region allows for the determination of the various carbon-nitrogen bonds present in the region. A residual of the plot fittings is shown at the bottom of the plot (and labeled as such). This value provides a visualization of the plot fittings accuracy with the horizontal line representing the fitted value and the other line is the measured value.

There are four different peaks shown in Figure 5.7 which correspond to the various types of Nitrogen-Carbon bonding. These are pyridinic-N, pyrrolic-N, graphitic-N, and oxidized-N. The values for these components are presented in Table 5.2. It should be noted that for the PAN-CNT-M there is no peak corresponding for pyrrolic-N. This could potentially be a result of pyrrolic-N being the least stable at high temperatures. Further investigation is necessary for this. Additionally, there are peaks labeled as oxidized-N. The current XPS data is not detailed enough to fully resolve what these peaks may correspond to. By using a higher resolution XPS it may be possible to better understand the significance. One such possibil-

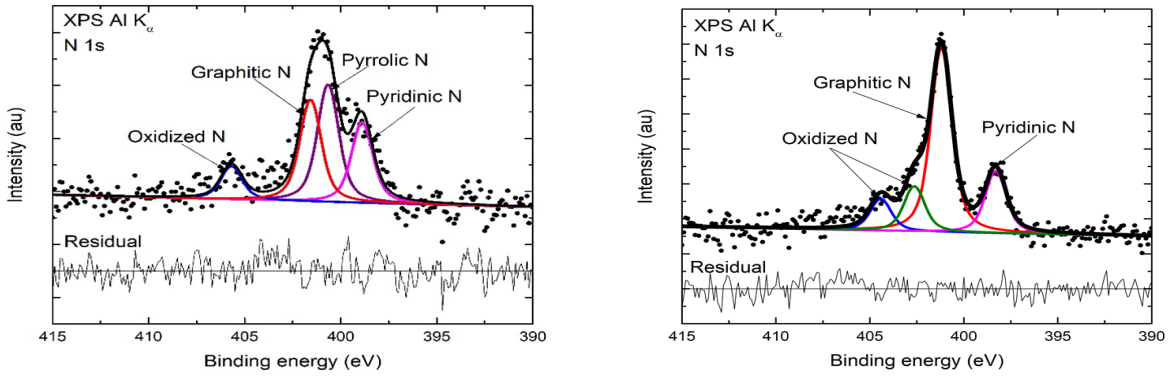

Figure 5.7: N 1s XPS spectra for both (a) PAN and (b) PAN-CNT-M. Figure from Pollack et al [148].

ity could include that these peaks relate to pyridinic-N oxide and graphitic-N oxide [127, 103].

Table 5.2: Nitrogen composition (values obtained from Pollack et al[148])

Element	Binding Energy (eV)	at. % PAN	at. % PAN-CNT-M
Carbon	285	86.5	94.5
Nitrogen	400	2.8	4.4
Oxygen	533	10.3	1.0
Pyridinic-N	398.5	24.14	19.21
Pyrrolic-N	400.1	35.29	0
Graphitic-N	401.3	30.58	56.97
Oxidized-N	405 & 402.6	9.99 & 0	13.97 & 9.85

From the results presented in Table 5.2 a direct comparison can be made between that of the pure PAN and the PAN-CNT-M. The clearest distinction comes from the difference in graphitic-N between the two where PAN has 30.58% compared to a 56.97% of the PAN-CNT-M. This large increase in graphitic-N is what would be expected based on the higher level of graphitization that is seen from the Raman and TEM data.

5.2.2 Oxygen Heteroatoms

In addition to the nitrogen peak there can also be a peak associated with oxygen bonds. This peak (O 1s) is deconvoluted in Figure 5.8 with its various peaks labeled. The presence of oxygen is interesting as it could be theorized it was doped in from the environment (either the stabilization or pyrolysis). While pure PAN, $(C_3H_3N_3)_n$, has no oxygen groups, when it is stabilized it will gain some because of oxidation. Potentially these oxygen's may remain in the final carbon structure. Alternatively, the oxygen could be from inside the furnace. During the normal procedure the furnace is purged of oxygen via a nitrogen flow for multiple hours. This purge may either be insignificant or there is a leak allowing some oxygen to flow into the furnace but just in low enough concentrations that the polymer does not burn. This could be a very interesting area to pursue further in how to control the remaining final oxygen content as well as the potential applications for having oxygen on the final structure such as with supercapacitors [202, 61, 184, 168].

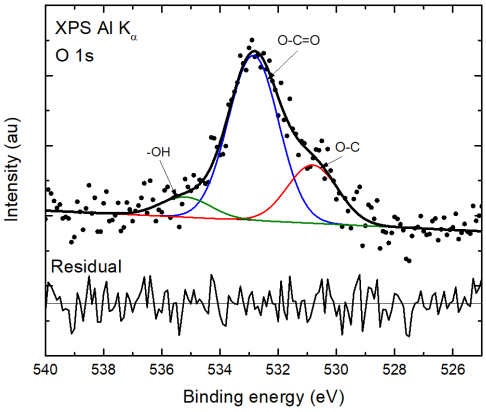

Figure 5.8: O 1s XPS spectra of PAN-CNT-M sample. Figure from Pollack et al [148]

Chapter 6

Electrochemical Characterization of Carbon

Electrochemical characterization was performed on the CNF materials to better understand the electrochemical performance. In this section the CNF mats where prepared as described in Section 4.1 and are referred to as the Working Electrode (WE) or simply the electrode. The electrode can be characterized using well understood analytes which can help to solve for parameters such as the electrode kinetics. Initially it is important to understand the electrodes surface area.

6.1 Surface Area of Carbon Nanofiber Electrodes

There are a variety of factors that can affect the surface area of the CNF electrodes and thus making the usage of the simple geometric area insufficient. The electrode is comprised of a complex 3D geometry that would invalidate some analytical methods such as the Randles-Sevcik equation from Eq. 4.4[26]. Additionally, because the electrode is reinforced with

PDMS there is potential to have the PDMS cover more area then anticipated before curing. When the PDMS cures it is optically clear and thin layers can be very difficult to detect. As such the EIS method for determining the surface area was chosen. This also has the benefit of determining the electrochemically active surface area rather than simply the uncoated surface area (that is the surface area that will react).

For EIS characterization an equivalent circuit was designed and fitted to the raw data from the experiment. The equivalent circuit was described and shown in Figure 4.6 from page 61. From the fitting of the data, the double layer capacitance can be calculated. From there the electrochemically active surface area can be solved as described from Eq. 4.5 on page 62.

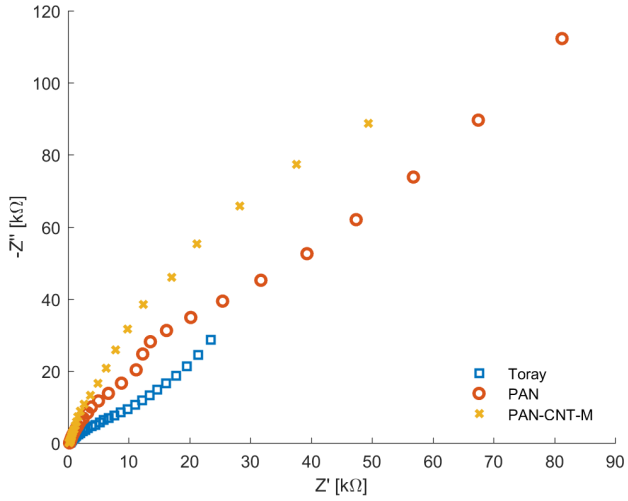

Figure 6.1: Electrochemical impedance spectroscopy plot of a commercially obtained Toray graphitic fiber mat, pure PAN mat, and a PAN-CNT-M mat. Figure adapted from Pollack et al[148]

When calculating the active surface area a useful parameter is the fraction (f) of the active surface area over the geometric (Eq. 6.1[46]). This fraction can provide some perspective on the increase in surface area. This ratio on its own does not necessarily provide insight but is useful when comparing between samples that allows for an appreciation of the increase in

active surface area due to processing.

$$f = \frac{A_{act}}{A_{geo}} \tag{6.1}$$

The various values obtained from the EIS tests are shown in Table 6.1 for some representative samples. The double layer capacitance (C_{dl}) is in units of $\left(\frac{\mu F}{cm^2}\right)$. The geometric ($A_g$) and active surface ($A_{act}$) areas are given in units of (cm^2) and the area fraction, f, is unit-less. Notably from this table is the improvements from the pure PAN sample to the Mechanically treated PAN and CNT sample (PAN-CNT-M). From the surface area fraction, it can be seen that the gains in surface area is almost twice as large then the gains in the untreated sample. This increase in active surface area could allow the electrode to be much smaller while still maintaining the same signal response as a pure PAN counterpart. Additionally, it would allow for higher sensitivity and lower limit of detection in sensing applications. Further surface area calculations can be tested via techniques such as nitrogen adsorption (also known as the Brunauer-Emmett-Teller or BET). This could provide additional details on the surface area (although not the active surface area). This could have been useful in determining the amount of electrode that became covered by the PDMS.

Table 6.1: Surface area of PAN and PAN-CNT-M electrodes (values obtained from Pollack et al[148])

Electrode	$C_{dl}\left(\frac{\mu F}{cm^2}\right)$	$A_g(cm^2)$	$A_{act}(cm^2)$	f
PAN	65.6	0.15	0.882	5.88
PAN-CNT-M	291.0	0.1	1.13	11.3

6.2 Heterogeneous Electron Transfer Rate of Electrodes

To better understand the electrodes electrochemical kinetics a redox probe was used. This is a well understood analyte that can be used to help determine the electrode kinetics of a material. An important consideration of an electrode material is the standard electrochemical rate constant, k^0, which only applies for a heterogeneous electron transfer. The kinetics of an electrode are important as it is related to the mass transport though-out the system.

In electrochemistry the reversibility of a reaction is defined by the electron transfer rate. A system is defined as reversible if the electron transfer rate between the electrode and the analyte is fast enough that there are no barriers presented by thermodynamics. This will manifest in cyclic voltammograms as a consistent peak seperation regardless of the scan rate. That is, the reaction becomes diffusion limited at the same potential regardless of how fast the potential is swept. This is considered an ideal situation and is rarely seen in practice. If the electron transfer rate is slow because of outside complications then the system is considered irreversible. A system in the middle would be considered quasi-reversible and this is the case as see from the cyclic voltammograms of the CNF electrodes. For quasi-reversible reactions the k^0 can be solved using the Nicholson method[12, 26] as seen in Eq. 6.2.

$$\Psi(\Delta E_{peak}) = \frac{\left(\frac{D_0}{D_R}\right)^{\frac{\alpha}{2}} k^0}{(\pi D_0 f v)^{\frac{1}{2}}} \tag{6.2}$$

Here Ψ is the kinetic parameter which was tabulated by Nicholson [135] for various peak-to-peak separation distances (ΔE_{peak}) for one step one electron processes. The charge transfer coefficient is given by α. The diffusion coefficients for the oxidized and reduced species are given by D_0 and D_R respectively. The scan rate is v given in $\frac{V}{s}$. The term f is simplified

from what is typically taken as a constant of $f = \frac{F}{RT}$. Where the Faraday Constant, F, is calculated by the constants $F = eN_A$. Here the elementary charge of an electron, e, is approximately $1.602 * 10^{19} C$ and Avogadro constant, N_A, is approximately $6.022 * 10^{23} mol^{-1}$. This results in the Faraday constant as $96485.333 \frac{C}{mol}$. The universal gas constant, R, is $8.314 \frac{J}{mol * K}$ and the temperature, T, is typically at room temperature of 300K (25 °C).

From Eq. 6.2 the system kinetics can be solved if the diffusion coefficient of the oxidezed and reduced species is known. As such ferri/ferrocynaide ($Fe(CN)_6^{3-/4-}$) is commonly used as an electrochemical probe[12]. With the knowledge of the diffusion coefficient[40] for ferricynaide as $7.26 * 10^{-6} \frac{cm^2}{s}$ and ferrocynaide as $6.67 * 10^{-6} \frac{cm^2}{s}$ then cyclic voltammetry could be performed as seen in Figure 6.2.

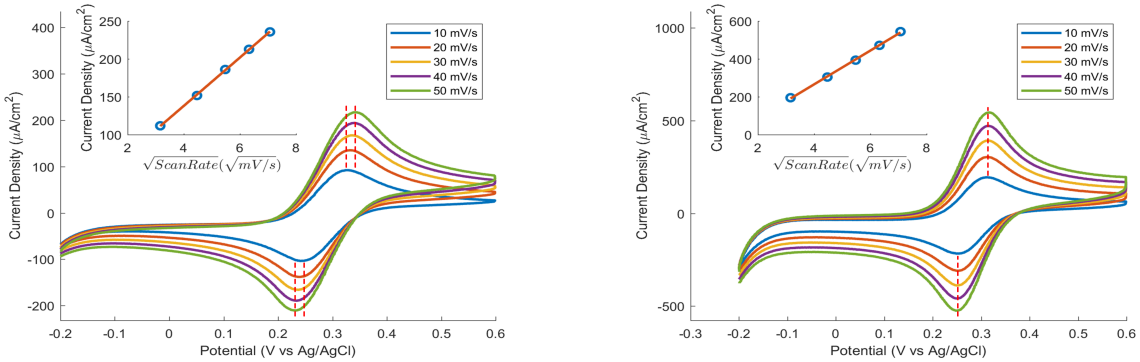

Figure 6.2: Cyclic voltammograms in 2M of KCl and 5mM $Fe(CN)_6^{3-/4-}$ at various scan rates of a (a) Pure PAN and (b) PAN-CNT-M electrodes. Inset plots the current density versus the square root of the scan rates. Figures adapted from Ghazinejad et al[69]

In Figure 6.2 the peak currents are plotted with a red dotted line. In the case of pure PAN electrodes (Figure 6.2a) it can clearly be seen that as the scan rates increase the peak-to-peak also increases. In comparison there is the PAN-CNT-M electrode (Figure 6.2b) shows a much more consistent peak-to-peak separation which remains the same separation regardless of the scan rate. The insets of the plots show the comparison of the current density versus the square root of the scan rate. The square root is taken because of the Randles-Sevcik equation

(Eq. 4.4 on page 59). As this plot deviates from linearity it is a sign of the reversibility of the system (i.e. the complications during electron transfer).

The kinetics, k^0, can now be calculated from Eq. 6.2 and Figure 6.2 which results in 0.0029 $\frac{cm}{s}$ for the Pure PAN electrodes and 0.0312 $\frac{cm}{s}$ for the PAN-CNT-M electrodes. This large increase in kinetics is expected as there are an increase in graphitic edges because of the addition of the mechanical treatment and CNT's[69, 26]. The PAN-CNT-M electrodes shows kinetic performance that is comparable with both graphene and graphene oxide which have values of $1.4 * 10^{-3}$ to $0.15 \frac{cm}{s}$[185, 23].

Adsorption of $Fe(CN)_6^{3-/4-}$ on Electrodes

An additional observation can be made when running an addition cyclic voltammetry on the electrodes immediately after the $Fe(CN)_6^{3-/4-}$ experiments. This was done in a blank electrolyte with the results plotted in Figure 6.3.

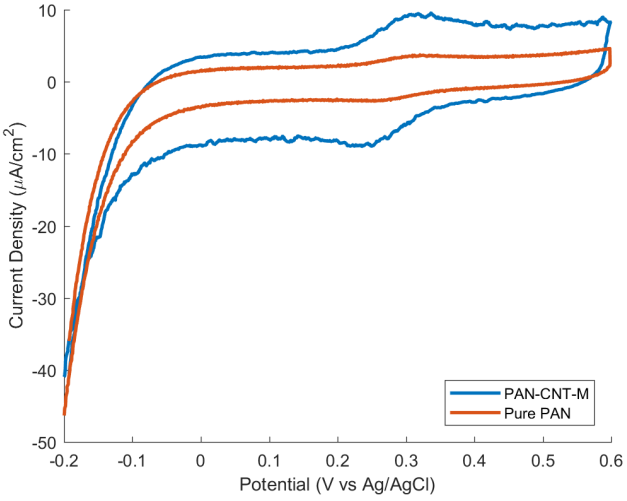

Figure 6.3: Cyclic voltammograms at a scan rate of 10 mV/s of Pure PAN and PAN-CNT-M electrodes immediately after $Fe(CN)_6^{3-/4-}$ Cyclic voltammetry in 2M KCl. Figures adapted from Ghazinejad et al[69]

The purpose of the of running a cyclic voltammograms in a blank electrolyte (2M KCl) is to

show any adsorption of the $Fe(CN)_6^{3-/4-}$ onto the electrode. Adsorption of $Fe(CN)_6^{3-/4-}$ has been shown to occur on the graphitic edges of carbon[27, 40]. Figure 6.3 demonstrates that there is a larger peak remaining on the electrode in the PAN-CNT-M compared to the pure PAN. Both electrodes have similar morphology's so it can be concluded that the $Fe(CN)_6^{3-/4-}$ is adsorbed rather than some remaining $Fe(CN)_6^{3-/4-}$ liquid trapped in the vacancies of the nanofiber mats.

Chapter 7

Theory For Unwinding Polymer Chain Towards Graphitization

The first step towards graphitization involves the alignment of the molecules from the electrospinning process. One area to note is that when speaking of molecular alignment, it is being referred to the polymer chains, not the alignment of the polymer nanofibers. This is also known as unwinding the molecular chain[69]. During the electrospinning there is an electrostatic force that applies a large shear force on the polymer. This shear force is strong enough that it will cause the macromolecules of the polymer to align[11, 100] along the axis of the polymer nanofiber. Depending on the solvent and polymer used there may be some relaxation of the stresses on the polymer fiber and as such the molecular orientation will become isotropic (randomly oriented) again[58]. One area to note is that it is typically accepted that in fully crystalline polymers, the formation of their crystals will occur faster and thus the collector plate may have no effect on the molecular orientation. Conversely when a polymer is fully amorphous the gains in molecular alignment from electrospinning will be lost if it's glass transition temperature (T_G, the temperature for when an amorphous polymer transitions from a hard glass like state to a softer one). If an amorphous polymer is

spun at the T_G then the orientation will not be preserved. Finally, semi-crystalline polymers (polymers with both regions of amorphous and regions of crystalline) such as in PAN, will have little effect in regards of the T_G to the molecular orientation[157]. The shear forces causing the alignment produce is known as the confinement mechanism[7].

An important observation about molecular alignment comes from the observations of how relative strength of a fiber increased exponentially as the fibers radius decreases. This was noted by Ji et al[90] where it was proposed that the large shear force applied to the nanofiber would cause orientation to occur along the shell of the fiber. The fiber unwinding depends on a ratio between the radius of the fiber, R, and the radius of gyration of the polymer (R_G, the size of the polymer coil). The ratio R/R_G could be used to predict the amount of polymer unwinding. As the ratio increased (that is, the fiber radius increased) then the properties of the fiber will be like that of the bulk polymer. This can be seen in Figure 7.1a where the fiber radius is close to that of the R_G. Additionally, in Figure 7.1b there is a much larger radius and as such only the fiber walls see any sort of unwinding.

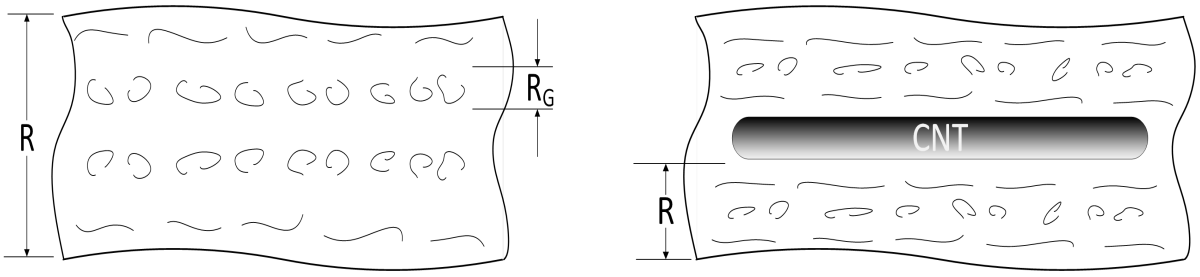

Figure 7.1: Molecular orientation diagram where the ratio of R/R_G is what will determine the molecular orientation. In (a) the fiber diameter is much larger, therefore only unwinding occurs at the edges of the fiber. The addition of CNT's in (b) allows for an additional interface to add shear force and unwind the molecular chain.

The addition of CNT's plays an important role in the molecular orientation as in the case seen in Figure 7.1b where the CNT acts as an additional interface. The CNT's will align with the fiber axis and provide an area of local shear forces which will allow for thicker fibers

to have more molecular alignment.

7.1 Carbon Nanotubes and Dielectrophoresis

Carbon Nanotubes (CNT) have long been added to various polymers during electrospinning to affect the nanofibers properties. Some common uses include the the increase in mechanical properties[82] and/or increasing electrical conductivity[186]. While the addition of CNT's into the CNF mats aided in these added properties, the larger reason is to be used for additional interfaces to increase the confinement effect and allow for thicker nanofibers to have aligned molecular chains[90].

During the electrospinning of a pure PAN solution (lacking CNT's), the solution is subjected to a uniform electric field. The addition of CNT's will introduce what is known as a dielectric phenomena. That is, the CNT's will cause local electric fields and thus the overall electric field would be non-uniform. A diagram of the Taylor region can be seen in Figure 7.2 with CNT's in the solution. Here the CNT's and polymer solution are being subjected to the electrostatic force. As the polymer jet forms, it will drag along the CNT.

As the CNT is being dragged by the polymer jet it will also be subjected to other forces as well. When any object moves through a fluid there will be a drag force in the opposite direction of motion. Here the CNT is being subjected to a drag force which will slow down the CNT relative to the polymer jet it is flowing in. As such this difference in velocity will cause a shear force to apply between the two. In addition, there will also be a force from the electric field known as a the dielectrophoretic force (F_{DEP}).

The dielectric field will induce a force which will act differently depending on the properties of the various elements inside the field. In the solution there are three elements with their own properties. There is the CNT's which were dispersed in a polymer, PAN, which is dis-

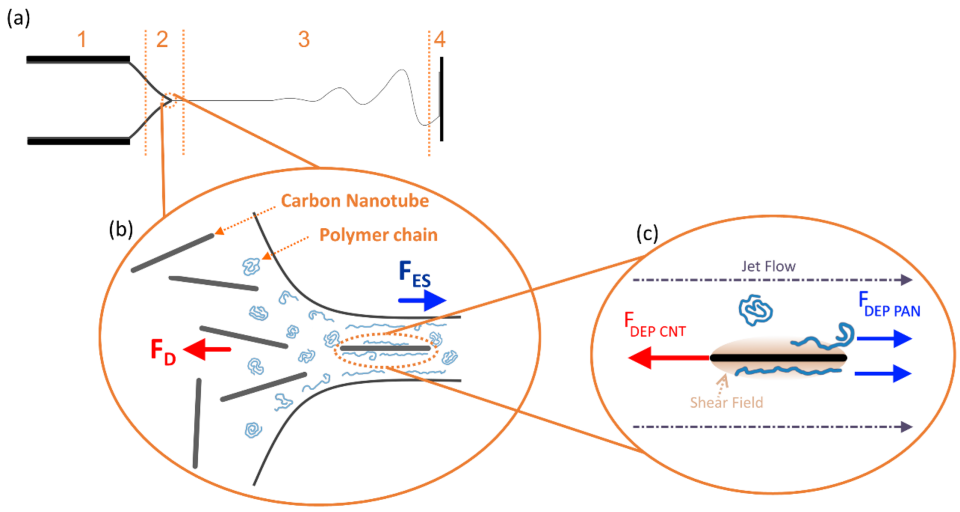

Figure 7.2: The effect of CNT's on unwinding the molecular chain of PAN. In the Taylor cone section, the electrostatic force is pulling and aligning the CNT's and polymer. As the polymer fiber narrows there is local shear fields against the surface of the CNT's. Figure adapted from Ref. [69]

solved in a solvent (DMF, Dimethylformamide). Key dielectrophoretic properties of these elements are listed in Table 7.1.

Table 7.1: Dielectrophoretic constants for PAN, CNT, and DMF (values obtained from Ghazinejad et al[69])

Material	CNT	PAN	DMF
Relative electrical permittivity, ϵ_r	$> 10^6 - j10^4$	5.5	36.7
Conductivity, $\sigma(S/m)$	10^5	10^{-11}	10^{-1}
Polarizability in DMF, $Re\{K\}$	+1	-0.395	N/A

From these properties the insight can be gained on the directions of various particles. The F_{DEP} occurs because the non-uniform electric field will induce a dipole moment. This will cause movement towards or away from the field's peaks based on the elements polarizability in its medium. This polarizability is given in Table 7.1 as the $Re\{K\}$ which is the real portion of the Clausius-Mossotti factor [17, 132, 192]. This Clausius-Mossotti factor is made up of the complex permittivities of the particle and the medium ($\tilde{\epsilon} = \epsilon - j\frac{\sigma}{\omega}$), where ϵ is the permittivity, σ is the conductivity, and ω is the angular frequency. The Clausius-Mossotti

factor can be calculated as seen in Eq. 7.1 where the subscripts "p" and "m" refer to the particle and medium respectively.

$$K(w) = \frac{\tilde{\epsilon_p} - \tilde{\epsilon_m}}{\tilde{\epsilon_p} + 2\tilde{\epsilon_m}} \tag{7.1}$$

The direction of the elements due to the F_{DEP} can then be seen in Eq. 7.2[147, 192, 69]:

$$F_{DEP} \propto \tilde{\epsilon_m} Re\{K(w)\} \nabla E^2 \tag{7.2}$$

Where ∇E^2 is the gradient of the electric field (calculated as the root-mean-square, rms). By using the values from Table 7.1 the direction of the F_{DEP} force on the CNT's are in the opposite direction of that from the polymer flow and away from the collector. This F_{DEP} and the drag increase the shear forces experienced on the polymer chain helping to unwind it. These forces are displayed in Figure 7.2. Although CNT's are ideal in this scenario, it may be desirable to replace them with a less expensive nanostructure so long as that nanostructure has dimensions smaller then that of the polymer jet and the polarizability is opposite than that of the polymer in the solvent. This should be investigated in future research.

Once the molecular alignment has been achieved via the above mechanisms then it must be maintained. When the solvent is fully evaporated the molecular orientation will be fixed. Prior to carbonization the polymer must be stabilized so cross-linking can occur between the polymer chains. In this process there is the potential for curling of the molecular chains and many of the gains from electrospinning could be lost.

7.2 Mechanically Stressed Polymer Stabilization

Prior to the pyrolysis step the PAN nanofibers need to undergo the process of stabilization. This process seems simple as it is the heat treatment of the polymer at ambient air pressure. It should be noted that the chemistry and reactions occurring in this process are complicated and still debated[149]. The crucial purpose of this process is to prepare the polymer for pyrolysis. During stabilization the PAN molecules undergo cross-linking[44] between neighboring atoms. This ladder causes the PAN to be more stable as the C≡N become C=N. The remaining bond will then form the cross-links between molecules of PAN as seen in Figure 7.3a.

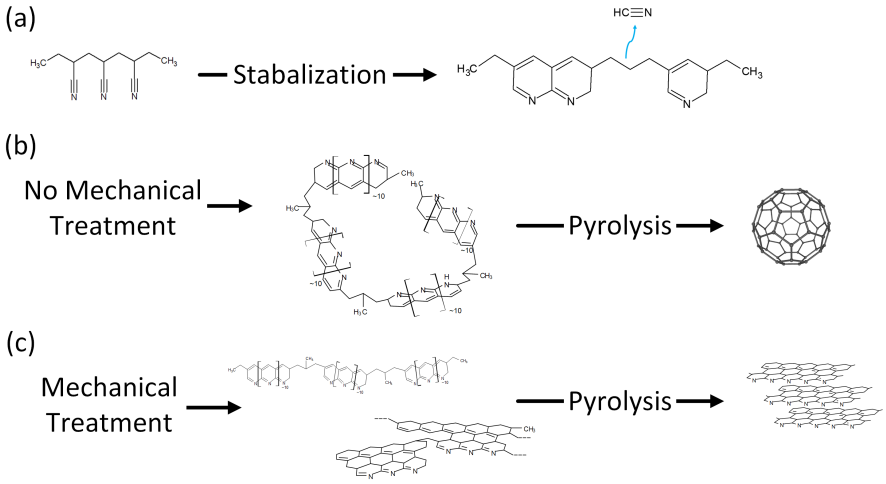

Figure 7.3: PAN stabilization (a) simplified PAN stabilization schematic. (b) When there is no mechanical treatment there can be a tendency to curl up which will lead to fullerene like structures after pyrolysis. (c) Alternatively, if there is mechanical treatment it can prevent the curling of the polymer chain which will help in the formation of graphitic structures after pyrolysis. Figure adapted from Ref. [69]

This formation of a ring is known as cyclization. In this process the undesirable sp^3 bonds are formed. The polymer chain will have a tendency to bend and curve. During pyrolysis this will result in penta- and hepta- carbon rings[69] as is seen in Figure 7.3b. Depending on the temperature of pyrolysis this could form either amorphous carbon or fullerenes. Once fullerenes are formed they become very difficult to break even at high temperatures.

This aspect of PAN is what has made it be called "non-graphitizing" since it will remain amorphous.

Ideally, the more sp^2 bonds which will lead to a more graphitic nature. During the heat treatment of stabilization, the fibers will tend towards curling up. By adding a mechanical compressive force, such as pressure, this is theorized to prevent the curling. From this conclusion there may be other methods of maintaining the gains from electrospinning beyond mechanical compressive force. With the polymer locked in place after stabilization then there will be less sp^3 bonds being formed and more sp^2 bonds, thus a more graphitic structure.

Chapter 8

Sensing Applications

The carbon nanofibers presented here with high graphitic content present the opportunity for many applications. A major area and the focus of this work is that of electrochemical devices. One of the simplest to prove is the area of sensing, that is where a voltage or current is applied to the electrode. This results in a current or voltage, respectively, which is produced via the electrochemical reaction occurring. The signal can then potentially be used to determine the type and quantity of a substance in the environment. Additionally, many other devices exist which could be found to have an advantage for using graphitic nanofibers. Sensing proves to be one of the simpler electrochemical devices to set up and as such it is one of the first applications to be attempted. Various analytes where tested, starting with hydrogen peroxide (H_2O_2).

8.1 Determination of Hydrogen Peroxide in a Solution

Hydrogen peroxide is an extremely important substance that can be found in everything from biochemistry to industrial products (such as in the paper, electronics, textile, wastewater,

or many others[29]). In terms of biochemistry, the hydrogen peroxide can be a product of many reactions and be used to indirectly monitor a substance. Its generation (and subsequent measuring) has been found to be a useful and accurate way in determining levels of important biological chemicals such as glucose, lactate, cholesterol, and many others[191]. As such, the ability to sense hydrogen peroxide is a very sought-after tool that has been accomplished using many methods.

The history of electrochemical sensing of hydrogen peroxide can arguably starts with enzymatic electrodes. Initially proposed by Clark et al[39], an enzyme will catalyze a reaction on the electrodes surface. A glucose sensor was able to me made by Updike et al[181] which determined glucose levels directly by attaching the enzyme glucose oxidase (GOx) to a gel on an oxygen electrode. When GOx and oxygen contacts with glucose it is reduced into hydrogen peroxide and gluconic acid. There will be a measurable current that is directly correlated to the amount of glucose in the system being measured. While there have been many generations of improvements to enzymatic sensors there are still some downsides such as the stability of the enzyme[141]. Even the most stable enzymes will be affected by various elements such as thermal fluctuations (as might be seen when being stored). Additionally, there is an innate complexity to electrode fabrication as the enzyme must be immobilized on the electrode. As such alternative sensing mechanisms have been investigated such as non-enzymatic electrodes. This is typically done via metals such as platinum and gold[36]. Here nanometal particles are placed on a conductive substrate (such as glass-like carbon) and act as a electrocatalyis for hydrogen peroxide. Metal based sensors have proven to be very capable but tend to be expensive. In the search for alternatives the carbon nanofiber as an electrode from the previous sections has shown promise in electrocatalyis for hydrogen peroxide and thus sensing.

8.1.1 Theory of Hydrogen Peroxide Sensing

There have been many studies on the active areas of nitrogen-doped carbons in their ability for electrocatalysis. The form of nitrogen takes on in the doped carbon can determine the electrochemical properties and as such is important to understand when optimizing the carbon structure. It has been shown that in regard to oxygen reduction the graphitic-N would enhance electron transfer because of the higher electronegativity of nitrogen compared with carbon. This will cause carbon to donate electrons to the nitrogen which would in turn back-donate an electron to an adjacent carbon causing an increase in current density[49, 105]. As such there will be enhanced charges of the carbons next to nitrogen when compared with a defect free graphene[197]. Alternatively, there are pyridinic-N sites which, because located on an edge plane, will have the nitrogen directly interact with the analyte using the nitrogen's lone electron. This in turn can cause the onset potential to be more positive[3].

when turning specifically to hydrogen peroxide the addition of nitrogen allows it to once again react differently depending on the surface of the carbon structure. For pyridinic-N and pyrrolic-N structures it was shown via modeling that they show stronger adsorption when compared to graphitic-N or pristine graphene[3]. This adsorption is based on a physisorption model. The O——O bonds in H_2O_2 can be broken in two different manners. In one the bond breaks into an a H^+, H_2O, and OH where the OH will stay bound to the carbon. In the second option the O——O bond will break into two OH groups which are both bonded to the carbons surface. The nitrogen doping can then facilitate the weakening of this bond[204]. The steps of hydrogen peroxide reduction have been broken down as two steps as seen here Equations 8.1 and 8.2[130, 81].

$$H_2O_2 + e^{-1} \rightarrow OH_{ad} + OH^- \tag{8.1}$$

$$OH_{ad} + e^{-1} \rightarrow OH^{-} \tag{8.2}$$

With thees two steps then cumulate with the net reaction seen in Equation 8.3 [182].

$$H_2O_2 + 2H^{+} + 2e^{-1} \rightarrow 2H_2O \tag{8.3}$$

8.1.2 Sensitivity and Limit of Detection of Hydrogen Peroxide

To demonstrate the ability of the mechanically treated CNF electrodes (PAN-CNT-M) to reduce hydrogen peroxide, electrochemical cyclic voltammetry and chronoamperometry were performed. Cyclic voltammetry (CV) was carried out to investigate the aptitude of the PAN-CNT-M electrodes in reduction and it was compared against other electrodes including a commercially available Toray® graphitic paper and a pure PAN CNF electrode. Phosphate Buffered Saline (PBS) was used as the background electrolyte since it will help mimic biological systems and will help eliminate effects from pH differences. Initially EIS was conducted and the active surface area was found so that the following results could be normalized and thus more easily compared. All results are thus viewed against the current density (A/cm^2).

In initial tests it was seen that hydrogen peroxide and oxygen will have very similar reduction peaks and as such it would be difficult to determine which is being reduced. As such all test cells were purged with nitrogen gas. A CV (not shown) was run in a blank solution of 1X PBS to determine the appropriate time for nitrogen purging for our testing. The time required to minimize the oxygen reduction peak was seen to be adequate after 20 min. In Figure 8.1a there is a comparison of the same PAN-CNT-M electrode run in a blank

electrolyte and then with the addition of 2.5 mM of H_2O_2 there is a very clear beak from the reduction current observed. This helps to confirm the removal of oxygen from the solution. There is still seen a small peak for the 1X PBS experiment which could be attributed to residual oxygen in the test cell. This provides further evidence that he electrode performs oxygen reduction.

The next CV was performed for the PAN-CNT-M electrode, a pure PAN electrode, and a Toray electrode in Figure 8.1b. All the electrodes were prepared in the same manner as described in Section 4.1. The results from the CV help to further demonstrate the increased performance of the PAN-CNT-M electrode. It is expected that the Toray electrode would show little electocatalysis as it is mostly graphitic structure lacking any nitrogen heteroatoms. Additionally, the Pure PAN electrode also demonstrates poor performance. This can be attributed to the amorphous nature of the CNF mat. Finally, the electrode with the largest signal is the PAN-CNT-M electrode. It is very clear from Figure 8.1b that the PAN-CNT-M sample shows the largest amount of reduction as well as the onset potential is increased compared to the other electrodes. This corresponds with what is seen in literature [49, 105] for graphitic N-doped materials.

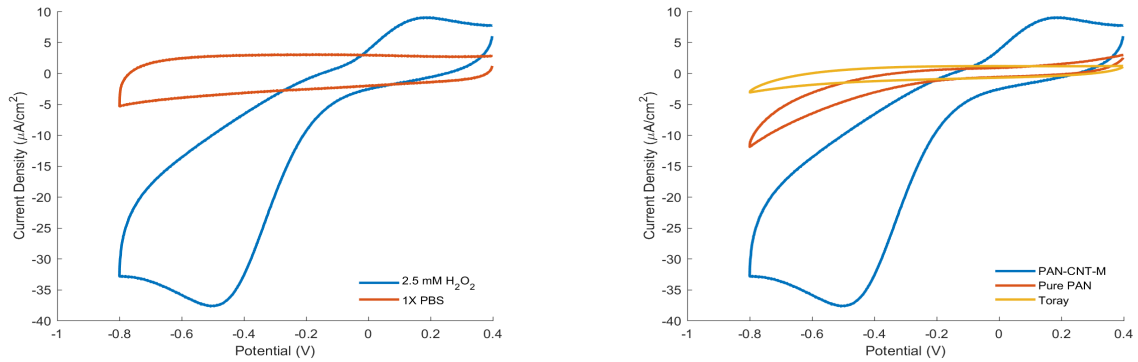

(a) **(b)**

Figure 8.1: Cyclic voltammogram of the various CNF mats run at 50 mV/s vs Ag/AgCl. (a) The PAN-CNT-M electrode tested in 1X PBS and in 2.5mM H_2O_2; (b) Electrodes of PAN-CNT-M, Pure PAN, and Toray in 2.5mM H_2O_2 Figure from Pollack et al[148]

From the Cyclic voltammogram of PAN-CNT-M there is the reduction peak seen when the

current density is at a maximum. This can be seen from Figure 8.1b at -0.5V vs Ag/AgCl. As such this was the potential chosen to run chronoamperometry (CA) which was used to better understand the electrodes sensitivity and lower limit of detection (LOD).

The use of CA would help determine the electrodes response to the carious additions of the H_2O_2 being added. Once the CA was started the current additions of H_2O_2 were added in fixed concentrations. The concentrations were added as 5, 10, 20, 100, 200, and 400 μM which summed up to a total concentration of about 2.5 mM H_2O_2. Each addition of H_2O_2 was added after the current stabilized from the previous addition and each concentration was added three times. The results as well as a calibration curve is shown in Figure 8.2.

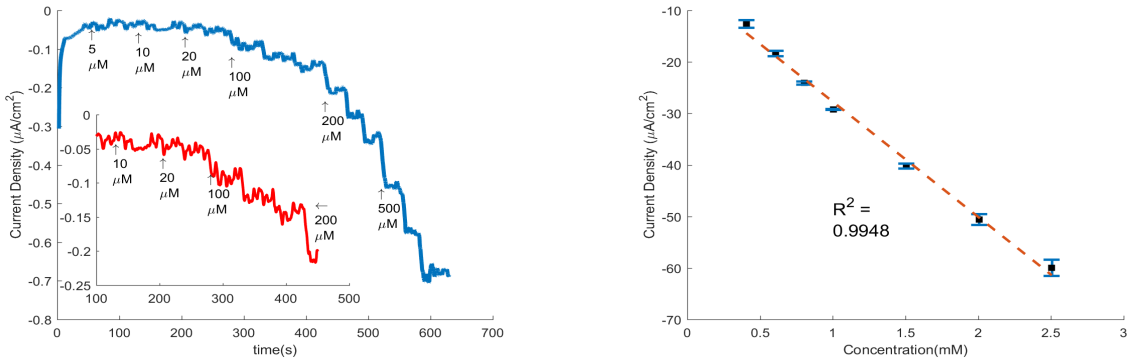

(a) **(b)**

Figure 8.2: (a) Chronoamperometry at -0.5 V vs Ag/AgCl of the PAN-CNT-M electrode and its response to the addition of H_2O_2 at the indicated concentrations. The inset plot is a zoomed in portion. The results were plotted as a standard curve (b) as concentration vs current density. Figure from Pollack et al [148]

From the CA plot in Figure 8.2a there can be seen an increase in current at right around the concentration of 20 μM, although more clearly at around 100 μM. At these insertions it can be seen that the change in current is larger than the noise of the system. As expected the increasing concentrations of H_2O_2 would result in a larger increase in current response where by the 100 μM additions the step response is very well defined. By looking at these step responses an average response time of about 4.6 seconds can be observed. The response time was calculated manually from the point of insertion of the analyte to the point of

stabilization. Various times were calculated and averaged out. From each step in Figure 8.2a the current vs concentration can then be plotted to make a calibration curve as was done in Figure 8.2b. To find the sensitivity a linear regression curve was calculated, and the slope was used. This can be seen in Equation 8.4.

$$I = -2.54C - 0.604 \tag{8.4}$$

Here I is the current density in $\frac{\mu A}{cm^2}$ and the concentration is C in mM. This results in a sensitivity of 2.54 $\frac{\mu A}{mM*cm^2}$ and a correlation coefficient (R^2) of 0.9948. The limit of detection (LOD) could then be calculated using Equation 4.3 on page 59 which would result in a LOD of 0.609 μM. The results are compared with other carbon-based sensors and tabulated in Table 8.1. Here it can be seen that the PAN-CNT-M electrodes produce very competitive results when compared to the other electrodes. A large advantage of the PAN-CNT-M electrode is its simplicity in fabrication where other carbon based sensors are using difficult to produce materials such as reduced graphene oxide (rGO) and/or expensive metals including gold (Au).

Table 8.1: Comparison of sensitivity of and LOD of various carbon based sensors on hydrogen peroxide

Material	Sensitivity ($\frac{\mu A}{mM*cm^2}$)	LOD (μM)	Reference
PAN-CNT-M	2.54	0.609	This work
Graphene–Carbon Nanotube Composite	32.91	9.4	[196]
rGO grafted with Aminothiophenol-Pd Nanoparticles	492.09	0.016	[210]
Graphene Oxide and Electrospun NiO Nanofibers	1100	0.77	[216]
Gold Nanoparticles on Nitrogen-Doped Graphene	186.22	0.12	[93]
Au-Nanoparticle/Polyoxometalate/Graphene Nanohybrids	58.87	1.54	[112]
MnO_2 Nanotubes/rGO Nanocomposite	194.5	1.29	[122]

The above tests were conducted in ideal conditions with precisely controlled concentrations. For a sensor to be useful it must being not only be sensitive but also selective. In practical applications there will be more than simply the desired analyte in the environment that is to be measured. As such some common substances should be tested to measure interference with that of H_2O_2. If another substance reduces at a potential near that of hydrogen peroxide, then it could add to the current response that is measured and give a false reading of the quantity of determined in the solution. To measure this potential interference chronoamperometry was conducted and additions of 1 mM H_2O_2, 0.15 mM Absorbic Acid (AA), 1mM Glucose (Glu), 0.5 mM Uric Acid (UA), and 1 mM H_2O_2 was added. Each addition was added only after the current had stabilized. The results are shown in Figure 8.3 where it can be seen that the only major change in response is because of the H_2O_2 additions. When the other analytes are added the only current response could be attributed to that of noise from the physical action of adding a solution into the test cell. This helps demonstrate the high selectivity of the PAN-CNT-M electrode in regard to detecting H_2O_2.

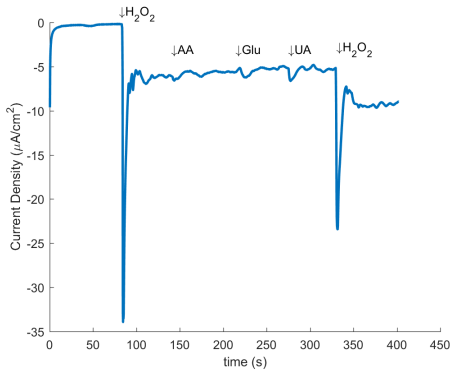

Figure 8.3: Chronoamperometry test to show the response of the PAN-CNT-M to 1 mM H_2O_2, 0.15 mM AA, 1mM Glu, 0.5 mM UA, and 1 mM H_2O_2 again. The potential is -0.5V vs Ag/AgCl. Figure from Pollack et al [148]

8.2 Other Analytes

The sensing of hydrogen peroxide is simply a case study of one analyte. In the interference test in Figure 8.3 various other substances where shown to have no effect on the overall current response from when at the -0.5V potential. This does not necessarily imply that these substances cannot be reduced by the electrode. Running a CV over a wide range of potentials allows for the determination for what potential is needed for each substance (if it even exists). In Figure 8.4 a cyclic voltammetry was performed with a potential window of -0.2 to 0.6 V in a 1X PBS solution with 2.5 mM of Ascorbic Acid (AA), Dopamine (DA), and Uric Acid (UA).

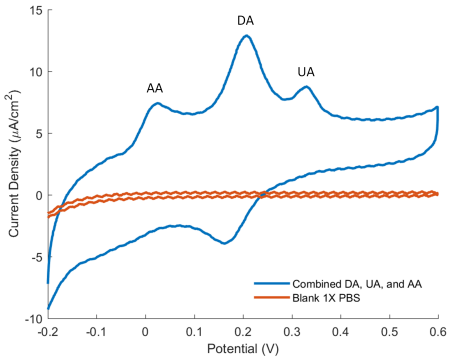

Figure 8.4: Cyclic voltammogram at 50 mV/s of a PAN-CNT-M electrode in the presence of Ascorbic Acid (AA), Dopamine (DA), and Uric Acid (UA)

From this figure there are three distinguished peaks that are labeled with their corresponding analyte respectively. This demonstrates the PAN-CNT-M sample's ability to reduce these analytes and subsequent chronoamperometry could be run at the potentials of 23, 207, and 330 mV for the AA, DA, and UA analytes respectively. The same procedure as what was done for the hydrogen peroxide could be completed to characterize the PAN-CNT-M electrode in terms of sensitivity and LOD. Interference tests should be run as well as some of the peaks may be interfering and distorting the signal such as the DA an UA peaks. Deconvolution methods could also potentially be used to separate the signals. This experiment also opens the possibility of sensing multiple substances with the electrode by switching potentials.

Other electrochemical techniques could be employed to sense other substances. A common technique could include stripping voltammetry[24] which has been used to detect extremely small concentrations of metals such as lead. In this technique the electrode is placed in a solution containing the metal to be detected. A pre-concentration step occurs where a current is run, and the metal will plate the electrode. After sufficient time there will be a stripping step where the current is reversed, and the metal coating is stripped off which causes cause an exchange of an electron. The peak potential will be indicative of what substance was stripped off while the current will provide insight to the concentration of said substance.

Chapter 9

Looking Forward

9.1 Insight into Current Work

Carbon structures are an exciting area of research with applications in an extremely wide range of fields from mechanical structures [113], electronics [188], energy generation [208], energy storage[206], electrochemical detection [148], and many more applications. Carbon can be presented in many forms and fabricated via many routes. A very popular route involves the pyrolysis of a polymer precursor to decompose the non-carbon molecules. Via this route one of the most popular precursors arouse as Polyacrylonitrile (PAN)[62]. The PAN precursor has been demonstrated to be used in each one of the applications stated above. One of the major issues with PAN is it is known as non-graphitizable[79]. As such PAN structures will either form glassy carbon or will need to be pyrolyzed at extremely high temperature such as 3000 °C[104]. The issue with high temperature pyrolysis involves both cost of equipment as well as at high temperatures the carbon will result in no remaining heteroatoms[218]. If heteroatoms are desired, they will need to be added via a doping post-process. Here a solution is shown to fabricate graphitic carbon from PAN at relatively low

temperatures (1000 °C). From this lower temperature the carbon was able to retain the content of heteroatoms such as nitrogen without any additional post-processing steps. The addition of nitrogen presents many advantages in carbon in both structural increases[98] as well as electrocatalytic properties[205].

To accomplish the task of low temperature pyrolysis of PAN towards graphitic carbon, a PAN solution was electrospun onto a rolling drum to produce a continuous randomly oriented nanofiber mat. The forces of electrospinning, the diameter of the fiber, and the addition of carbon nanotubes (CNT) caused the molecular chains of PAN to unwind and align as they collect onto their target. This unwinding is thought to be typically lost when PAN is cross-linked via stabilization. To maintain the molecular alignment mechanical stress was applied to the nanofiber mats before and during the stabilization process. Finally, when the PAN nanofiber mats were pyrolyzed the aligned molecular fibers allowed the carbon to be formed with graphitic planes rather than curl up into fullerenes and become glass-like carbon.

The graphitic nature of the PAN carbon nanofiber mats (CNF) was shown via the utilization of various characterization techniques. Conductivity measurement was performed with a four-probe setup that showed the mechanically treated PAN CNF (PAN-CNT-M) had a conductivity of over 33 times more than a simple PAN CNF. Raman spectroscopy was also utilized to show about a 20% decrease in disorder in the PAN-CNT-M samples when looking at the I_D/I_G peak ratios. Additionally, TEM was performed to look at the microstructure where there is a very noticeable increase in the graphitic planes. Finally, XPS was able to confirm the existence of nitrogen groups in the carbon structure as well as a large increase in the graphitic nitrogen's when compared to the pure PAN samples.

The benefits of the graphitic nature and presence of nitrogen were shown via electrochemical testing. Electrochemically active surface areas were able to be determined using EIS. This showed an almost twofold increase in the electrochemically active surface area between the PAN-CNT-M and a pure PAN electrode. This potentially translated to better heterogeneous

electron transfer rates as tested with ferri/ferrocynaide via cyclic voltammetry. The PAN-CNT-M demonstrated an almost eleven-fold improvement in these kinetics. Additionally, there was increased adsorption of ferri/ferrocynaide on the PAN-CNT-M electrodes as well. These improved properties of the PAN-CNT-M electrodes helps to further demonstrate the improved graphitization of the PAN electrode.

From these improved properties and the nitrogen function groups it became apparent that the PAN-CNT-M electrodes would show promise for hydrogen peroxide reduction and thus as a sensor. Cyclic voltammetry and chronoamperometry were performed to demonstrate and characterize the PAN-CNT-M electrode as a sensor. From these experiments a sensitivity of 2.5 $\frac{\mu A}{mM*cm^2}$ and a limit of detection of 0.609 μM was determined which are very competitive results when compared with other carbon based hydrogen peroxide sensors. Many of these competitive sensors involve much more complicated and expensive fabrication steps, some involve graphene and rare metals such as gold. Hydrogen peroxide sensing is simply one application possibility of the PAN-CNT-M electrode. The electrode showed good selectivity with other common biological chemicals such as dopamine. There are many other potential applications where the PAN-CNT-M material could show good potential.

9.2 Potential Applications

Beyond the sensing application shown in Chapter 8 there are other functions the mechanically treated carbon nanofiber mats could be used in. While not an exhaustive list, there has been enough data presented to suggest that using the CNF mats for energy generation in a fuel cell could potentially replace expensive materials such as platinum. Additionally, the CNF mat could be used in energy storage in the form of a super-capacitor.

9.2.1 Fuel Cells

In the world of energy generation fuel cells look like a promising path forward compared to traditional thermal methods. Typically, electricity is generated via mechanical work being converted into electrical. A gas-powered generator (such as an internal combustion engine or a gas turbine) will utilize chemical energy that it combusts. This combustion is transformed into mechanical work in mechanisms such as a crank shaft or a turbine. The mechanical work will then be used to generate electricity. Along this process there is a lot of waste energy. A fuel cell simplifies this process greatly and thus is more efficient by extracting electrical energy directly from a fuel via electrochemistry. In a simple fuel cell there is a anode which may have hydrogen flowing thought it and a cathode which could have oxygen (from air) flowing. They are separated by an electrolyte and a proton exchange barrier (which is a membrane where only protons can pass). Hydrogen will be flowed into the fuel cell where it will it is oxidized. This splits the hydrogen into a proton (H^+) and an electron (e^-). The electron is then flowed to power a load as well as to the opposite electrode where it reduces the oxygen with the proton to produce water as waste. This is known as a Proton exchange membrane (PEM) fuel cell. In both sides of the fuel cell there are catalysts which typically are made of expensive platinum. A musch researched area is to replace the platinum with a material such as carbon. From Chapter 8, it was discussed that with the hydrogen peroxide reduction there was also strong electrocatalytic ability to reduce oxygen as well. The reduction of oxygen is a much-studied area in fuel cells known as the oxygen reduction reaction (ORR)[213]. In addition to using oxygen on the cathode there have been research as using hydrogen peroxide[3]. Beyond the generation of energy via a device such as a fuel cell, the carbon naonfiber mats present the opportunity to be used in the energy storage.

9.2.2 Energy Storage

With the generation of energy, a way to store it is critical. Typically, this is done via batteries or in capacitors. The main difference in the two is the method of storing energy. A battery is an electrochemical device that stores the electrical energy in chemical form while a capacitor will store the energy as an accumulation of charge (via an electric field). The carbon nanofiber mats can be utilized in both applications.

Capacitors

Capacitors are a common electrical device used in almost every piece of electronics used today. A capacitor is made up of two conductors that are separated by an dielectric (insulating) material. Electrical charge will accumulate on the conducting plate in what is known as capacitance. The level of capacitance is inversely proportional to that of the gap between the conductors and as such the smaller the gap the higher the capacitance. The common capacitor used in electronic devices is the electrolytic capacitors which can be made between a metal foil sandwiched around a thin dielectric. To increase the capacitance to much larger values (such that it becomes a super-capacitor) the phenomena of the electric double layer can be utilized which would place the gap on the order of nanometers. The carbon nanofiber mats (CNF) have a very high surface area compared to their flat analogs which has been shown to increase the specific capacitance[115]. Additionally, the various heteroatoms such as oxygen and nitrogen have been shown to increase the capacitance of carbon materials[139, 202, 213].

Bibliography

[1] K. Akagi, M. Nishiguchi, H. Shirakawa, Y. Furukawa, and I. Harada. One-dimensional conjugated carbyne - synthesis and properties. *Synthetic Metals*, 17(1-3):557–562, 1987.

[2] S. Al Khabouri, S. Al Harthi, T. Maekawa, Y. Nagaoka, M. E. Elzain, A. Al Hinai, A. Al-Rawas, A. Gismelseed, and A. A. Yousif. Composition, Electronic and Magnetic Investigation of the Encapsulated ZnFe2O4 Nanoparticles in Multiwall Carbon Nanotubes Containing Ni Residuals. *Nanoscale Research Letters*, 10(1):262, 2015.

[3] S. J. Amirfakhri, D. Binny, J. L. Meunier, and D. Berk. Investigation of hydrogen peroxide reduction reaction on graphene and nitrogen doped graphene nanoflakes in neutral solution. *Journal of Power Sources*, 257:356–363, 2014.

[4] K. Angoni. Remarks on the structure of carbon materials on the basis of Raman spectra. *Carbon*, 31(4):537–547, 1993.

[5] J. Antal Michael Jerry and G. Varhegyi. Cellulose Pyrolysis Kinetics: The Current State of Knowledge. *Ind. Eng. Chem. Res.*, 34(3):703–717, 1995.

[6] J. Anu Bhushani and C. Anandharamakrishnan. Electrospinning and electrospraying techniques: Potential food based applications. *Trends in Food Science and Technology*, 38(1):21–33, 2014.

[7] A. Arinstein. Confinement mechanism of electrospun polymer nanofiber reinforcement. *Journal of Polymer Science, Part B: Polymer Physics*, 51(9):756–763, 2013.

[8] M. Armand and J.-M. Tarascon. Building better batteries. *Nature*, 451(7179):652–657, 2008.

[9] N. Arora and N. N. Sharma. Arc discharge synthesis of carbon nanotubes: Comprehensive review. *Diamond and Related Materials*, 50:135–150, 2014.

[10] P. Avouris. Molecular electronics with carbon nanotubes. *Accounts of Chemical Research*, 35(12):1026–1034, 2002.

[11] A. Baji, Y. W. Mai, S. C. Wong, M. Abtahi, and P. Chen. Electrospinning of polymer nanofibers: Effects on oriented morphology, structures and tensile properties. *Composites Science and Technology*, 70(5):703–718, 2010.

[12] A. J. Bard and L. R. Faulkner. *ELECTROCHEMICAL METHODS*, volume 2. wiley, 2000.

[13] R. H. Baughman, A. a. Zakhidov, and W. a. de Heer. Carbon nanotubes — the route toward applications. *Science*, 297(5582):787–92, 2002.

[14] R. Beams, L. Gustavo Cançado, and L. Novotny. Raman characterization of defects and dopants in graphene. *Journal of Physics: Condensed Matter*, 27(8):083002, 2015.

[15] F. Béguin, K. Szostak, G. Lota, and E. Frackowiak. A Self-Supporting Electrode for Supercapacitors Prepared by One-Step Pyrolysis of Carbon Nanotube / Polyacrylonitrile Blends. *Advanced Materials*, 17:2380–2384, 2005.

[16] E. Bekyarova, Y. Ni, E. B. Malarkey, V. Montana, L. Jared, R. C. Haddon, V. Parpura, J. L. McWilliams, R. C. Haddon, and V. Parpura. Applications of carbon nanotubes in biotechnology and biomedicine. *Journal of biomedical nanotechnology*, 1(1):3, 2005.

[17] L. Benguigui and I. J. Lin. More about the dielectrophoretic force. *Journal of Applied Physics*, 53(2):1141–1143, 1982.

[18] B. Bhushan, B. K. Gupta, G. W. Vancleef, C. Capp, and J. V. Coe. Fullerene (C-60) Films for Solid Lubrication. *Tribology Transactions*, 36(4):573–580, 1993.

[19] A. Bianco, K. Kostarelos, and M. Prato. Applications of carbon nanotubes in drug delivery. *Current Opinion in Chemical Biology*, 9(6):674–679, 2005.

[20] P. Błoński, J. Tuček, Z. Sofer, V. Mazánek, M. Petr, M. Pumera, M. Otyepka, and R. Zboil. Doping with Graphitic Nitrogen Triggers Ferromagnetism in Graphene. *Journal of the American Chemical Society*, 139(8):3171–3180, 2017.

[21] L. Bokobza, J. L. Bruneel, and M. Couzi. Raman spectroscopy as a tool for the analysis of carbon-based materials (highly oriented pyrolitic graphite, multilayer graphene and multiwall carbon nanotubes) and of some of their elastomeric composites. *Vibrational Spectroscopy*, 74:57–63, 2014.

[22] A. S. Bondarenko and G. A. Ragoisha. EIS Spectrum Analyser.

[23] S. Boopathi, T. N. Narayanan, and S. Senthil Kumar. Improved heterogeneous electron transfer kinetics of fluorinated graphene derivatives. *Nanoscale*, 6(17):10140–10146, 2014.

[24] A. Bott. Stripping Voltammetry, 1993.

[25] C. Boys. LVII. On the production, properties, and some suggested uses of the finest threads. *Philosophical Magazine Series 5*, 23(145):489–499, 1887.

[26] D. A. C. Brownson and C. E. Banks. *The Handbook of Graphene Electrochemistry*. Springer London, 2014.

[27] D. a. C. Brownson, D. K. Kampouris, and C. E. Banks. *Graphene electrochemistry: fundamental concepts through to prominent applications*, volume 41. 2012.

[28] L. D. Burke and P. F. Nugent. The electrochemistry of gold: I the redox behaviour of the metal in aqueous media. *Gold Bulletin*, 30(2):43–53, 1997.

[29] J. M. Campos-Martin, G. Blanco-Brieva, and J. L. Fierro. Hydrogen peroxide synthesis: An outlook beyond the anthraquinone process, 2006.

[30] G. Canton. *Development of Electro-Mechanical Spinning for Controlled Deposition of Carbon Nanofiber*. PhD thesis, University of California, Irvine, 2014.

[31] G. Canton, L. Kulinsky, and M. J. Madou. Electro-Mechanical Spinning: A new manufacturing technique for micro/nano-fabrication of carbon fibers. *Proceedings - International Symposium on Advanced Packaging Materials*, 4(Paper 9):230–239, 2013.

[32] Y. Cao, H. Yu, J. Tan, F. Peng, H. Wang, J. Li, W. Zheng, and N. B. Wong. Nitrogen-, phosphorous- and boron-doped carbon nanotubes as catalysts for the aerobic oxidation of cyclohexane. *Carbon*, 57:433–442, 2013.

[33] G. Centi and S. Perathoner. Carbon nanotubes for sustainable energy applications. *ChemSusChem*, 4(7):913–925, 2011.

[34] F. Cervantes-Sodi, G. Csányi, S. Piscanec, and A. C. Ferrari. Edge-functionalized and substitutionally doped graphene nanoribbons: Electronic and spin properties. *Physical Review B - Condensed Matter and Materials Physics*, 77(16):1–13, 2008.

[35] C. Y. Chang-Chien, C. H. Hsu, H. P. Lin, C. Y. Tang, and C. Y. Lin. Synthesis of porous carbon and silica spheres using PEO-PF polymer blends. *Journal of Porous Materials*, 13(3):195–199, 2006.

[36] S. Chen, R. Yuan, Y. Chai, and F. Hu. Electrochemical sensing of hydrogen peroxide using metal nanoparticles: A review. *Microchimica Acta*, 180(1-2):15–32, 2013.

[37] S. Y. Chou, P. R. Krauss, and P. J. Renstrom. Imprint Lithography with 25-Nanometer Resolution. *Science*, 272(5258):85–87, 1996.

[38] A. Chuvilin, U. Kaiser, E. Bichoutskaia, N. A. Besley, and A. N. Khlobystov. Direct transformation of graphene to fullerene. *Nature Chemistry*, 2(6):450–453, 2010.

[39] L. C. Clark and C. Lyons. Electrode systems for continuous monitoring in cardiovascular surgery. *Annals Of The New York Academy Of Sciences*, 102(1):29–45, 1962.

[40] K. K. Cline, M. T. Mcdermott, and R. L. Mccreery. Anomalously Slow Electron Transfer at Ordered Graphite Electrodes: Influence of Electronic Factors and Reactive Sites. *J. Phys. Chem.*, 98:5314–5319, 1994.

[41] F. C. Cowlard and J. C. Lewis. Vitreous Carbon - A New Form of Carbon. *J Mater Sci*, 2(507):507–512, 1967.

[42] A. Cuesta, P. Dhamelincourt, J. Laureyns, A. Martínez-Alonso, and J. M. Tascón. Raman microprobe studies on carbon materials. *Carbon*, 32(8):1523–1532, 1994.

[43] N. Daems, X. Sheng, I. F. J. Vankelecom, and P. P. Pescarmona. Metal-free doped carbon materials as electrocatalysts for the oxygen reduction reaction. *J. Mater. Chem. A*, 2(12):4085–4110, 2014.

[44] L. I. David and A. F. Ismail. Influence of the thermastabilization process and soak time during pyrolysis process on the polyacrylonitrile carbon membranes for O2/N2 separation. *Journal of Membrane Science*, 213(1-2):285–291, 2003.

[45] W. H. De Jong and P. J. A. Borm. Drug delivery and nanoparticles:applications and hazards. *International journal of nanomedicine*, 3(2):133–49, 2008.

[46] M. De Leo, A. Kuhn, and P. Ugo. 3D-ensembles of gold nanowires: Preparation, characterization and electroanalytical peculiarities. *Electroanalysis*, 19(2-3):227–236, 2007.

[47] M. F. L. De Volder, S. H. Tawfick, R. H. Baughman, and A. J. Hart. Carbon Nanotubes: Present and Future Commercial Applications. *Science*, 339(6119):535–539, 2013.

[48] J. Deitzel, J. Kleinmeyer, D. Harris, and N. Beck Tan. The effect of processing variables on the morphology of electrospun nanofibers and textiles. *Polymer*, 42(1):261–272, 2001.

[49] D. Deng, X. Pan, L. Yu, Y. Cui, Y. Jiang, J. Qi, W. X. Li, Q. Fu, X. Ma, Q. Xue, G. Sun, and X. Bao. Toward N-doped graphene via solvothermal synthesis. *Chemistry of Materials*, 23(5):1188–1193, 2011.

[50] R. J. Diefendorf. The deposition of pyrolytic graphite. *GENERAL ELECTRIC CO SCHENECTADY NY*, 60(No. RL-2432M), 1960.

[51] M. S. Dresselhaus and P. C. Eklund. Phonons in carbon nanotubes. *Advances in Physics*, 49(6):705–814, 2000.

[52] Y. Dror, W. Salalha, R. L. Khalfin, Y. Cohen, A. L. Yarin, and E. Zussman. Carbon nanotubes embedded in oriented polymer nanofibers by electrospinning. *Langmuir*, 19(17):7012–7020, 2003.

[53] B. Duan, X. Yuan, Y. Zhu, Y. Zhang, X. Li, Y. Zhang, and K. Yao. A nanofibrous composite membrane of PLGA-chitosan/PVA prepared by electrospinning. *European Polymer Journal*, 42(9):2013–2022, 2006.

[54] A. G. Dumanl and A. H. Windle. Carbon fibres from cellulosic precursors: a review. *J Mater Sci*, 47:4236–4250, 2012.

[55] A. Einstein. Concerning an heuristic point of view toward the emission and transformation of light. *Ann. Phys*, 17(132), 1905.

[56] C. P. Ewels and M. Glerup. Nitrogen Doping in Carbon Nanotubes. *Journal of Nanoscience and Nanotechnology*, 5(9):1345–1363, 2005.

[57] C. S. Fadley. X-ray photoelectron spectroscopy: Progress and perspectives. *Journal of Electron Spectroscopy and Related Phenomena*, 178-179(C):2–32, 2010.

[58] S. F. Fennessey and R. J. Farris. Fabrication of aligned and molecularly oriented electrospun polyacrylonitrile nanofibers and the mechanical behavior of their twisted yarns. *Polymer*, 45(12):4217–4225, 2004.

[59] A. C. Ferrari and D. M. Basko. Raman spectroscopy as a versatile tool for studying the properties of graphene. *Nature Publishing Group*, 8(4):235–246, 2013.

[60] A. C. Ferrari and J. Robertson. Interpretation of Raman spectra of disordered and amorphous carbon. *Physical Review B*, 61(20):14095–14107, 2000.

[61] E. Frackowiak. Carbon materials for supercapacitor application. *Physical Chemistry Chemical Physics*, 9(15):1774, 2007.

[62] E. Frank, F. Hermanutz, and M. R. Buchmeiser. Carbon fibers: Precursors, manufacturing, and properties. *Macromolecular Materials and Engineering*, 297(6):493–501, 2012.

[63] S. Frank. Carbon Nanotube Quantum Resistors. *Science*, 280(5370):1744–1746, 1998.

[64] R. E. Franklin. Crystallite Growth in Graphitizing and Non-Graphitizing Carbons. *Proceedings of the Royal Society of London A: Mathematical, Physical and Engineering Sciences*, 209(1097):196–218, 1951.

[65] A. FUJISHIMA and K. HONDA. Electrochemical Photolysis of Water at a Semiconductor Electrode. *Nature*, 238(5358):37–38, 1972.

[66] J. Gatford and Delv0n2. Electrospinning.

[67] A. K. Geim and K. S. Novoselov. The rise of graphene. *Nature Materials*, 6(3):183–191, 2007.

[68] D. Geng, Y. Y. Chen, Y. Y. Chen, Y. Li, R. Li, X. Sun, S. Ye, and S. Knights. High oxygen-reduction activity and durability of nitrogen-doped graphene. *Energy & Environmental Science*, 4(3):760, 2011.

[69] M. Ghazinejad, S. Holmberg, O. Pilloni, L. Oropeza-Ramos, and M. Madou. Graphitizing Non-graphitizable Carbons by Stress-induced Routes. *Scientific Reports*, 7(1):16551, dec 2017.

[70] A. Goel, J. B. Howard, and J. B. Sande. Size analysis of single fullerene molecules by electron microscopy. *Carbon*, 42(10):1907–1915, 2004.

[71] K. Gong, F. Du, Z. Xia, M. Durstock, L. Dai, D. R. Paul, W. J. Koros, R. Y. F. Liu, Y. S. Hu, E. Baer, A. Hiltner, H. D. Keith, R. Y. F. Liu, A. Hiltner, E. Baer, R. E. Cohen, A. Bellare, R. J. Albalak, W. Hu, and G. Reiter. Nitrogen-doped carbon nanotube arrays with high electrocatalytic activity for oxygen reduction. *Science*, 323(FEBRUARY):760–764, 2009.

[72] F. G. Gonon. Nonlinear relationship between impulse flow and dopamine released by midbrain dopaminergic neurons as studied by in vitro electrochemistry. *Neuroscience*, 24(1):19–28, 1988.

[73] J. J. Gooding. Nanostructuring electrodes with carbon nanotubes: A review on electrochemistry and applications for sensing. *Electrochimica Acta*, 50(15):3049–3060, 2005.

[74] R. Gopal, S. Kaur, Z. Ma, C. Chan, S. Ramakrishna, and T. Matsuura. Electrospun nanofibrous filtration membrane. *Journal of Membrane Science*, 281(1-2):581–586, 2006.

[75] B. Guo, Q. Liu, E. Chen, H. Zhu, L. Fang, and J. R. Gong. Controllable N-doping of graphene. *Nano Letters*, 10(12):4975–4980, 2010.

[76] S. Guo and S. Dong. Graphene nanosheet: synthesis, molecular engineering, thin film, hybrids, and energy and analytical applications. *Chemical Society reviews*, 40(5):2644–2672, 2011.

[77] T. Guo, C. Jin, and R. E. Smalley. Doping bucky: formation and properties of boron-doped buckminsterfullerene. *The Journal of Physical Chemistry*, 95(13):4948–4950, 1991.

[78] T. Han, A. L. Yarin, and D. H. Reneker. Viscoelastic electrospun jets: Initial stresses and elongational rheometry. *Polymer*, 49(6):1651–1658, 2008.

[79] P. J. F. Harris. Structure of non-graphitising carbons. *International Materials Reviews*, 42(5):206–218, 1997.

[80] P. Heide. *X-ray Photoelectron Spectroscopy: An Introduction to Principles and Practices*. John Wiley & Sons, Ltd, 2011.

[81] M. Honda, T. Kodera, and H. Kita. Electrochemical behavior of H2O2 at Ag in HClO4 aqueous solution. *Electrochimica Acta*, 31(3):377–383, 1986.

[82] H. Hou, J. J. Ge, J. Zeng, Q. Li, D. H. Reneker, A. Greiner, and S. Z. Cheng. Electrospun polyacrylonitrile nanofibers containing a high concentration of well-aligned multiwall carbon nanotubes. *Chemistry of Materials*, 17(5):967–973, 2005.

[83] Y.-Y. Huang, S. K. Sharma, R. Yin, T. Agrawal, L. Y. Chiang, and M. R. Hamblin. Functionalized Fullerenes in Photodynamic Therapy. *J Biomed Nanotechnol*, 10(9):1918–1936, 2014.

[84] Z. M. Huang, Y. Z. Zhang, M. Kotaki, and S. Ramakrishna. A review on polymer nanofibers by electrospinning and their applications in nanocomposites. *Composites Science and Technology*, 63(15):2223–2253, 2003.

[85] A. T. Hubbard, R. M. Ishikawa, and J. Katekaru. Study of platinum electrodes by means of electrochemistry and low-energy electron diffraction. *Journal of Electroanalytical Chemistry and Interfacial Electrochemistry*, 86(2):271–288, 1978.

[86] S. Iijima. Helical microtubules of graphitic carbon, 1991.

[87] L. G. Isaacs. The Graphitization of Organic Compounds: III. Heterocyclic Nitrogen Derivatives of Anthracene and Phenanthrene. *Carbon*, 8(1):118, 1966.

[88] A. Jaworek and A. T. Sobczyk. Electrospraying route to nanotechnology: An overview. *Journal of Electrostatics*, 66(3-4):197–219, 2008.

[89] G. M. Jenkins and K. Kawamura. Structure of glassy carbon. *Nature*, 231:175–176, 1971.

[90] Y. Ji, C. Li, G. Wang, J. Koo, S. Ge, B. Li, J. Jiang, B. Herzberg, T. Klein, S. Chen, J. C. Sokolov, and M. H. Rafailovich. Confinement-induced super strong PS/MWNT composite nanofibers. *EPL (Europhysics Letters)*, 84(5):56002, 2008.

[91] J.J.Kipling, J.N.Sherwood, P.V.Shooter, and N.R.Thompson. Factors influencing the graphitization of polymer carbons. *Carbon*, 1(3):315–320, 1964.

[92] A. Jorio, R. Saito, G. Dresselhaus, and M. S. Dresselhaus. *Raman Spectroscopy in Graphene Related Systems The Authors.* Wiley-VCH Verlag GmbH & Co. KGaA, 2011.

[93] J. Ju and W. Chen. In situ growth of surfactant-free gold nanoparticles on nitrogen-doped graphene quantum dots for electrochemical detection of hydrogen peroxide in biological environments. *Analytical Chemistry*, 87(3):1903–1910, 2015.

[94] C.-H. Jung, W.-J. Kim, C.-H. Jung, I.-T. Hwang, D. Khim, D.-Y. Kim, J.-S. Lee, B.-C. Ku, and J.-H. Choi. A simple PAN-based fabrication method for microstructured carbon electrodes for organic field-effect transistors. *Carbon*, 87(C):257–268, 2016.

[95] M. V. Kakade, S. Givens, K. Gardner, K. H. Lee, D. B. Chase, and J. F. Rabolt. Electric field induced orientation of polymer chains in macroscopically aligned electrospun polymer nanofibers. *Journal of the American Chemical Society*, 129(10):2777–2782, 2007.

[96] N. Ketabi, T. de Boer, M. Karakaya, J. Zhu, R. Podila, A. M. Rao, E. Z. Kurmaev, and A. Moewes. Tuning the electronic structure of graphene through nitrogen doping: experiment and theory. *RSC Adv.*, 6(61):56721–56727, 2016.

[97] O. V. Kharissova and B. I. Kharisov. Variations of interlayer spacing in carbon nanotubes. *RSC Adv.*, 4(58):30807–30815, 2014.

[98] M.-A. Kim, D. Jang, S. Tejima, R. Cruz-Silva, H.-I. Joh, H. C. Kim, S. Lee, and M. Endo. Strengthened PAN-based carbon fibers obtained by slow heating rate carbonization. *Scientific Reports*, 6(March):22988, 2016.

[99] E. A. Kiyatkin, R. A. Wise, and A. Gratton. Drug and behaviorassociated changes in dopaminerelated electrochemical signals during intravenous heroin selfadministration in rats. *Synapse*, 14(1):60–72, 1993.

[100] T. Kongkhlang, K. Tashiro, M. Kotaki, and S. Chirachanchai. Electrospinning as a New Technique To Control the Crystal Morphology and Molecular Orientation of Polyoxymethylene Nanofibers. *Journal of the American Chemical Society*, 130(46):15460–15466, 2008.

[101] K. Koziol, B. O. Boskovic, and N. Yahya. *Synthesis of carbon nanostructures by CVD method*, volume 1. Springer Berlin Heidelberg, 2010.

[102] M. Kumar and Y. Ando. Chemical Vapor Deposition of Carbon Nanotubes: A Review on Growth Mechanism and Mass Production. *Journal of Nanoscience and Nanotechnology*, 10(6):3739–3758, 2010.

[103] S. Kundu, T. C. Nagaiah, W. Xia, Y. Wang, S. V. Dommele, J. H. Bitter, M. Santa, G. Grundmeier, M. Bron, W. Schuhmann, and M. Muhler. Electrocatalytic Activity and Stability of Nitrogen-Containing Carbon Nanotubes in the Oxygen Reduction Reaction. *The Journal of Physical Chemistry C*, 113(32):14302–14310, 2009.

[104] T. Kyotani, N. Sonobe, and A. Tomita. Formation of highly orientated graphite from polyacrylonitrile by using a two-dimensional space between montmorillonite lamellae. *Nature*, 331:331–333, 1988.

[105] L. Lai, J. R. Potts, D. Zhan, L. Wang, C. K. Poh, C. Tang, H. Gong, Z. Shen, J. Lin, and R. S. Ruoff. Exploration of the active center structure of nitrogen-doped graphene-based catalysts for oxygen reduction reaction. *Energy & Environmental Science*, 5(7):7936, 2012.

[106] B. J. Landi, M. J. Ganter, C. D. Cress, R. A. DiLeo, and R. P. Raffaelle. Carbon nanotubes for lithium ion batteries. *Energy & Environmental Science*, 2(6):638, 2009.

[107] C. Lee, X. Wei, J. W. Kysar, and J. Hone. of Monolayer Graphene. *Science*, 321(July):385–388, 2008.

[108] D. Li, Y. Wang, and Y. Xia. Electrospinning of polymeric and ceramic nanofibers as uniaxially aligned arrays. *Nano Letters*, 3(8):1167–1171, 2003.

[109] N. Li, Z. Wang, K. Zhao, Z. Shi, Z. Gu, and S. Xu. Large scale synthesis of N-doped multi-layered graphene sheets by simple arc-discharge method. *Carbon*, 48(1):255–259, 2010.

[110] X. Li, W. Cai, J. An, S. Kim, J. Nah, D. Yang, R. Piner, A. Velamakanni, I. Jung, E. Tutuc, S. K. Banerjee, L. Colombo, and R. S. Ruoff. Large-Area Synthesis of High-Quality and Uniform Graphene Films on Copper Foils. *Science*, 324(5932):1312–1314, 2009.

[111] X.-F. Li, K.-Y. Lian, L. Liu, Y. Wu, Q. Qiu, J. Jiang, M. Deng, and Y. Luo. Unraveling the formation mechanism of graphitic nitrogen-doping in thermally treated graphene with ammonia. *Scientific Reports*, 6(1):23495, 2016.

[112] R. Liu, S. Li, X. Yu, G. Zhang, S. Zhang, J. Yao, B. Keita, L. Nadjo, and L. Zhi. Facile synthesis of Au-nanoparticle/polyoxometalate/graphene tricomponent nanohybrids: An enzyme-free electrochemical biosensor for hydrogen peroxide. *Small*, 8(9):1398–1406, 2012.

[113] Y. Liu and S. Kumar. Recent progress in fabrication, structure, and properties of carbon fibers. *Polymer Reviews*, 52(3-4):234–258, 2012.

[114] D. Long, W. Li, L. Ling, J. Miyawaki, I. Mochida, and S. H. Yoon. Preparation of nitrogen-doped graphene sheets by a combined chemical and hydrothermal reduction of graphene oxide. *Langmuir*, 26(20):16096–16102, 2010.

[115] D. Lozano-Castello, D. Lozano-Castello, D. Cazorla-Amoros, D. Cazorla-Amoros, a. Linares-Solano, a. Linares-Solano, S. Shiraishi, S. Shiraishi, H. Kurihara, H. Kurihara, a. Oya, and a. Oya. Influence of pore structure and surface chemistry on electric double layer capacitance in non-aqueous electrolyte. *Carbon*, 41:1765–1775, 2003.

[116] C. J. Luo, S. Loh, E. Stride, and M. Edirisinghe. Electrospraying and Electrospinning of Chocolate Suspensions. *Food and Bioprocess Technology*, 5(6):2285–2300, 2012.

[117] Z. Luo, S. Lim, Z. Tian, J. Shang, L. Lai, B. MacDonald, C. Fu, Z. Shen, T. Yu, and J. Lin. Pyridinic N doped graphene: synthesis, electronic structure, and electrocatalytic property. *Journal of Materials Chemistry*, 21(22):8038, 2011.

[118] P. X. Ma and R. Zhang. Synthetic nano-scale fibrous extracellular matrix. *Journal of Biomedical Materials Research*, 46(1):60–72, 1999.

[119] M. J. Madou, V. H. Perez-Gonzalez, and B. Pramanick. *Carbon : The Next Silicon? - Book 2*. Momentum Press Engineering, 2016.

[120] M. J. Madou, V. H. Perez-Gonzalez, and B. Pramanick. *Carbon : The Next Silicon? Book 1*. Momentum Press Engineering, 2016.

[121] A. Maghsoumi, L. Brambilla, C. Castiglioni, K. Müllen, and M. Tommasini. Overtone and combination features of G and D peaks in resonance Raman spectroscopy of the C ₇₈ H ₂₆ polycyclic aromatic hydrocarbon. *Journal of Raman Spectroscopy*, 46(9):757–764, 2015.

[122] M. R. Mahmoudian, Y. Alias, W. J. Basirun, P. M. Woi, and M. Sookhakian. Facile preparation of MnO2 nanotubes/reduced graphene oxide nanocomposite for electrochemical sensing of hydrogen peroxide. *Sensors and Actuators, B: Chemical*, 201:526–534, 2014.

[123] L. M. Malard, M. A. Pimenta, G. Dresselhaus, and M. S. Dresselhaus. Raman spectroscopy in graphene. *Physics Reports*, 473(5-6):51–87, 2009.

[124] S. Maldonado, S. Morin, and K. J. Stevenson. Structure, composition, and chemical reactivity of carbon nanotubes by selective nitrogen doping. *Carbon*, 44(8):1429–1437, 2006.

[125] X. Mao, X. Yang, G. C. Rutledge, and T. A. Hatton. Ultra-Wide-Range Electrochemical Sensing Using Continuous Electrospun Carbon Nano fi bers with High Densities of States. *Applied Materials & Interfaces*, 2014.

[126] T. Matsumoto. Mesophase pitch and its carbon fibers. *Pure and Applied Chemistry*, 57(11):1553–1562, 1985.

[127] P. H. Matter, L. Zhang, and U. S. Ozkan. The role of nanostructure in nitrogen-containing carbon catalysts for the oxygen reduction reaction. *Journal of Catalysis*, 239(1):83–96, 2006.

[128] J. A. Matthews, G. E. Wnek, D. G. Simpson, and G. L. Bowlin. Electrospinning of collagen nanofibers. *Biomacromolecules*, 3(2):232–238, 2002.

[129] A. D. McNaught, A. Wilkinson, M. Nic, J. Jirat, B. Kosata, and A. Jenkins. *IUPAC. Compendium of Chemical Terminology, 2nd ed. (the "Gold Book")*. Blackwell Scientific Publications, Oxford, 2nd editio edition, 2006.

[130] R. Memming, J. E. Soc, and R. Memming. Mechanism of the Electrochemical Reduction of Persulfates and Hydrogen Peroxide Mechanism of the Electrochemical Reduction of Persulfates and Hydrogen Peroxide. *Journal of The Electrochemical Society*, 116(6):785–790, 1969.

[131] W. S. L. Mok, M. J. Antal, P. Szabo, G. Varhegyi, and B. Zelei. Formation of Charcoal from Biomass in a Sealed Reactor. *Industrial and Engineering Chemistry Research*, 31(4):1162–1166, 1992.

[132] A. Mortadi, A. El Melouky, E. G. Chahid, R. El Moznine, and O. Cherkaoui. Studies of the clausiusMossotti factor. *Journal of Physical Studies*, 20(4):4001–1–4001–4, 2016.

[133] J. F. Moulder, W. F. Stickle, P. E. Sobol, and K. D. Bomben. *Handbook of X-ray Photoelectron Spectroscopy*. Perkin-Elmer Corporation, 1992.

[134] S. H. Nam, H. S. Shim, Y. S. Kim, M. A. Dar, J. G. Kim, and W. B. Kim. Ag or Au nanoparticle-embedded one-dimensional composite TiO2 nanofibers prepared via electrospinning for use in lithium-ion batteries. *ACS Applied Materials and Interfaces*, 2(7):2046–2052, 2010.

[135] R. S. Nicholson. Theory and Application of Cyclic Voltammetry for Measurement of Electrode Reaction Kinetics. *Analytical Chemistry*, 37(11):1351–1355, oct 1965.

[136] T. Nishimura. Electrochemical behavior of rust formed on carbon steel in a wet/dry environment containing chloride ions. *Corrosion*, 56(9):935–941, 2000.

[137] C. Niu, E. K. Sichel, R. Hoch, D. Moy, and H. Tennent. High power electrochemical capacitors based on carbon nanotube electrodes. *Applied Physics Letters*, 70(11):1480–1482, 1997.

[138] K. S. Novoselov, A. K. Geim, S. V. Morozov, D. Jiang, Y. Zhang, S. V. Dubonos, I. V. Grigorieva, and A. A. Firsov. Electric field effect in atomically thin carbon films. *Science*, 306(5696):666–669, 2004.

[139] Y. J. Oh, J. J. Yoo, Y. I. Kim, J. K. Yoon, H. N. Yoon, J. H. Kim, and S. B. Park. Oxygen functional groups and electrochemical capacitive behavior of incompletely reduced graphene oxides as a thin-film electrode of supercapacitor. *Electrochimica Acta*, 116:118–128, 2014.

[140] T. Ondarçuhu and C. Joachim. Drawing a single nanofibre over hundreds of microns. *Europhysics Letters (EPL)*, 42(2):215–220, 1998.

[141] S. Park, H. Boo, and T. D. Chung. Electrochemical non-enzymatic glucose sensors. *Analytica Chimica Acta*, 556(1):46–57, 2006.

[142] B. Partoens and F. M. Peeters. From graphene to graphite: Electronic structure around the K point. *Physical Review B - Condensed Matter and Materials Physics*, 74(7):1–11, 2006.

[143] J. R. Pels, F. Kapteijn, J. A. Moulijn, Q. Zhu, and K. M. Thomas. Evolution of nitrogen functionalities in carbonaceous materials during pyrolysis. *Carbon*, 33(11):1641–1653, 1995.

[144] V. Penmatsa, H. Kawarada, and C. Wang. Fabrication of carbon nanostructures using photo-nanoimprint lithography and pyrolysis. *Journal of Micromechanics and Microengineering*, 22(4):045024, 2012.

[145] H. O. Pierson. Handbook of Carbon, Graphite, Diamond and Fullerenes. *Handbook of Carbon, Graphite, Diamond and Fullerenes*, pages 25–69, 1993.

[146] O. Y. Podyacheva and Z. R. Ismagilov. Nitrogen-doped carbon nanomaterials: To the mechanism of growth, electrical conductivity and application in catalysis. *Catalysis Today*, 249:12–22, 2015.

[147] H. A. Pohl. The motion and precipitation of suspensoids in divergent electric fields. *Journal of Applied Physics*, 22(7):869–871, 1951.

[148] B. Pollack, S. Holmberg, D. George, I. Tran, M. Madou, M. Ghazinejad, R. Ragan, M. Madou, and M. Ghazinejad. Nitrogen-Rich Polyacrylonitrile-Based Graphitic Carbons for Hydrogen Peroxide Sensing. *Sensors*, 17(10):1–15, 2017.

[149] M. S. A. Rahaman, A. F. Ismail, and A. Mustafa. A review of heat treatment on polyacrylonitrile fiber. *Polymer Degradation and Stability*, 92(8):1421–1432, 2007.

[150] S. Ramakrishna, R. Jose, P. S. Archana, A. S. Nair, R. Balamurugan, J. Venugopal, and W. E. Teo. Science and engineering of electrospun nanofibers for advances in clean energy, water filtration, and regenerative medicine. *Journal of Materials Science*, 45(23):6283–6312, 2010.

[151] C. V. Raman. A Change of Wave-length in Light Scattering, 1928.

[152] C. V. Raman. A new radiation. *Proceedings of the Indian Academy of Sciences - Section A*, 37(3):333–341, 1928.

[153] R. Ramaseshan, S. Sundarrajan, R. Jose, and S. Ramakrishna. Nanostructured ceramics by electrospinning. *Journal of Applied Physics*, 102(11), 2007.

[154] A. Reina, X. Jia, J. Ho, D. Nezich, H. Son, V. Bulovic, M. S. Dresselhaus, and J. Kong. Supporting Information Large Area , Few-Layer Graphene Films on Arbitrary Substrates by Chemical Vapor Deposition. *Nano letters*, 9(1):1–8, 2009.

[155] D. H. Reneker and A. L. Yarin. Electrospinning jets and polymer nanofibers. *Polymer*, 49(10):2387–2425, 2008.

[156] D. Reznik, C. H. Olk, D. A. Neumann, and J. R. D. Copley. X-ray powder diffraction from carbon nanotubes and nanoparticles. *Physical Review B*, 52(1):116–124, 1995.

[157] M. Richard-Lacroix and C. Pellerin. Molecular orientation in electrospun fibers: From mats to single fibers. *Macromolecules*, 46(24):9473–9493, 2013.

[158] J. Robertson. Properties of diamond-like carbon, 1992.

[159] S. D. ROBERTSON. Graphite Formation from Low Temperature Pyrolysis of Methane over some Transition Metal Surfaces. *Nature*, 221:1044–1046, 1969.

[160] W. N. W. Salleh, A. F. Ismail, T. Matsuura, and M. S. Abdullah. Precursor Selection and Process Conditions in the Preparation of Carbon Membrane for Gas Separation : A Review in the Preparation of Carbon Membrane for Gas Separation : A Review. *Separation & Purification Reviews*, 40:261–311, 2011.

[161] O. J. Schueller, S. T. Brittain, and G. M. Whitesides. Fabrication of glassy carbon microstructures by soft lithography. *Sensors and Actuators A: Physical*, 72(2):125–139, 1999.

[162] F. Schwierz. Graphene transistors. *Nature Nanotechnology*, 5(7):487–496, 2010.

[163] Y. Shao, J. Wang, H. Wu, J. Liu, I. A. Aksay, and Y. Lin. Graphene based electrochemical sensors and biosensors: A review. *Electroanalysis*, 22(10):1027–1036, 2010.

[164] Y. Shao, S. Zhang, M. H. Engelhard, G. Li, G. Shao, Y. Wang, J. Liu, I. A. Aksay, and Y. Lin. Nitrogen-doped graphene and its electrochemical applications. *Journal of Materials Chemistry*, 20(35):7491, 2010.

[165] C. S. Sharma, A. Sharma, and M. Madou. Multiscale carbon structures fabricated by direct micropatterning of electrospun mats of SU-8 photoresist nanofibers. *Langmuir*, 26(4):2218–2222, 2010.

[166] H. Shi, Y. Shen, F. He, Y. Li, A. Liu, S. Liu, and Y. Zhang. Recent advances of doped carbon as non-precious catalysts for oxygen reduction reaction. *J. Mater. Chem. A*, 2(38):15704–15716, 2014.

[167] S. Silva and P. Ravi. *Properties of amorphous carbon*. Iet, 29 edition, 2003.

[168] M. D. Stoller and R. S. Ruoff. Best practice methods for determining an electrode material's performance for ultracapacitors. *Energy & Environmental Science*, 3(9):1294, 2010.

[169] A. M. Stortini, L. M. Moretto, A. Mardegan, M. Ongaro, and P. Ugo. Arrays of copper nanowire electrodes: Preparation, characterization and application as nitrate sensor. *Sensors and Actuators, B: Chemical*, 207(Part A):186–192, 2015.

[170] D. Sun, C. Chang, S. Li, and L. Lin. Near-field electrospinning. *Nano Letters*, 6(4):839–842, 2006.

[171] H. Tan. Roller nanoimprint lithography. *Journal of Vacuum Science & Technology B: Microelectronics and Nanometer Structures*, 16(6):3926, 1998.

[172] S. J. Tans, A. R. M. Verschueren, and C. Dekker. Room-temperature transistor based on a single carbon nanotube. *Nature (London)*, 393(6680):49–52, 1998.

[173] G. Taylor. Disintegration of Water Drops in an Electric Field. *Proceedings of the Royal Society A: Mathematical, Physical and Engineering Sciences*, 280(1382):383–397, 1964.

[174] G. Taylor. Electrically Driven Jets. *Proceedings of the Royal Society A: Mathematical, Physical and Engineering Sciences*, 313(1515):453–475, 1969.

[175] W.-E. Teo, R. Inai, and S. Ramakrishna. Technological advances in electrospinning of nanofibers. *Science and Technology of Advanced Materials*, 12(1):013002, 2011.

[176] W. E. Teo and S. Ramakrishna. A review on electrospinning design and nanofibre assemblies. *Nanotechnology*, 17(14):R89–R106, 2006.

[177] D. Teweldebrhan, F. Miao, C. N. Lau, a. a. Balandin, S. Ghosh, W. Z. Bao, and I.Caligo. Superior thermal conductivity of single layer graphene. *Nano Letters*, 8:902, 2008.

[178] E. T. Thostenson, Z. Ren, and T.-W. Chou. Advances in the science and technology of carbon nanotubes and their composites: a review. *Composites Science and Technology*, 61(13):1899–1912, 2001.

[179] N. Tucker, J. Stanger, M. Staiger, H. Razzaq, and K. Hofman. The History of the Science and Technology of Electrospinning from 1600 to 1995. *Journal of Engineered Fibers and Fabrics*, 7(SPECIAL ISSUE):63–73, 2012.

[180] F. Tuinstra, J. L. Koenig, and L. Koenig. Raman Spectrum of Graphite. *The Journal of Chemical Physics*, 53(3):1126–1130, 1970.

[181] S. J. Updike and G. P. Hicks. The Enzyme Electrode. *Nature*, 214(5092):986–988, 1967.

[182] T. G. Van Venrooij and M. T. Koper. Bursting and mixed-mode oscillations during the hydrogen peroxide reduction on a platinum electrode. *Electrochimica Acta*, 40(11):1689–1696, 1995.

[183] P. Vandenabeele. *Practical Raman Spectroscopy*. John Wiley & Sons, Ltd, The Atrium, Southern Gate, Chichester, West Sussex, PO19 8SQ, United Kingdom, 2013.

[184] M. Vangari, T. Pryor, and L. Jiang. Supercapacitors: Review of Materials and Fabrication Methods. *Journal of Energy Engineering*, 139(2):72–79, 2012.

[185] M. Velický, D. F. Bradley, A. J. Cooper, E. W. Hill, I. A. Kinloch, A. Mishchenko, K. S. Novoselov, H. V. Patten, P. S. Toth, A. T. Valota, S. D. Worrall, and R. A. Dryfe. Electron transfer kinetics on mono- and multilayer graphene. *ACS Nano*, 8(10):10089–10100, 2014.

[186] G. Wang, Z. K. Tan, X. Q. Liu, S. Chawda, J. S. Koo, V. Samuilov, and M. Dudley. Conducting MWNT/poly(vinyl acetate) composite nanofibres by electrospinning. *Nanotechnology*, 17(23):5829–5835, 2006.

[187] H. Wang, T. Maiyalagan, and X. Wang. Review on recent progress in nitrogen-doped graphene: Synthesis, characterization, and its potential applications, 2012.

[188] W. Wang, Z. Li, X. Xu, B. Dong, H. Zhang, Z. Wang, C. Wang, R. H. Baughman, and S. Fang. Au-doped polyacrylonitrile-polyaniline core-shell electrospun nanofibers having high field-effect mobilities. *Small*, 7(5):597–600, 2011.

[189] Y. Wang, D. C. Alsmeyer, and R. L. McCreery. Raman Spectroscopy of Carbon Materials: Structural Basis of Observed Spectra. *Chemistry of Materials*, 2(5):557–563, 1990.

[190] Y. Wang, Z. Li, J. Wang, J. Li, and Y. Lin. Graphene and graphene oxide: Biofunctionalization and applications in biotechnology. *Trends in Biotechnology*, 29(5):205–212, 2011.

[191] S. Watabe, Y. Sakamoto, M. Morikawa, R. Okada, T. Miura, and E. Ito. Highly sensitive determination of hydrogen peroxide and glucose by fluorescence correlation spectroscopy. *PLoS ONE*, 6(8):1–5, 2011.

[192] C. Wei, T. Y. Wei, C. H. Liang, and F. C. Tai. The separation of different conducting multi-walled carbon nanotubes by AC dielectrophoresis. *Diamond and Related Materials*, 18(2-3):332–336, 2009.

[193] D. Wei, Y. Liu, Y. Wang, H. Zhang, L. Huang, and G. Yu. Synthesis of N-doped graphene by chemical vapor deposition and its electrical properties., Nano Lett. *Nano Letters*, 9(5):1752–1758, 2009.

[194] Q. Wei, X. Tong, G. Zhang, J. Qiao, Q. Gong, and S. Sun. Nitrogen-Doped Carbon Nanotube and Graphene Materials for Oxygen Reduction Reactions. *Catalysts*, 5(3):1574–1602, 2015.

[195] M. S. Wellons, P. a. Berseth, and R. Zidan. Novel catalytic effects of fullerene for LiBH4 hydrogen uptake and release. *Nanotechnology*, 20(20):204022, 2009.

[196] S. Woo, Y. R. Kim, T. D. Chung, Y. Piao, and H. Kim. Synthesis of a graphene-carbon nanotube composite and its electrochemical sensing of hydrogen peroxide. *Electrochimica Acta*, 59:509–514, 2012.

[197] P. Wu, P. Du, H. Zhang, and C. X. Cai. Microscopic effects of the bonding configuration of nitrogen-doped graphene on its reactivity toward hydrogen peroxide reduction reaction. *Physical Chemistry Chemical Physics*, 15:6920–6928, 2013.

[198] X. Wu, R. D. Oleschuk, and N. M. Cann. Characterization of microstructured fibre emitters: in pursuit of improved nano electrospray ionization performance. *Analyst*, 137(18):4150, 2012.

[199] Y. Wu, M. S. Johannes, and R. L. Clark. AFM-based voltage assisted nanoelectrospinning. *Materials Letters*, 62(4-5):699–702, 2008.

[200] Z. S. Wu, W. Ren, L. Gao, B. Liu, C. Jiang, and H. M. Cheng. Synthesis of high-quality graphene with a pre-determined number of layers. *Carbon*, 47(2):493–499, 2009.

[201] Xinran Wang, X. Li, L. Zhang, Y. Yoon, P. K. Weber, H. Wang, J. Guo, and H. Dai. N-Doping of Graphene Through Electrothermal Reactions with Ammonia. *Science*, 324(May):768–771, 2009.

[202] B. Xu, S. Yue, Z. Sui, X. Zhang, S. Hou, G. Cao, and Y. Yang. What is the choice for supercapacitors: graphene or graphene oxide? *Energy & Environmental Science*, 4(8):2826, 2011.

[203] J. B. Xu and T. S. Zhao. Mesoporous carbon with uniquely combined electrochemical and mass transport characteristics for polymer electrolyte membrane fuel cells. *RSC Advances*, 3(1):16, 2013.

[204] Z. W. Xu, H. J. Li, B. Yin, Y. Shu, X. N. Zhao, D. S. Zhang, L. J. Zhang, K. Z. Li, X. H. Hou, and J. H. Lu. N-doped graphene analogue synthesized by pyrolysis of metal tetrapyridinoporphyrazine with high and stable catalytic activity for oxygen reduction. *RSC Advances*, 3(24):9344, 2013.

[205] R. Yadav and C. Dixit. Synthesis, characterization and prospective applications of nitrogen-doped graphene: A short review. *Journal of Science: Advanced Materials and Devices*, 2(2):141–149, 2017.

[206] X. Yang, D. Wu, X. Chen, and R. Fu. Nitrogen-enriched nanocarbons with a 3-D continuous mesopore structure from polyacrylonitrile for supercapacitor application. *Journal of Physical Chemistry C*, 114(18):8581–8586, 2010.

[207] A. L. Yarin, S. Koombhongse, and D. H. Reneker. Taylor cone and jetting from liquid droplets in electrospinning of nanofibers. *Journal of Applied Physics*, 90(9):4836–4846, 2001.

[208] S. Ye, A. K. Vijh, and L. H. Dao. A New Fuel Cell Electrocatalyst Based on Carbonized Polyacrylonitrile Foam. *Journal of The Electrochemical Society*, 144(1):90, 1997.

[209] B. K. Yen, B. E. Schwickert, and M. F. Toney. Origin of low-friction behavior in graphite investigated by surface x-ray diffraction. *Applied Physics Letters*, 84(23):4702–4704, 2004.

[210] J. M. You, D. Kim, S. K. Kim, M. S. Kim, H. S. Han, and S. Jeon. Novel determination of hydrogen peroxide by electrochemically reduced graphene oxide grafted with aminothiophenol-Pd nanoparticles. *Sensors and Actuators, B: Chemical*, 178:450–457, 2013.

[211] W. Yuan, Y. Zhou, Y. Li, C. Li, H. Peng, J. Zhang, Z. Liu, L. Dai, and G. Shi. The edge- and basal-plane-specific electrochemistry of a single-layer graphene sheet. *Scientific Reports*, 3(Cvd):2248, 2013.

[212] C. Zhang, L. Fu, N. Liu, M. Liu, Y. Wang, and Z. Liu. Synthesis of nitrogen-doped graphene using embedded carbon and nitrogen sources. *Advanced Materials*, 23(8):1020–1024, 2011.

[213] J. Zhang, Z. Xia, and L. Dai. Carbon-based electrocatalysts for advanced energy conversion and storage. *Science Advances*, 1(7):e1500564–e1500564, 2015.

[214] Y. Zhang, H. Gu, and S. Iijima. Single-wall carbon nanotubes synthesized by laser ablation in a nitrogen atmosphere. *Applied Physics Letters*, 73(26):3827–3829, 1998.

[215] Y. Zhang, X. He, J. Li, Z. Miao, and F. Huang. Fabrication and ethanol-sensing properties of micro gas sensor based on electrospun SnO2 nanofibers. *Sensors and Actuators, B: Chemical*, 132(1):67–73, 2008.

[216] Y. Zhang, Y. Wang, J. Jia, and J. Wang. Nonenzymatic glucose sensor based on graphene oxide and electrospun NiO nanofibers. *Sensors and Actuators, B: Chemical*, 171-172:580–587, 2012.

[217] Z. Zhang, D. Molina Piper, S. B. Son, S. C. Kim, K. H. Oh, S. H. Lee, and Y. Ding. Carbon nanopatterns and nanoribbons from directly nanoimprinted polyacrylonitrile: Correlation between crystallite orientation and nanoimprint process. *Polymer (United Kingdom)*, 54(21):5936–5941, 2013.

[218] Q. Zhu, S. L. Money, A. E. Russell, and K. M. Thomas. Determination of the Fate of Nitrogen Functionality in Carbonaceous Materials during Pyrolysis and Combustion Using X-ray Absorption Near Edge Structure Spectroscopy. *Langmuir*, 13(7):2149–2157, 1997.